TÉCNICO LISBOA

Effect of stairs on the seismic behaviour of columns

Cláudia Sá Nogueira Pereira

Thesis to obtain the Master of Science Degree in

Civil Engineering

Supervisor: Prof. Mário Manuel Paisana dos Santos Lopes

Examination Committee

Chairperson: Prof. António Manuel Figueiredo Pinto da Costa
Supervisor: Prof. Mário Manuel Paisana dos Santos Lopes
Member of the Committee: Prof. Carlos Alberto Ferreira de Sousa Oliveira

March 2018

Acknowledgements

To begin with, I would like to express my sincere gratitude and appreciation to my thesis supervisor Prof. Mário Lopes for sharing with me his knowledge and contagious passion for earthquake engineering while, at the same time, challenging me to see beyond the obvious. Without his constant support, motivation and availability, the end result achieved would certainly not be possible.

I would also wish to acknowledge the contributions made by Dr Rita Peres who so kindly and promptly addressed my concerns associated with the structural program used.

Last but not least, I would like to express my deepest gratitude to my friends for their genuine companionship, as well as, to my family, in particular to my aunt for her words of wisdom, my brother for his encouragement and my parents for their support and immeasurable love.

Resumo

Esta dissertação foca-se no estudo dos efeitos não-lineares produzidos por deslocamentos impostos por acções sísmicas em pilares de edifícios que suportam escadas a meia altura entre pisos. Para o efeito, efectuam-se análises computacionais sobre uma sub-estrutura de betão armado de um piso, constituída por duas vigas,dois pilares e uma escada.

Numa fase inicial apresenta-se uma revisão bibliográfica referente ao desenvolvimento de alguns conceitos relevantes na área de Engenharia Sísmica. Seguidamente, efectua-se uma apresentação do funcionamento do programa de elementos finitos utilizado – SeismoStruct (2016), assim como uma calibração dos modelos referentes às análises estruturais não-lineares a realizar. Por fim, executam-se dois tipos de análises estruturais, uma estática linear, com o objectivo de analisar o nível de esforços obtidos, e uma estática não-linear, considerando diferentes quantidades de armaduras longitudinais e transversais, assim como diferentes níveis de compressão a nível dos pilares para avaliar a capacidade de deformação da estrutura em estudo.

Demonstrou-se que se se efectuar uma análise linear, como é corrente em projecto, a presença da escada na estrutura conduz à obtenção de elevados esforços no pilar que suporta a escada. Consequentemente, existe uma necessidade de aumentar a quantidade de armaduras de flexão. Contudo, pelas análises não-lineares efectuadas, é demonstrado que o aumento da armadura de flexão, diminui a ductilidade e aumenta a probabilidade de ocorrência de rotura por esforço transverso. Pelo contrário, o aumento do nível de confinamento, pelo aumento da quantidade de armaduras transversais, aumenta a ductilidade disponível melhorando o desempenho sísmico. Também se observou que o aumento do nível de esforço axial, aplicado aos pilares, influenciava negativamente a ductilidade disponível.

Palavras-Chave: Escadas, Pilar, Deslocamentos Impostos, Ductilidade, Confinamento, Acção Sísmica

Abstract

This dissertation focuses on the study of the nonlinear effects produced by imposed displacements due to seismic actions on columns of buildings that support stairs at their mid-height level. To this purpose, a single storey reinforced concrete sub-structure will be analysed, consisting of two columns, two beams and stairs.

Firstly, a literature review on the development of some relevant concepts regarding earthquake engineering is presented. Subsequently, the main modules of the finite element software used - SeismoStruct (2016) - are introduced and a calibration of the nonlinear analyses to be performed is carried out. Lastly, two types of structural analyses are executed. One static linear, with the objective of analysing the internal forces obtained, and one static pushover nonlinear, considering different quantities of longitudinal and transverse reinforcement and different compressive forces applied on the columns, to evaluate the deformation capacity of the structure being studied.

It is demonstrated that in the framework of linear analyses, common in design practice, the presence of stairs in the structure leads to high levels of internal forces in the column that supports the stairs. Consequently, there is a need to increase the quantity of flexural reinforcement considered. Nevertheless, the static pushover analyses have shown that an increase in the flexural reinforcement reduces the ductility and increases the probability of a shear induced type of failure. Conversely, the increase in the confinement level, through the use of transverse reinforcement, increases the ductility availability and improves the seismic performance. Additionally, it was observed that an increase in the axial forces applied on the columns, negatively influenced the ductility availability.

Keywords: Stairs, Column, Imposed Displacements, Ductility, Confinement, Seismic Action

Table of Contents

List of Figures

List of Tables

Symbols

A_a	one-half of the total amount of flexural reinforcement (tensile reinforcement)
A_c	cross sectional area of concrete
A_c	section core area within centre lines of hoops including the longitudinal steel area
A_{cc}	area of core within centre lines of hoops excluding area of longitudinal steel
A_e	area of effectively confined core concrete
A_i	total area of ineffectively confined core concrete at the level of hoops
A_s	area of longitudinal reinforcement
$A_{s,max}$	maximum area of longitudinal reinforcement
$A_{s,min}$	minimum area of longitudinal reinforcement
A_{sx}/s	total area of transverse bars per unit length in the x direction
A_{sy}/s	total area of transverse bars per unit length in the y direction
b	section width
b_c	concrete core dimension to centre line of perimeter hoop in x direction
c	cover thickness
c_u	neutral axis depth near collapse
c_y	neutral axis depth at yield
d_c	concrete core dimension to centre line of perimeter hoop in y direction
EA	axial stiffness
EI_{sec}	secant flexural stiffness at yield
E_c	modulus of elasticity of concrete
E_h	post-yield stiffness of reinforcing steel
EI_1	flexural stiffness about minor axis
EI_2	flexural stiffness about major axis
E_s	modulus of elasticity of reinforcing steel
E_{sec}	secant modulus of confined concrete at peak stress
f_c	peak compressive stress of concrete

f'_{cc}	compressive strength of confined concrete
f'_{co}	compressive strength of unconfined concrete
f'_{cc}/f'_{co}	confinement factor
f_{cm}	mean compressive strength of concrete
f_{ct}	maximum tensile strength of concrete
f_{ctm}	mean tensile strength of concrete
f_{cu}	ultimate compressive strength of concrete
f_l	lateral pressure from the transverse reinforcement
f'_l	effective lateral confining stress (Annex E - EN1998-2)
f'_{lx}	effective lateral confining stress in x direction
f'_{ly}	effective lateral confining stress in y direction
f_y	yield strength of reinforcing steel
f_{yh}	yield strength of transverse reinforcement
GJ	torsional stiffness
H	height of the element
h	sectional dimension perpendicular to the flexural axis
h	section height
IS	integration section
k_e	confinement effectiveness coefficient
L	free height of the element
L	length of the element
M	bending moment
M_u	ultimate bending moment
M_y	yield bending moment
n	number of longitudinal bars
N	axial force
N	compressive force applied on top of columns
PP	self-mass per length

r	quotient between modulus of concrete
R	force reduction factor
s	hoop spacing
s'	clear vertical spacing between hoop bars
V	shear force
V_E	elastic base shear
V_D	design base shear
w_i'	i^{th} clear distance between adjacent longitudinal bars
x	quotient between the concrete strain and the strain at maximum concrete stress
Υ	material specific weight
δ	applied displacement
δ_u	ultimate displacement
δ_y	yield displacement
Δ_u	ultimate displacement
Δ_y	yield displacement
ε_c	concrete strain
ε_c^+	strain of confined concrete
ε_s^+	strain of reinforcing steel under tension
ε_{co}	strain at maximum stress of unconfined concrete
ε_{cc}	strain at maximum stress of confined concrete
ε_{cu}	ultimate concrete compressive strain
ε_{cy}	strain at maximum stress of concrete
ε_{sp}	concrete spalling strain
ε_{su}	ultimate strain of reinforcing steel
ε_{sy}	yield strain of reinforcing steel
λ	shear ratio
μ	strain hardening parameter of reinforcing steel
μ_Δ	displacement ductility capacity

ρ_{cc}	ratio of area of longitudinal reinforcement to area of core of section
ρ_s	total transversal volumetric reinforcement ratio
ρ_w	volumetric ratio of the transverse reinforcement
σ	stress
σ_{sy}	yield stress of reinforcing steel
σ_u	ultimate stress of reinforcing steel
σ_y	yield stress of reinforcing steel
$\sum w_i^2$	square sum of clear distances between adjacent longitudinal bars
$\sum_{i=1}^{n} \frac{(w_i')^2}{6}$	total area of ineffectively confined core concrete at level of hoops
Φ , χ	curvature
χ_u	ultimate curvature
χ_y	yield curvature

1. Introduction

1.1. Overview

These days, in the current design practice, stairs are usually not included in the global modelling of buildings. In fact, stair elements are often treated as being secondary elements whose design is made separately from the main structure with the intention of only withstanding vertical loadings.

Nevertheless, when building structures are subjected to imposed horizontal displacements and stairs are connected to columns at an intermediate level between storeys, these stairs can produce negative effects in the local behaviour of the structure, namely, a short column effect. This effect can significantly damage the columns that are so important to withstand the vertical loads.

In this sense, it is important to analyse the effects that the stairs produce in columns of buildings, when subjected to horizontal displacements, in terms of ductility and through nonlinear analyses.

1.2. Objectives

The principal objective of this dissertation is to contribute to a better understanding of the structural behaviour of columns that support stairs at a mid-height level between storeys, under the effects of seismic actions. To this purpose, a single storey framed structure consisting of two columns, two beams and a slab of stairs, will be analysed while being subjected to a relative imposed horizontal displacement between the levels of the two beams, which simulates the effects resulting from an earthquake action. This single storey framed structure is intended to represent part of a multi storey building of approximately ten floors.

In the current design codes, generally, the effects produced by seismic actions are solely represented by inertia forces being applied on the structures. It is also nowadays known that considering imposed horizontal displacements to simulate the effects of seismic actions produces more adequate results than considering applied inertia forces. When considering imposed displacements, the results are more adequate because the deformation capacity of the structures is explicitly taken into account.

This dissertation is intended to highlight the nonlinear effects on a column that supports a slab of stairs at the mid-height level. The term used to describe these nonlinear effects is commonly referred to as being the short-column effect. This effect is known for reducing the structural deformation capacity whilst significantly increasing the levels of shear forces as well as the ductility demand in terms of curvatures and displacements.

It will be demonstrated that the overall structure performance significantly improves with the increase of the confinement level in the columns, through the use of transverse reinforcement, rather than improving through the increase of flexural reinforcement. The measurement of the deformation capacity of the structure will provide the means to assess the overall structure performance. The deformation capacity will be measured by the evaluation of the values of material strains, curvatures as well as displacements achieved, beyond the elastic phase, in the nonlinear range of the analyses.

1.3. Thesis Organisation and Contents

This dissertation is divided into five chapters. Aside from this current introductory chapter, a brief description regarding the contents of each chapter is presented in the following paragraphs.

Chapter 2 includes a literature review based on the studies of several researchers, such as Nigel Priestley, John Mander and António Brito, among others. This chapter presents a historical background on the development of seismic design as well as some conceptual assumptions regarding current seismic design codes. Furthermore, the effects produced by imposed displacements on reinforced concrete structures and the assumed concrete stress-strain behaviour are also indicated.

Chapter 3 focuses on the calibration of the structural nonlinear analyses to be subsequently performed. In this chapter, the main modelling assumptions of the finite element software SeismoStruct (2016) as well as a brief description of the different modules, regarding the input data to build the structural models, are introduced. In the end, after the consideration of several different modelling strategies, one strategy is chosen to carry out the subsequent analyses, one that minimised the potential emergence of convergence problems and maximised the ductility demand, in terms of displacements and curvatures.

Chapter 4 comprises two main subchapters, the first concerns static analyses, considering non-variable loadings, while the second is related to the static pushover analyses to be executed. The static analyses involve two single storey framed structures: the first consists of two columns and two beams; the second, in addition to the representation of two beams connected by two columns, it also considers the presence of stairs. A certain displacement is applied on both structures to assess and compare the internal forces reached. The static pushover analyses only involve the structure that considers the representation of stairs, wherein three models are studied, considering different column reinforcement details and different levels of compressive forces being applied on the columns. In this type of analysis, comparisons are established between the displacements, curvatures and bending moments obtained.

Finally, Chapter 5 briefly summarises the main conclusions derived from the results achieved in the previous chapters.

2. Literature Review

This literature review chapter will outline several studies regarding the assumptions of current seismic design codes and the effects of imposed displacements on reinforced concrete structures. The latter is relatively important considering that, in general, structures, such as buildings and bridges, when subjected to seismic actions, not only have to transmit horizontal inertia forces to the foundations but also have to exhibit the ability to accommodate imposed displacements. This structural ability to accommodate imposed displacements is one of the objectives intended to be studied in this dissertation.

Firstly, a brief overview into the historical development of seismic design will be introduced, followed by the presentation of the equal displacement theory, which is inherent to force-based procedures, as well as the definition of the concept of ductility. Subsequently, based on the studies of Brito (2011), the behaviour of reinforced concrete elements subjected to imposed displacements will be discussed and, lastly, the assumed concrete behaviour proposed by Mander et al. (1988) will be presented.

2.1. Historical Background on Seismic Design

The first steps made in what is known today as seismic design, date back to the early 20th century, where a number of deadly earthquakes occurred in different countries, such as Italy, Japan, New Zealand and the United States of America (Lopes 2008; Calvi and Sullivan 2009; Priestley et al. 2007, cited in Camacho 2012, p.5).

Across the globe, these earthquakes strongly contributed to realise that the structures should be designed to withstand horizontal solicitations caused by the seismic actions. At the time, these horizontal solicitations were often treated as horizontal forces, equivalent to a certain percentage of the structure weight, regardless of its period (Calvi and Sullivan 2009; Camacho 2012). It was only after the Long Beach earthquake of 1933 that, according to Lopes (2008), the first concerns of ensuring the structures' ability to accommodate, horizontal forces as well as imposed displacements, triggered by the seismic solicitations, arisen.

As stated by Priestley (2000), from that period onwards, the concepts of "strength" and "performance" were considered to be synonymous in the codes design for seismic resistance until the development of the capacity design principles in New Zealand by Park and Paulay (1976), cited in Priestley (2000). Ever since then, there has been a rising concern in evaluating the overall performance of buildings, especially considering that many structures had been able to endure inertia forces, calculated assuming an elastic behaviour, larger than their own structural strength (Priestley 2000; Calvi and Sullivan 2009; Camacho 2012).

Nonetheless, the current design codes, namely Eurocode 8, still follow a force-based approach with a subsequent checking of the displacements achieved. In other words, as stated by Priestley (2000), the structure performance is not directly addressed at the initial stages of the design process. Instead, use

is made of the concept of ductility, first introduced in the 60s or 70s, to measure the inelastic deformation capacity (Priestley 2000). According to Priestley (2000), the ductility used to be expressed in terms of displacements (μ_Δ) and it was assumed to have a direct correspondence with the force reduction factor (R), as seen in the equations below.

$$\mu_\Delta = R \tag{1}$$

$$R = \frac{V_E}{V_D} \tag{2}$$

$$\mu_\Delta = \frac{\Delta_u}{\Delta_y} \tag{3}$$

This force reduction factor was used to reduce the elastic base shear strength to acceptable design levels and, in the current codes, is commonly referred to as behaviour coefficient.

Over the years, after several experimental and analytical researches into determining the available ductility capacity of different structural systems and, by association, the appropriate force reduction factors, it became clear that this approach implicitly assumed displacement capacity, instead of force capacity, as the basis for design. Despite these facts, the design process continued to be based in terms of required strength and the displacement capacity was only evaluated at final steps of the design procedure (Calvi and Sullivan 2009). Currently, this design procedure is advocated by the Eurocode 8 and many other codes around the world.

During the 90s, the investigations started to lay more emphasis on the explicitly consideration of the structures capacity to support displacements, as opposed to the ductility capacity of the structural systems, and the concept of performance based seismic design started to develop (Camacho 2012).

2.2. Equal Displacement Theory and Ductility Concept

Figure 1 (Priestley 2000, p.2) illustrates the basis of the equal displacement approximation, together with the problems concerning the definition of yield and ultimate displacement, which has been quite vague and non-consensual within the research community. The numeric symbols in the figure below, indicate the various defining possibilities of yield and ultimate displacements.

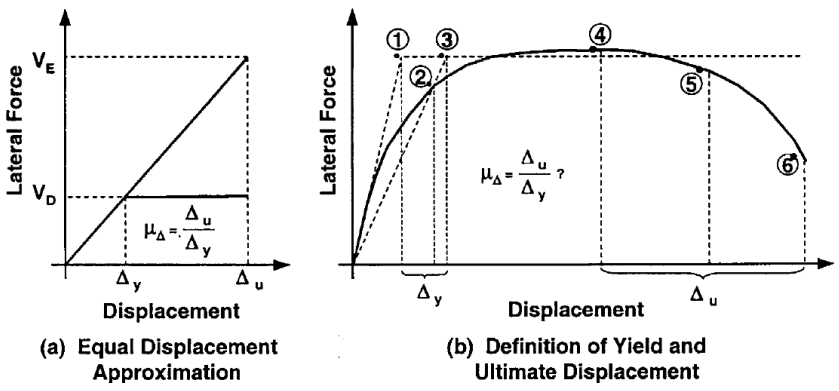

Figure 1 – Problems with the definition of ductility capacity (Priestley 2000)

According to Priestley et al. (2008), cited in Camacho (2012, p.4), the equal displacement theory basically assumes that, within the same applied action, the displacements suffered by a structure that responds inelastically are equal to the displacements that would arise, had the structure responded in an elastic manner. The difficulty lies in defining, exactly, the points at which the yield or ultimate displacements occur. For instance, Priestley (2000) stated that the yield displacement had been defined as being the intersection of initial tangent stiffness with the nominal strength or the displacement at first yield while, on the other hand, the ultimate displacement had been defined as being the displacement at peak strength or the displacement at initial fracture of transverse reinforcement. This ambiguity greatly contributed to the obtainment of different displacement ductility values in structures.

Another noteworthy aspect of this force-based approach, referred by Priestley (2000), is the assumption that particular structural systems can be associated with characteristic ductility capacities and, as a consequence, characteristic force-reduction factors. When in reality, the displacement ductility capacity of concrete structures depends on a number of factors, such as axial load, reinforcement ratio and structural geometry.

Among the different conceptual problems of the force-based design approaches discussed by Priestley (2000), one that should be highlighted is the need of specifying the initial stiffness of the structural members, which wrongly suggests that the structural stiffness does not depend on strength and that, yield displacements or yield curvatures are proportional to strength. Different investigators, such as Priestley (2000), Smith and Tso (2002), Brito (2011) and Camacho (2012), showed that not only does the structural stiffness of members vary proportionally with strength, but also the yield curvatures or yield displacements are almost independent of strength, as illustrated in Figure 2 (Priestley 2000, p.7).

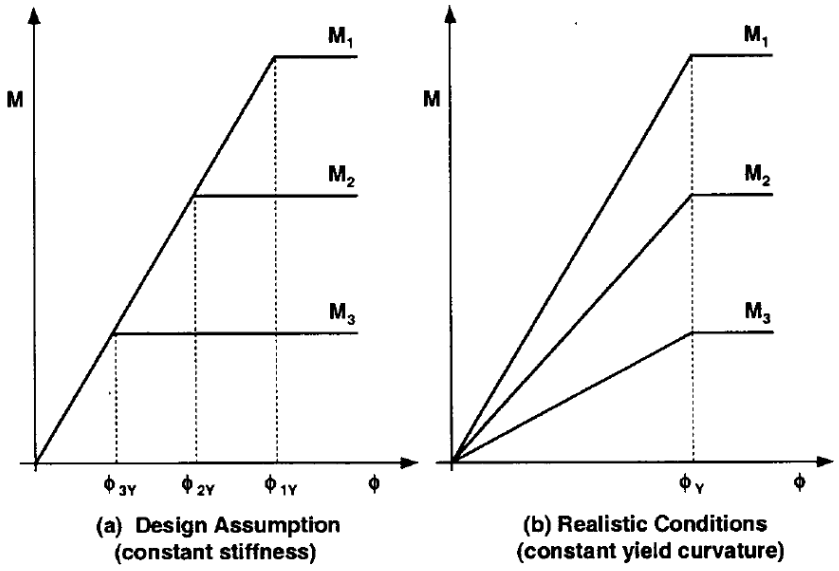

Figure 2 – Influence of strength on moment-curvature relationship (Priestley 2000)

Since the majority of the expressions used to estimate the initial stiffness of the structural members are completely independent of the quantity of flexural reinforcement and solely dependent on the

cross-sectional dimensions, the values of flexural resistance are directly proportional to yield curvatures, as it is possible to observe in the equation represented below.

$$EI = \frac{M}{\Phi} \tag{4}$$

All in all, these conceptual problems and inadequate assumptions regarding force-based seismic design would not exist if the structures, under seismic actions, did not yield and only responded along the linear range. However, that is not the case, since those structures respond along the inelastic range and elastic characteristics are still being used to give an indication on the structural inelastic performance.

2.3. Effects of Imposed Displacements on Reinforced Concrete Elements

2.3.1. Redefinition of basic concepts

The current design practice, regarding reinforced concrete structures subjected to an imposed displacement, usually involves a linear elastic analysis and the division of the internal forces obtained by a behaviour coefficient, to take into account the nonlinear effects. The objective is to ensure that the structure has an adequate resistant capacity to support the internal forces generated. If the considered behaviour coefficient in a structure were to be equal to unity, then a linear response would be expected and yielding would not occur in the structure, under seismic actions.

Brito (2011) clarified the main concepts behind this design methodology whilst resorting to the study of a fixed beam, with a constant section, wherein one of the ends was capable of supporting a horizontal translation to allow the application of displacements (Figure 3 – Brito 2011, p.111).

Brito (2011) started with admitting that there was no axial force being applied onto the beam. From then, the yield curvature of the cross-section was estimated by assuming that the maximum strain of the reinforcing steel was the one corresponding to its yield strain. By having the curvature value and the neutral axis position, the strains diagram of the cross-section was obtained, and subsequently, the materials stresses and the bending moment (through stresses integration) were obtained, as well.

Figure 3 – Fixed beam modelling (Brito 2011)

Even though the approach herein outlined was only an approximation to the actual behaviour of the reinforced concrete, Brito (2011) drew the following conclusions:

- if the neutral axis depth does not significantly vary, it can be said that the yield curvatures are dependent on the section dimension of the flexural plane;
- if the distribution of the flexural reinforcement does not vary, then it can be said that the neutral axis depth does not depend on the amount of flexural reinforcement;
- from the first two points, the strains diagram of the cross-section, at yielding, does not considerably vary with the amount of flexural reinforcement considered;
- the yield curvature and the strain diagram are almost independent from the amount of flexural reinforcement, therefore are independent from the yielding bending moment [Priestley (2000) and CEB-FIB (2003), cited in Brito (2011, p.112)];
- the yielding bending moment of the cross-section is a product that depends on the quantity of flexural reinforcement considered, as opposed to being the starting point of the analysis.

In the current design practice of reinforced concrete elements under flexion, the bending moment at yield obtained in the elastic analysis is what conditions the definition of the longitudinal reinforcement. For instance, the effects of imposed displacements are defined by static variables, such as bending moments, instead of kinematic variables, such as deformations. The determination of the amount of flexural reinforcement is based on the value of the bending moments obtained on a given analysis. Furthermore, the curvatures and strains diagrams are dependent on the value of bending moment and flexural reinforcement considered.

If, on the other hand, the effects of imposed displacements were to be taken into consideration in terms of kinematic variables, it would only be necessary a guarantee that the curvatures ductility demand was lower than the curvatures ductility availability. Moreover, there would not be a necessity to ensure a certain quantity of flexural reinforcement to withstand an imposed displacement. The flexural reinforcement would only be needed to resist applied forces.

2.3.2. Column analysis under imposed displacements

To reiterate the main consequences, discussed in the previous subchapter, Brito (2011) further analysed the column of Figure 3, considering two compact cross-sections. The first, Section A, is a circular section, where the longitudinal reinforcement is distributed along the perimeter. The second, Section B, is a rectangular section, where the longitudinal reinforcement is distributed near the extremities, parallel to the flexural axis. Figure 4 (adapted from Brito 2011, p.116) depicts the two types of cross-sections considered and their dimensions. Figure 5 (adapted from Brito 2011, p.116) illustrates the stress-strain relationships considered whilst Table 1 and Table 2 (both adapted from Brito 2011, p.116) show the defining parameters of the stress-strain relationships for the reinforcing steel and the concrete, respectively.

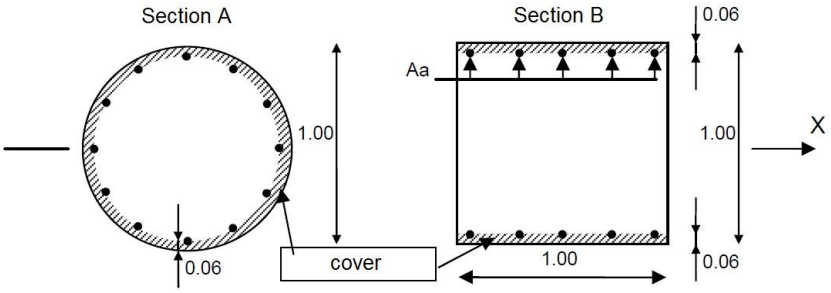

Figure 4 – Circular section A and rectangular section B (adapted from Brito 2011)

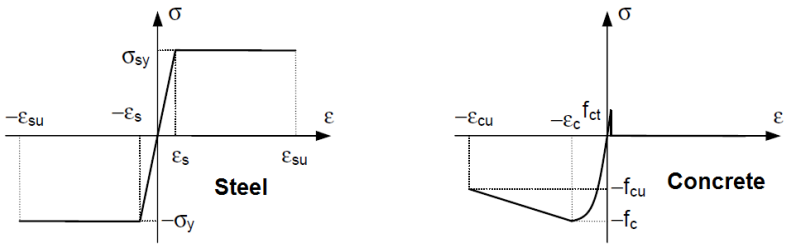

Figure 5 – Stress-strain relationships of reinforcing steel and concrete (adapted from Brito 2011)

Table 1 – Reinforcing steel parameters (adapted from Brito 2011)

ε_{sy} (‰)	ε_{su} (‰)	σ_{sy} (MPa)
2,175	200	435

Table 2 – Concrete parameters (adapted from Brito 2011)

ε_{cy} (‰)	ε_{cu} (‰)	f_c (MPa)	f_{cu} (MPa)	f_{ct} (MPa)
2,0	15,0	35	25	0

The parameters considered were intended to simulate plausible design values, except for the ultimate strain of the reinforcing steel that considers relatively high a value, not commonly found in structural reinforcement, in order to avoid a type of failure induced by the excessive reinforcement deformation. Additionally, the influence of the concrete tensile strength, the concrete cover and the reinforcement hardening were disregarded.

Table 3 (adapted from Brito 2011, p.117) shows the quantities of flexural reinforcement under tension considered for the two cross-sections. In the circular section, the reinforcement under tension was considered to be half the total amount of reinforcement in the section.

Table 3 – Flexural tensile reinforcement (adapted from Brito 2011)

Case	1	2	3
A_a (cm^2)	20	50	125

The moment-curvature diagrams obtained for both cross-sections and for the various amounts of longitudinal reinforcement are represented in Figure 6 (adapted from Brito 2011, p.117). No axial forces were applied on the cross-sections.

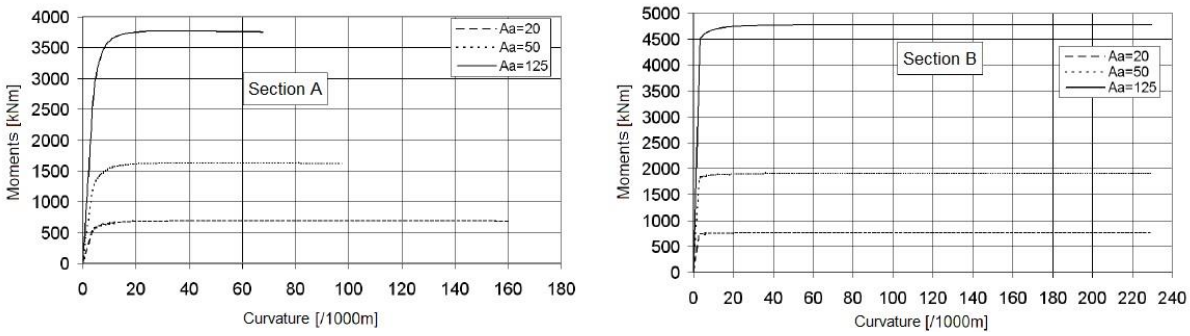

Figure 6 – Bending-moment-curvature diagrams for sections A and B with different amounts of flexural reinforcement (adapted from Brito 2011)

From the diagrams obtained, it was possible to observe that in Section A, the ultimate curvatures achieved decreased with the increase of flexural reinforcement. On the contrary, in Section B, the ultimate curvatures achieved were not influenced by the amount of flexural reinforcement considered. Brito (2011) explained this difference by analysing the type of failures that had occurred.

The ultimate curvatures achieved in Section A were associated with the occurrence of concrete failure. The reinforcement distribution in Section A, forced the concrete contribution in the absorption of the compressive forces. Consequently, the neutral axis depth in Section A significantly increased with the increase in the amount of flexural reinforcement considered, which led to the obtainment of smaller values of ultimate curvatures. It is evidenced in the equation below that great variations in the neutral axis depth, near failure, lead to the obtainment of great variations in the ultimate curvatures.

$$\chi_u = \frac{\varepsilon_{cu}}{c_u} \tag{5}$$

Unlike Section A, where concrete failure occurred, Section B experienced failure due to the excessive reinforcement deformation. Even though, the ultimate reinforcement strain was far superior than the ultimate concrete strain, Section B experienced this type of failure, because the reinforcement concentration, near the extremities, greatly contributed to the absorption of the compressive forces and, as a result, the neutral axis depths obtained near failure were all very small and, most importantly, practically the same for the different amounts of flexural reinforcement considered. As a result, the ultimate curvatures achieved in Section B were all numerically very close and almost not influenced by the quantity of flexural reinforcement, due to the very small variations in the neutral axis depths near failure, as evidenced in the equation below.

$$\chi_u = \frac{\varepsilon_{su}}{h - c_u} \tag{6}$$

The data in Table 4 (adapted from Brito 2011, p.118) summarises the most relevant variables, at yield and failure, regarding sections A and B. It should be noted that the depth of the compressive zone was

measured to the centre of the reinforcement under compression and most further away from the neutral axis.

Table 4 – Yield and ultimate variables associated with sections A and B (adapted from Brito 2011)

Case	χ_y (‰/m)	χ_u (‰/m)	c_y (m)	c_u (m)	M_y (kN.m)	M_u (kN.m)	$\frac{EI_{sec}}{A_a}$ (MN)	$\frac{M_y}{A_a}$ (kN/m)	$\frac{M_u}{A_a}$ (kN/m)
Section A (circular)									
1	3.104	160.535	0.179	0.093	472.24	685.89	76.07	236 120	342 945
2	3.391	97.238	0.239	0.154	1108.90	1615.89	65.40	221 780	323 178
3	3.772	67.577	0.303	0.221	2604.85	3751.29	55.25	208 388	300 103
Section B (rectangular)									
1	2.870	229.029	0.122	0.008	716.28	765.36	124.78	358 140	382 680
2	3.105	229.335	0.179	0.009	1789.92	1914.05	115.29	357 984	382 810
3	3.444	229.641	0.248	0.009	4415.22	4785.02	102.56	353 218	382 802

The results in the table above indicated that, as the flexural reinforcement significantly increased, up to 525%, the levels of bending moments also increased proportionally while the yield curvatures only increased up to 21%. The increase of the neutral axis depth at yield was not strong enough to produce great curvatures variations. This can be explained by the fact that the depth reduction of the zone under tension is relatively less significant than the relative increase of the length of the compressive zone. The equation below shows the calculation of yield curvatures and Figure 7 (Brito 2011, p.119) illustrates the small influence that variations in the neutral axis depths cause on yield curvatures.

$$\chi_y = \frac{\varepsilon_{sy}}{h - c_y} \tag{7}$$

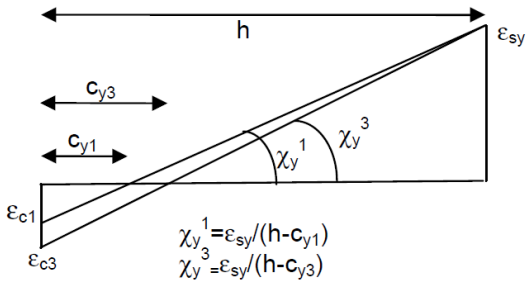

Figure 7 – Comparison between yield curvatures (Brito 2011)

Brito (2011) then concluded that the values of reinforcement yield strains and the geometry of cross-sections, unlike the amounts of flexural reinforcement, considerably influenced the values of yield curvatures achieved. In addition, it was also concluded that the levels of bending moments increased proportionally with the increase of flexural reinforcement. Thus, at yield, the flexural stiffness almost had a proportional variation with the quantity of longitudinal reinforcement.

Lastly, if Section B had experienced concrete failure, as opposed to failure due to excessive reinforcement deformation, the ultimate curvatures achieved would be influenced by the amount of flexural reinforcement considered. Nevertheless, the variations between the ultimate curvatures in Section B would be smaller than the ultimate curvatures variations in Section A, taking into account the different reinforcement distribution of the two sections. In Section B, the reinforcement concentration near the extremities, parallel to the flexural axis, would strongly contribute to the absorption of the compressive forces and would somewhat limit the increase of the neutral axis extension, with the increase of the flexural reinforcement. Therefore, the reinforcement concentration near the extremities constitutes an efficient possibility to increase the deformation capacity of the cross-section.

2.3.3. Influencing Factors on the Ductility of Reinforced Concrete Structures

This subchapter, also based on the studies conducted by Brito (2011), will further assess the influence of some other aspects concerning the deformation capacity of cross-sections, namely:

- geometry of the cross-section;
- resistant capacity of the materials;
- flexural reinforcement ratio and distribution;
- concrete tensile strength;
- axial force load;
- ratio between the ultimate and yield reinforcing steel stresses and post-yield stiffness of reinforcing steel;
- concrete cover;
- shear force load;
- slope of the descending portion of the concrete stress-strain relationship.

The first four factors were analysed at the cross-sectional level while the effects of the remaining aspects were studied on structural elements. The last two factors, the shear force load and the slope of the descending portion of concrete constitutive relationship, were only assessed in a qualitative manner.

The following subsections of this subchapter will indicate the various aspects that influence the ductility of reinforced concrete structures. The column represented in Figure 3 will serve as the basis for this analysis. It is noteworthy to mention that the deformation capacity of the cross-sections, in terms of ultimate curvatures, strongly depends on the values of the ultimate compressive concrete strains which, in turn, are dependent on the extension of the neutral axis depths.

2.3.3.1. Geometry of the Cross-section

The influence of the cross-sections dimensions was studied considering the sections represented in Figure 8 (adapted from Brito 2011, p.129), where one is a circular section, with a 2m diameter, while

the other is square section, 2m wide. The reinforcement quantity was increased - four times the initial considered value - in order to maintain the geometric percentage between the flexural reinforcement and the concrete area.

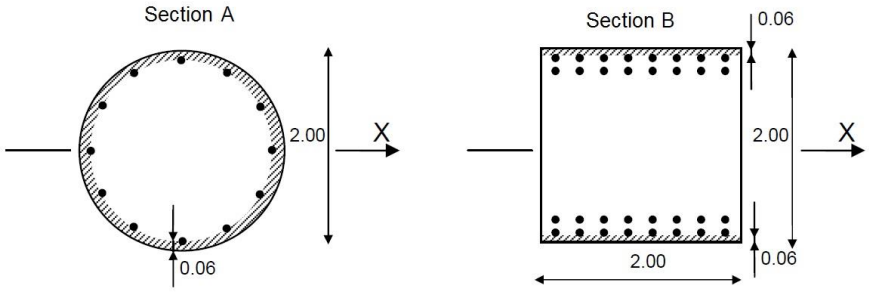

Figure 8 - Circular section A and square section B (adapted from Brito 2011)

Figure 9 (adapted from Brito 2011, p.129) depicts the bending-moment-curvature diagrams obtained for the two sections and the various amounts of flexural reinforcement considered.

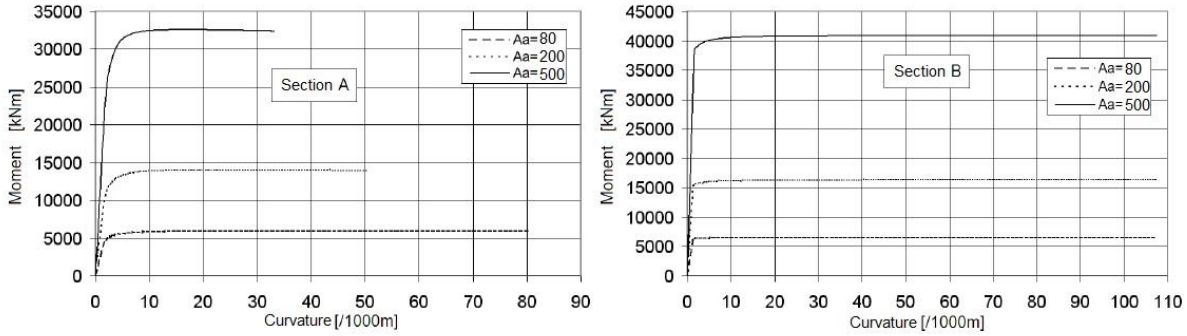

Figure 9 – Bending-moment-curvature diagrams for the new sections A and B (adapted from Brito 2011)

The data in Table 5 (adapted from Brito 2011, p.130) summarises the most relevant variables, at yield and at failure, regarding the new sections A and B, considering various amounts of flexural reinforcement.

Table 5 - Yield and ultimate variables associated with the new sections A and B (adapted from Brito 2011)

Case	A_a (cm^2)	χ_y (‰/m)	χ_u (‰/m)	c_y (m)	c_u (m)	M_y (kN.m)	M_u (kN.m)
Section A (new)							
1	80	1.44	80.20	0.367	0.187	4085.1	5905.5
2	200	1.57	50.28	0.490	0.298	9612.4	13948.9
3	500	1.74	33.17	0.628	0.452	22491.8	32387.1
Section B (new)							
1	80	1.34	107.31	0.254	0.016	6131.3	6538.2
2	200	1.45	107.43	0.374	0.018	15370.6	16344.3
3	500	1.60	107.49	0.521	0.019	37893.5	40883.3

It was possible to observe that the resistant capacity of the sections significantly increased in relation to the resistant capacity of initial sections considered in Table 4. The same type of failures occurred, concrete failure in Section A and reinforcement failure in Section B, since the reinforcement/concrete ratio was maintained. The depths of the neutral axis also varied in a proportional manner with the increase of the cross-sections dimensions. Considering that the materials strains at yield and near failure remained unchanged and the proportional increase of the neutral axes depth, the curvatures obtained were smaller than the ones initially attained.

All things considered, Brito (2011) confirmed that the deformation capacity of the cross-sections decreased with the increase of the dimension, perpendicular to the flexural axis, provided that there are not great variations in the reinforcement ratio and distribution.

2.3.3.2. Materials Resistant Capacity

It has been shown that slenderer reinforced concrete elements perform better under imposed displacements. Nevertheless, there are limits to the slenderness ratio considering the fact that the elements usually have to withstand the effects of applied forces (Brito 2011). One possibility to increase the elements resistant capacity is to increase the materials strength in order to maximise, as much as possible, the slenderness ratio (Camacho 2012).

As the concrete strength increases, brittle type of concrete failures tends to occur near the aggregates, rather than the cement grout. On the other hand, the maximum strains are not greatly influenced by the increase of concrete strength. The maximum strains of unconfined concrete only reduce for strength values higher than 55MPa. As a consequence, increasing the concrete strength can help diminishing the extensions of the neutral axes and, thus, it can also lead to the obtainment of greater curvature values. Nevertheless, the same cannot be said about confined concrete, whose maximum strain values can be more influenced by the increase of strength (Brito 2011).

In what concerns the type of reinforcing steel considered, as the reinforcement strength increases, the tensile forces to be equilibrated also increase, leading to the obtainment of larger depths of neutral axes, which can diminish the deformation capacity of the cross-sections. In addition, high-strength reinforcing steels are generally less ductile. All in all, the reinforcement strength considered must be high enough to not only ensure the resistant capacity to support applied forces, but it must also ensure the ability to consider slenderer elements.

2.3.3.3. Flexural Reinforcement Distribution and Ratio

This subsection shows an analysis conducted by Brito (2011) that considered a different flexural reinforcement distribution, with the purpose of exclusively studying its influence on the ductility capacity. Figure 10 (Brito 2011, p.132) illustrates Section B with the new flexural reinforcement distribution considered, which is perpendicular to the flexural axis and near to the extremities. Three different quantities of reinforcement were studied to produce the same levels of bending moments as the original Section B.

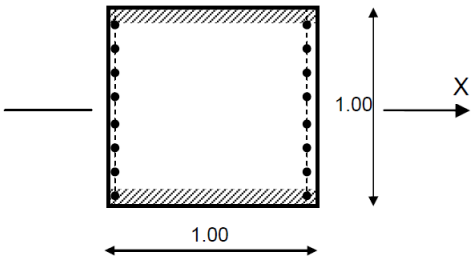

Figure 10 – Section B with reinforcement perpendicular to the flexural axis (Brito 2011)

Figure 11 (adapted from Brito 2011, p.132) depicts the bending-moment-curvature diagram in Section B for the different amounts of flexural reinforcement considered.

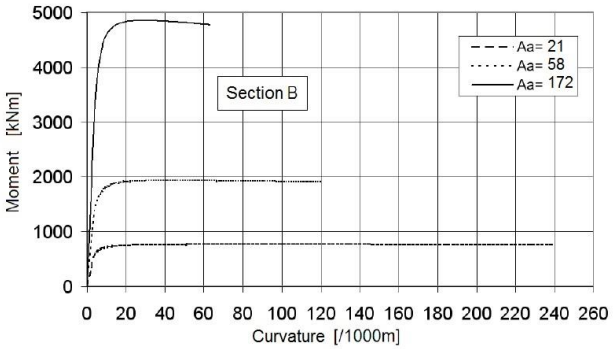

Figure 11 – Bending-moment-curvature diagram (adapted from Brito 2011)

Table 6 (adapted from Brito 2011, p.133) evidences the most relevant variables, at yield and at failure, regarding the analysis of Section B considering different amounts of longitudinal reinforcement.

Table 6[1] - Yield and ultimate variables associated with Section B (adapted from Brito 2011)

Case	A_a (cm^2)	χ_y (‰/m)	χ_u (‰/m)	c_y (m)	c_u (m)	M_y (kN.m)	M_u (kN.m)
1	21.2 (20)	2.89 (2.87)	242.25 (229.029)	0.127 (0.122)	0.054 (0.008)	463.9 (716.28)	762.6 (765.36)
2	58.1 (50)	3.16 (3.105)	120.68 (229.335)	0.191 (0.179)	0.124 (0.009)	1156.5 (1789.92)	1906.6 (1914.05)
3	171.9 (125)	3.61 (3.444)	63.08 (229.641)	0.277 (0.248)	0.238 (0.009)	2963.7 (4415.22)	4772.4 (4785.02)

It was observed that for Case 1, the section failure occurred due to the excessive reinforcement deformation. The necessary concrete contribution to balance the tensile forces in the reinforcement was very small and, therefore, the neutral axis depth at failure was also very small. In the remaining cases, it was observed that a concrete type of failure had occurred.

When comparing to the results obtained in the original Section B, the yield curvatures in the table above were slightly higher than the original yield curvatures obtained, because the neutral axes

[1] The data in brackets concerns the results of when the reinforcement was distributed near the extremities, parallel to the flexural axis.

depths at yield were also slightly higher. It would have been expected for these neutral axes depths to be even greater, considering the lack of compressive reinforcement. However, when the first longitudinal bars yield, the remaining tensile bars were still in the pre-yield elastic range, which inhibited the further extension of the neutral axes. As a consequence, the level of mobilised forces was slightly lower, which explained the smaller intensities of bending moments at yield.

The neutral axes depths obtained near failure were considerably higher than the original Section B. In addition, as the quantity of reinforcement increased, the neutral axes depths near failure also increased. Particularly, for Case 2 and Case 3, where concrete failure occurred, the increase of the neutral axes depths negatively influenced the ultimate curvatures achieved. Near failure, the majority of the longitudinal bars were at the post-yield phase of the constitutive relationship.

Given the new reinforcement distribution, the lever arm was much lower than the original situation. In order to guarantee the same level of resistant capacity in this present situation, the quantity of flexural reinforcement has to be greater. If the quantity of reinforcement has to be greater, then the level of tensile forces needed to be equilibrated is also higher and the neutral axis depth has to necessarily increase. Moreover, the lack of compressive reinforcement near the extremities parallel to the flexural axis, also contributes to the increase of the neutral axis depth near failure. Lastly, another aspect that increases the neutral axes depths is the concrete strength degradation for great levels of deformations, which is associated with the descending portion of the constitutive relationship. This effect is less relevant when considering confined concrete.

It was concluded that a reinforcement distribution near the extremities parallel to the flexural axis constituted an effective tactic in maximising the deformation capacity of cross-sections.

In relation to the reinforcement ratio between the compressive and tensile longitudinal bars, despite not being explicitly studied, it was possible to conclude that a diminishing of that factor increases the neutral axis depth and, thus, reduces the cross-sectional ductility. The neutral axis depth increase can be explained by the greater concrete contribution that must balance the lack of compressive reinforcement, in order to equilibrate the mobilised forces of the reinforcement under tension.

2.3.3.4. Concrete Tensile Strength

The concrete tensile strength increases the flexural stiffness of the cross-sections by limiting the evolution of the cracked zone. Nevertheless, it has been argued by Brito (2011) that not taking into consideration the value of the concrete tensile strength in monotonic analyses that intend to study the effects of seismic actions, which are by nature cyclic actions, only slightly underestimates the curvature values possibly achievable. As a result, in this dissertation, in all of the analyses performed, that concrete tensile strength considered was equal to zero.

2.3.3.5. Axial Force Load

Compressive axial forces on reinforced concrete elements produce a negative influence on the deformation capacity of cross-sections, since the neutral axes depths increase and the sectional failure occurs under smaller values of curvatures. Brito (2011) analysed the original sections A and B,

considering confined concrete with a normalised axial force of about 40%. The following equations show the axial forces adopted in Section A and Section B, respectively.

$$N = \frac{\pi \times 1.0^2}{4} \times 0.4 \times 35 \times 10^3 \approx 11\,000\ kN \quad (8)$$

$$N = 1.0^2 \times 0.4 \times 35 \times 10^3 \approx 14\,000\ kN \quad (9)$$

Figure 12 (adapted from Brito 2011, p.139) depicts the bending-moment-curvature diagrams for the two sections under compression, considering different amounts of flexural reinforcement.

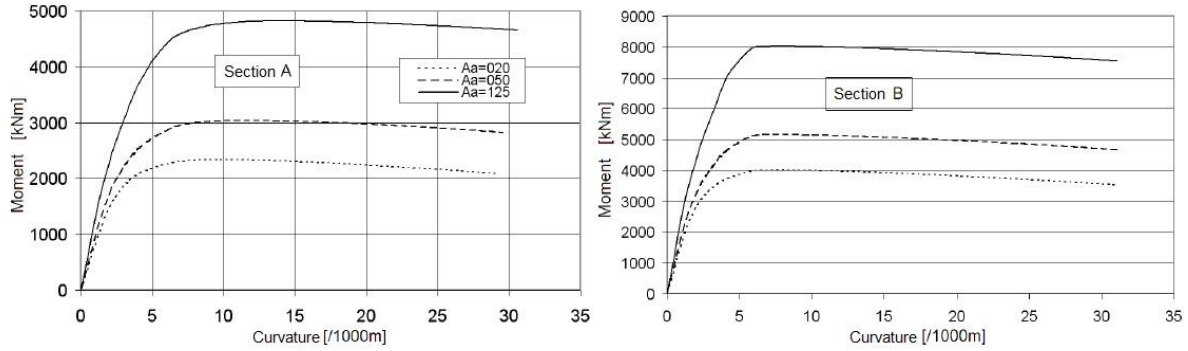

Figure 12 – Bending-moment-curvature diagrams for sections under compression (adapted from Brito 2011)

The bending-moment-curvature diagrams evidenced a descending portion that led to the obtainment of ultimate bending moments smaller than the values of yielding bending moments. The descending portion was explained by the existence of another descending portion in the considered confined concrete stress-strain relationship, as well as the fact that steel hardening parameter was disregarded, which could potentially attenuate the descending portion on the bending-moment-curvature diagrams.

Table 7 (adapted from Brito 2011, p.139) evidences the most relevant variables, at yield and at failure, regarding the analysis of sections A and B under the effects of a compressive axial force, considering different amounts of longitudinal reinforcement. Comparing the data in Table 7 with the results obtained that did not consider the effects of the axial forces, Brito (2011) drew the following conclusions:

- the axial force increased the depth of the neutral axes at yield and, therefore, the yield curvatures also increased;
- all of the different cross-sections experienced concrete failure because of the increase of the neutral axis depths;
- the ultimate curvatures were not significantly influenced by the increase of flexural reinforcement, since the neutral axis depths in the various cases were all numerically close.
- the quantity of flexural reinforcement is significantly influenced by the resistant capacity of cross-sections unlike the deformation capacity, which is not significantly influenced by the quantity of flexural reinforcement;
- the ultimate curvatures achieved were considerably lower than the ones that did not consider the influence axial forces.

Table 7[2] - Yield and ultimate variables associated with the compressed sections A and B (adapted from Brito 2011)

Case	A_a (cm^2)	χ_y (‰/m)	χ_u (‰/m)	c_y (m)	c_u (m)	M_y (kN.m)	M_u (kN.m)
Section A (circular)							
1	20	6.515 (3.104)	29.337 (160.535)	0.546 (0.179)	0.511 (0.093)	2289.64 (472.24)	2085.73 (685.89)
2	50	6.311 (3.391)	29.792 (97.238)	0.535 (0.239)	0.503 (0.154)	2899.95 (1108.90)	2824.85 (1615.89)
3	125	5.978 (3.772)	30.625 (67.577)	0.516 (0.303)	0.490 (0.221)	4413.92 (2604.85)	4655.94 (3751.29)
Section B (rectangular)							
1	20	5.942 (2.870)	31.191 (229.029)	0.514 (0.122)	0.481 (0.008)	3986.47 (716.28)	3515.79 (765.36)
2	50	5.938 (3.105)	31.191 (229.335)	0.514 (0.179)	0.481 (0.009)	5129.27 (1789.92)	4664.65 (1914.05)
3	125	5.928 (3.444)	31.191 (229.641)	0.513 (0.248)	0.481 (0.009)	7988.07 (4415.22)	7535.72 (4785.02)

In regards to the third point, the values of neutral axis depth near failure were quite similar, in the various cases, because the flexural reinforcement ratio between compressive and tensile bars maintained practically the same. In Section B, as the reinforcement increased, the forces that needed to be equilibrated increased as well, almost the same in both the compressive and tensile sides. In Section A, since the values of neutral axis depth were close to the centre of gravity of the cross-section, the flexural reinforcement ratio practically remained unchanged with the increase of reinforcement.

All of the conclusions presented, in particular the last two points, emphasise the negative effects that the axial forces cause in the deformation capacity of cross-sections.

2.3.3.6. Concrete Cover

Brito (2011) studied the influence the concrete cover on the ductility, observing that the consideration of the concrete cover on the analyses expectedly led to the obtainment of stronger bending moments, for a given level of curvature. In other words, the stiffness of cross-sections increased if the concrete cover was directly taken into account in the analyses. Additionally, it was observed that, as the extension of the zones without concrete cover, in the element studied, decreased, the ductility demand increased. In the end, Brito (2011) concluded that, in general, it can be acceptable to disregard the influence of the concrete cover on the ductility of cross-sections.

[2] The data in brackets concerns the results that did not consider the effects of the axial force.

2.3.3.7. Ratio between the ultimate and yield reinforcing steel stresses and post-yield stiffness of reinforcing steel

The quotient between the ultimate and yield reinforcing steel stresses gives an indication on the spread of plasticity in the plastic hinge regions. The greater the difference between those stresses, the greater can be the plastic hinge dimension. Considering that a trilinear stress-strain relationship was adopted for the reinforcing steel, as seen in Figure 13 (Brito 2011, p.122), the post-yield stiffness also influences the plastic hinge dimension, since it defines how quickly the ultimate stress is achieved and, therefore, the length of the hardening phase.

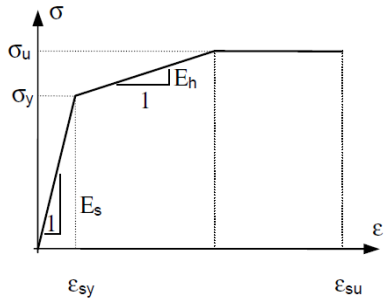

Figure 13 – Trilinear constitutive relationship of reinforcing steel (Brito 2011)

As soon as the ultimate reinforcing steel stress is achieved, if it is not possible to increase the resistant bending moment in the cross-section, then the spread of plasticity in the plastic hinge comes to a halt. The majority of the post-yield deformations occur in the plastic hinge regions, where the stiffness is reduced upon their formation. The smaller the plastic hinge length, the greater will be the demand of curvatures to ensure a certain relative rotation between the ends of the plastic hinge (Brito 2011).

Brito (2011) studied the effects of the reinforcing steel hardening on the ductility, by analysing the column of Figure 3, considering Section A and a transverse displacement of 2.5δ_y and 6δ_y. The ratios between the post-yield stiffness and initial elastic stiffness, also known as the hardening parameters, were of 1%, 2% and 5%. In addition, two quotients between the ultimate and yield reinforcing steel stresses were adopted (σ_u/σ_y = 1.3 and 1.2). Figure 14 (adapted from Brito 2011, p.148) depicts the bending-moment-curvature diagrams obtained for the three reinforcement quantities previously considered and for 1.3 quotient between the ultimate and yield stresses of the reinforcing steel. Table 8 (adapted from Brito 2011, p.148) and Table 9 (adapted from Brito 2011, p.148) indicate the maximum curvatures obtained in the column, for the cases where the imposed displacement was achieved before failure.

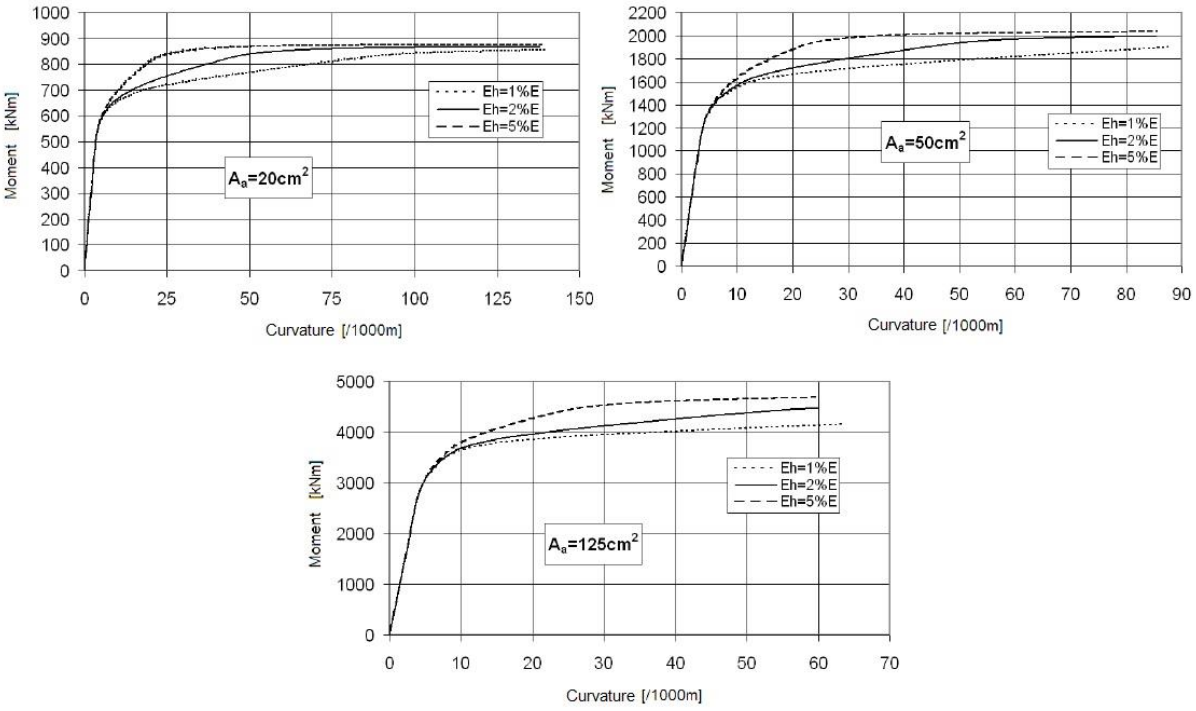

Figure 14 – Bending-moment-curvature diagrams for different steel hardening parameters (adapted from Brito 2011)

Table 8 - Maximum curvature at the column base section (Section A – δ = 2.5 δ_y; adapted from Brito 2011)

A_a (cm^2)	σ_u/σ_y=1.2			σ_u/σ_y=1.3		
	E_h/E_s=0.01	E_h/E_s=0.02	E_h/E_s=0.05	E_h/E_s=0.01	E_h/E_s=0.02	E_h/E_s=0.05
20	20.41	17.75	14.41	20.41	17.75	14.41
50	18.69	16.30	13.62	18.69	16.30	13.62
125	18.15	16.07	13.44	18.15	16.07	13.44

Table 9 – Maximum curvature at the column base section (Section A – δ = 6.0 δ_y; adapted from Brito 2011)

A_a (cm^2)	σ_u/σ_y=1.2			σ_u/σ_y=1.3		
	E_h/E_s=0.01	E_h/E_s=0.02	E_h/E_s=0.05	E_h/E_s=0.01	E_h/E_s=0.02	E_h/E_s=0.05
20	62.50	104.40	---	62.12	47.98	---
50	68.50	---	---	67.53	51.39	---
125	---	---	---	---	56.63	---

In Table 8 it was observed that the quotient between the ultimate and yield stresses did not influence the maximum curvatures achieved, because in both cases the quotient did not reach 1.2. It was concluded that for small ductility demands, the quotient between ultimate and yield stresses was not relevant.

As of Table 9, in some cases the imposed displacement was not reached because failure occurred under smaller displacement levels. It was observed that, in general, the increase of the quotient

between ultimate and yield reinforcing steel stresses diminished the ductility demand for a certain level of imposed displacement.

In what regards the effects of the hardening parameters, it was observed that out of all the hardening parameters, within the same levels of imposed displacement, the value of 2% led to the obtainment of smaller levels of ductility demand. This was explained by the shape of the bending-moment-curvature diagrams, where the diagrams associated with the hardening parameter of 2% most deviated from the shape of a perfect elastic-plastic diagram. It is noteworthy to mention that the ultimate bending moment is equal to the yielding bending moment in a perfect elastic-plastic diagram.

In the cases associated with a hardening parameter of 1%, the increase of the bending moment post-yielding was very small and the section failure occurred before the ultimate steel stress was reached. In comparison with the other values of hardening parameters, not only was the spread of plasticity smaller but also the ductility demand tended to be greater.

In the cases associated with a hardening parameter of 5%, the ultimate reinforcing steel stress was quite rapidly achieved and, as a consequence, the ultimate strains achieved were relatively low. The plastic hinge lengths were similar to the ones obtained with a hardening parameter of 2%. In the zones where the bending moment was lower than the ultimate bending moment, the curvatures were low and the ductility demand, in terms of curvatures, on the end node of the plastic hinge was higher.

Brito (2011) concluded that the constitutive relationship of the reinforcing steel could significantly influence the levels of curvatures achieved, in the post-yield phase of reinforced concrete elements.

2.3.3.8. Shear Force

The shear influence can be assessed through the value of shear ratio where h is the section dimension perpendicular to the flexural axis.

$$\lambda = \frac{M}{V.h} \tag{10}$$

Concrete elements with a compact cross-section, a quantity of transverse reinforcement not excessively small and a small or moderate level of axial force, are not highly susceptible to experiencing shear failure for shear ratio values higher than three. Strong levels of shear forces are usually associated with small levels of shear ratio and produce the following effects:

- diminishing of the plastic hinge length and, as a consequence, the diminishing of the ductility and the energy dissipation capacity;
- shear failure at curvature levels smaller than the maximum achievable, in other words, the local ductility of structural elements is reduced.

Brito (2011) concluded that as long as the capacity design principles are adopted in the structures design process and a shear induced type of mechanism is avoided, the levels of shear forces do not influence the ductility of reinforced concrete structures.

2.3.3.9. Descending Portion of the Concrete Stress-Strain Relationship

The stress-strain relationships of confined concrete usually include a descending portion, associated with the concrete strength degradation under strong levels of deformation. This strength degradation leads to an increase in the neutral axes depths and, consequently, a decrease in the ultimate curvatures achieved. The effects of strength degradation are stronger in lightly reinforced concrete sections or in sections subjected to strong levels of axial forces. The use of medium to strong levels of confinement can minimise the slope of the descending portion of the concrete stress-strain relationship (Brito 2011).

2.4. Concrete Stress-Strain Behaviour

The behaviour of concrete is strongly influenced by its own level of confinement. In order to take into account this effect in the static pushover analysis performed in this dissertation, the theoretical stress-strain model for both confined and unconfined concrete proposed by Mander et al. (1988) was adopted and is illustrated in Figure 15 (Mander et al. 1988, p.1807).

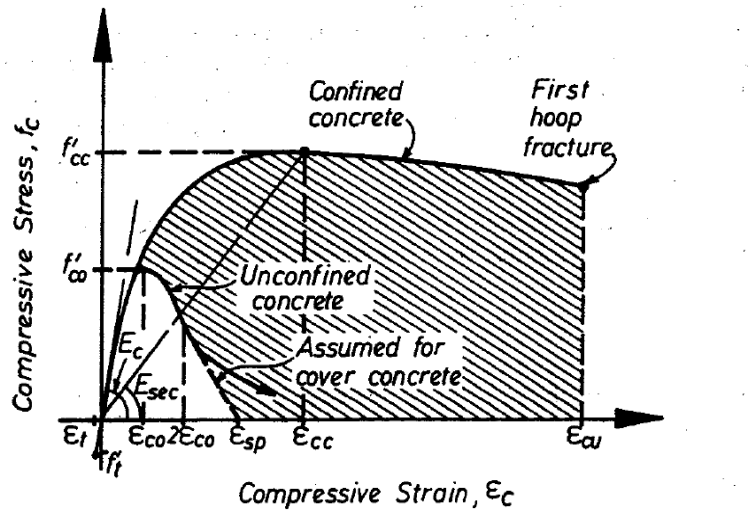

Figure 15 - Stress-strain model for confined and unconfined concrete (Mander et al. 1988)

The longitudinal compressive concrete stress (f_c) for a quasi-static monotonic loading is given by:

$$f_c = \frac{f'_{cc} x r}{r - 1 - x^r} \tag{11}$$

The obtainment of the compressive strength of confined concrete (f'_{cc}) will be explained later. The quotient between the compressive concrete strain (ε_c) and the strain at maximum concrete stress (ε_{cc}) is represented by the letter x.

$$x = \frac{\varepsilon_c}{\varepsilon_{cc}} \tag{12}$$

The strain at maximum concrete stress (ε_{cc}) is defined by:

$$\varepsilon_{cc} = \varepsilon_{co}\left[1 + 5\left(\frac{f'_{cc}}{f'_{co}} - 1\right)\right] \quad (13)$$

Usually the value assumed for the strain at maximum stress of unconfined concrete (ε_{co}) is 0.002. Finally, the quotient r can be written as:

$$r = \frac{E_c}{E_c - E_{sec}} \quad (14)$$

where the concrete modulus of elasticity (E_c) is given by:

$$E_c = 5{,}000\sqrt{f'_{co}} \quad [MPa] \quad (15)$$

and the secant modulus of confined concrete at peak stress (E_{sec}) is defined by:

$$E_{sec} = \frac{f'_{cc}}{\varepsilon_{cc}} \quad (16)$$

The spalling strain (ε_{sp}) defines the behaviour of the unconfined concrete cover once the stress reaches zero, while the ultimate concrete compressive strain at first hoop fracture (ε_{cu}), for orthogonal hoops, can be determined as, according to Eurocode 8 - Part 2, E.2.1.(c):

$$\varepsilon_{cu} = 0{,}004 + \frac{1{,}4 \times 2\rho_w f_{yh}\varepsilon_{su}}{f'_{cc}} \quad (17)$$

The Eurocode 2 - Part 1, 3.2.2(2) assumes for the mean reinforcement steel elongation at maximum force (ε_{su}), a value greater than or equal to 0,075 for reinforcement bars of Class C.

Alternatively, in addition to the approach described above, the ultimate compressive concrete strain could be obtained through the expressions proposed by Scott et al. (1982), cited in Brito (2011, p. 182). However, Brito (2011) favoured the use of the Eurocode 8 formulation, concluding that not only was it more conservative, under certain circumstances, but it was also the most recent method. It is now important to obtain the effective lateral confining pressure (f'_l) as well as the confinement effectiveness coefficient for rectangular concrete sections (k_e).

The confinement reinforcement generates a transverse pressure in the concrete core that can only achieve its maximum effectively in the zone under arching action which causes the full development of the confining stress. This arching effect assumed to occur vertically between the levels of hoop reinforcement and horizontally between restrained longitudinal bars is represented in Figure 16 (Mander et al. 1988, p.1810).

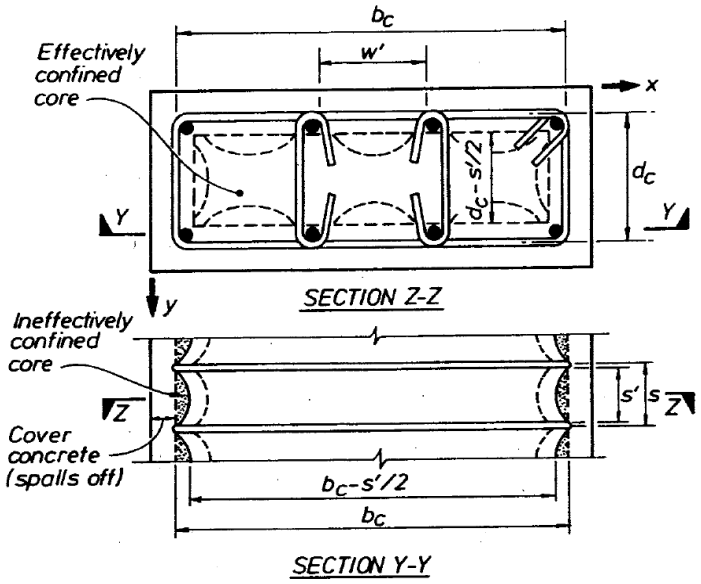

Figure 16 – Effectively confined core for rectangular hoop reinforcement (Mander et al. 1988)

The effective lateral confining pressure is given by:

$$f_l' = f_l k_e \tag{18}$$

where the confinement effectiveness coefficient (k_e) can be written as:

$$k_e = \frac{A_e}{A_{cc}} \tag{19}$$

where the area of effectively confined concrete core (A_e) is:

$$A_e = \left(b_c d_c - \sum_{i=1}^{n} \frac{(w_i')^2}{6}\right)\left(1 - \frac{s'}{2b_c}\right)\left(1 - \frac{s'}{2d_c}\right) \tag{20}$$

and the confined concrete area (A_{cc}), which is assumed to be the area within the centre lines of hoops excluding the longitudinal steel area, can be obtained as follows:

$$A_{cc} = A_c(1 - \rho_{cc}) \tag{21}$$

Therefore, the confinement effectiveness coefficient (k_e) can simply be written as:

$$k_e = \frac{\left(1 - \sum_{i=1}^{n} \frac{(w_i')^2}{6 b_c d_c}\right)\left(1 - \frac{s'}{2b_c}\right)\left(1 - \frac{s'}{2d_c}\right)}{(1 - \rho_{cc})} \tag{22}$$

Since it is common to have in the x and y directions of rectangular cross sections different quantities of transverse reinforcement, the ratios between the transverse reinforcement and the respective concrete core dimension are given by:

$$\rho_x = \frac{A_{sx}}{s d_c} \tag{23}$$

$$\rho_y = \frac{A_{sy}}{sb_c} \tag{24}$$

The lateral confining stresses on the concrete in both directions is given by:

$$f_{lx} = \rho_x f_{yh} \tag{25}$$

$$f_{ly} = \rho_y f_{yh} \tag{26}$$

As a result, the effective lateral confining stresses in both directions can be written as:

$$f'_{lx} = k_e \rho_x f_{yh} \tag{27}$$

$$f'_{ly} = k_e \rho_y f_{yh} \tag{28}$$

Lastly, to obtain the confinement factor, denominated in Mander et al. (1988) as the confined strength ratio, use was made of the graphic in Figure 17 which involves the multiaxial failure surface described by William and Warnke (1975), cited in Mander et al. (1988, p. 1812). As illustrated below, the confinement factor is the quotient between the confined concrete compressive strength (f'_{cc}) and the unconfined concrete compressive strength (f'_{co}).

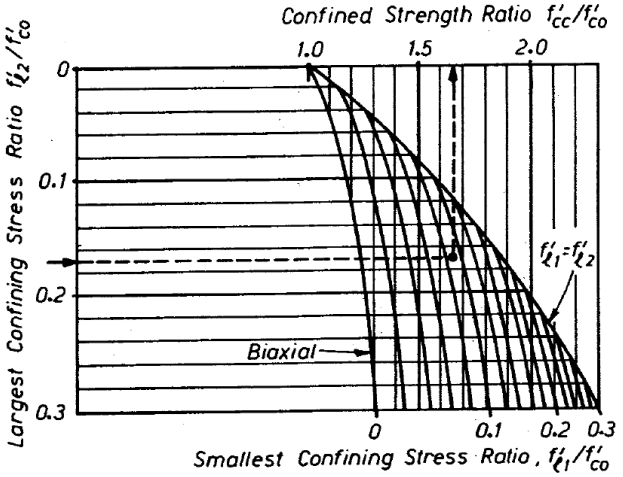

Figure 17 – Confined strength from lateral confining stresses for rectangular sections (Mander et al. 1988)

When the confinement factor was too small to be determined in the graphic represented above, the effective lateral confining stress was estimated according to the Annex E of the Eurocode 8-Part 2, considering the presence of orthogonal hoops, as:

$$f'_l = \sqrt{f'_{lx} f'_{ly}} \tag{29}$$

Consequently, the confinement factor was obtained as follows:

$$\frac{f'_{cc}}{f'_{co}} = -1{,}254 + 2{,}254\sqrt{1 + \frac{7{,}94 f'_l}{f'_{co}}} - 2\frac{f'_l}{f'_{co}} \tag{30}$$

3. Model Calibration

The main objective of this chapter is to calibrate the structural model of the static pushover analyses to be performed. To this effect, use will be made of the finite element program SeismoStruct (2016) to assess the structural behaviour.

Firstly, important modelling assumptions of the SeismoStruct software regarding the geometric nonlinearity and the material inelasticity will be presented.

Secondly, emphasis will be laid on the different tabs of the program that are vital for the models construction. The type of materials, sections, restraints, loadings, as well as the rupture definition on the structural models, will be presented.

Lastly, with the various structural models assembled, a choice will be made on the model that will serve as the basis for the nonlinear analyses. These structural models include inelastic force-based elements, whose type of discretisation, number of integration sections and section fibres were varied during the selection process to evaluate the different levels of ductility achieved, in terms of displacements and curvatures, on the different elements.

3.1. Modelling Assumptions

3.1.1. Geometric Nonlinearity

The geometric nonlinearity in the SeismoStruct software is implemented through a total co-rotational formulation developed by Correia and Virtuoso (2006), cited in SeismoStruct User Manual (2016, p.272), which takes into consideration large displacements, large rotations and large independent deformations (P-Delta effects) with regard to the frame element's chord. Figure 18 shows the local chord system of the beam-column elements, defined in the software, which includes six degrees-of-freedom and their corresponding internal forces.

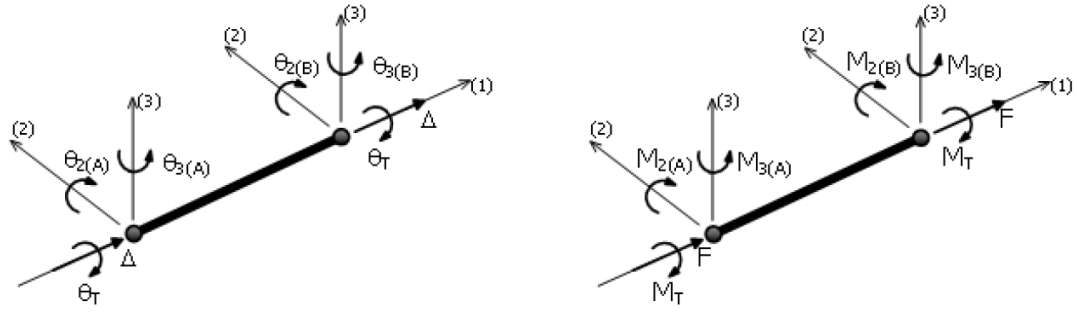

Figure 18 – Local chord system of the beam-column element (SeismoStruct User Manual 2016)

3.1.2. Material Inelasticity

The material inelasticity in the SeismoStruct program is modelled with distributed inelasticity framed elements. As pointed out by Calabrese et al. (2010), the entire member is modelled as an inelastic

element and the source of inelasticity is defined at a sectional level, in the controlling sections known as integration sections. These sections are refined into fibres that are individually associated with a material uniaxial inelastic behaviour. The global inelasticity of the frame is obtained through the numerical integration of the response provided by each integration section (Calabrese et al. 2010). Figure 19 shows a generic beam-column element with six integration sections as well as the discretisation into fibres of a reinforced concrete cross-section.

It should be stated, however, that this numerical integration is only approximate since it heavily depends on the number of controlling sections within a certain element. Furthermore, it is also important to emphasise that there is no need to establish in advance the length at which the inelastic response is expected to occur, since the integration sections of a given member can all enter in the inelastic range.

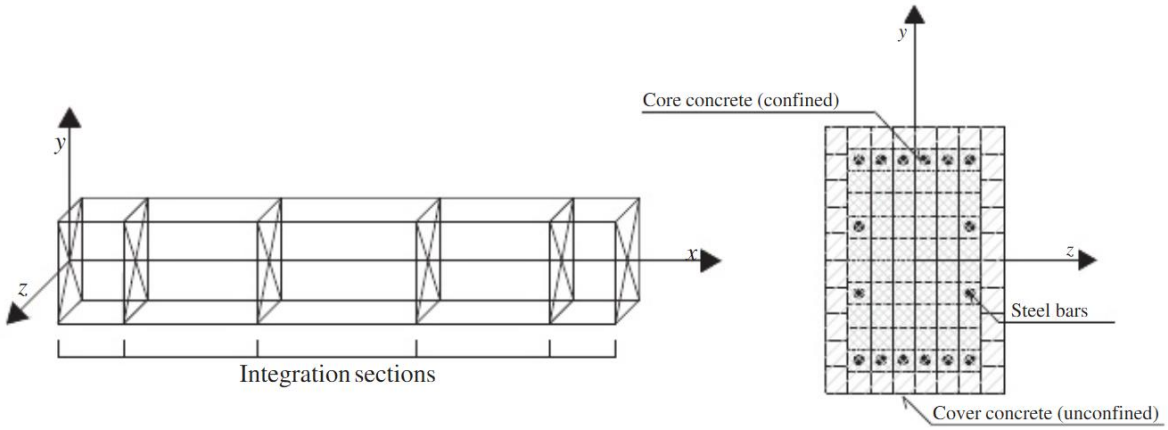

Figure 19 – Integration sections and sectional fibres discretisation (Calabrese et al. 2010)

There are two alternate formulations to implement the distributed inelasticity modelling. One is the displacement-based, which will not be discussed herein since it will not be used in this work. The other is the force-based approach where equilibrium is satisfied, a linear moment variation is enforced between the defined displacement increments and the inelastic deformations can occur freely both along the member length and the section depth.

According to Calabrese et al. (2010), cited in SeismoStruct User Manual (2016, p.274), theoretically, force-based elements do not need discretisation, besides the subdivision into integration sections within the element, unless localisation issues are expected to occur. The term localisation is associated with the fact that the sustained damage in any given element is concentrated only in one zone. Calabrese et al. (2010) further stated that, from a numerical point of view, localisation is a phenomenon that can be interpreted as being a finite element problem that happens under a softening constitutive sectional behaviour. In other words, this localisation is a concentration of inelasticity which is highly variable, not only in terms of numerical results but also with the type of discretisation and number of integrations sections defined.

In what regards the numerical integration, the Gauss quadrature is used for two or three integration sections while the Lobatto quadrature is used where four to ten integration sections are defined. Their approximate coordinates along the elements length measured from their barycentre are:

- 2 integration sections: [-0.577 0.577] x L/2
- 3 integration sections: [-1 0.0 1] x L/2
- 4 integration sections: [-1 -0.447 0.447 1] x L/2
- 5 integration sections: [-1 -0.655 0.0 0.655 1] x L/2
- 6 integration sections: [-1 -0.765 -0.285 0.285 0.765 1] x L/2
- 7 integration sections: [-1 -0.830 -0.469 0.0 0.469 0.830 1] x L/2
- 8 integration sections: [-1 -0.872 -0.592 -0.209 0.209 0.592 0.872 1] x L/2
- 9 integration sections: [-1 -0.900 -0.677 -0.363 0.0 0.363 0.677 0.900 1] x L/2
- 10 integration sections: [-1 -0.920 -0.739 -0.478 -0.165 0.165 0.478 0.739 0.920 1] x L/2

It should be noted that force-based elements do not possess less than three integration sections in order to avoid under-integration and ensure the obtainment of solid results regarding, for instance, the moment-curvature diagrams.

3.2. Structural Modelling

3.2.1. Materials

The first step in modelling the frame structure was to define the materials in order to characterise the cross-sections of the inelastic structural elements to be utilised. For this purpose, the strength class C30/37 was used for the concrete while the grade A500 was used for the reinforcing steel.

Regarding the materials' models in SeismoStruct, the "Mander et al. nonlinear concrete model" and the "Bilinear steel model" were used. According to SeismoStruct User Manual (2016), the first is a uniaxial nonlinear model in which the confining pressure is constant and the constitutive relationship is the one suggested by Mander et al. (1988) (see Figure 20). In the previous chapter, a succinct explanation of the stress-strain concrete behaviour proposed by Mander et al. (1988) was presented. The second is a uniaxial bilinear stress-strain model with a kinematic strain hardening rule assumed to have a linear variation with the increment of plastic strains (see Figure 21).

The mechanical properties were specified according to Eurocode 2 Part 1-1. Table 10 and Table 11 show the parameters necessary to fully describe the materials' models which include strength, modulus of elasticity and strains, among others.

The mean concrete tensile strength (f_{ctm}) was not considered in this phase of the model calibration. In this study, the consideration of the concrete tensile strength in the static pushover analysis to be performed would undoubtedly increase the overall stiffness of the structure since it would minimise the extension of the cracking zone. Nevertheless, under a cyclic loading such as the seismic action, once the concrete cracks, it no longer resists to tensile stresses. As a result, a monotonic model with a significant non-linear behaviour that does not consider the tensile strength, actually approximates more to the response of a model with a cyclic behaviour because if the magnitude of the deformation is high, the whole cross-section cracks, at least for one loading direction.

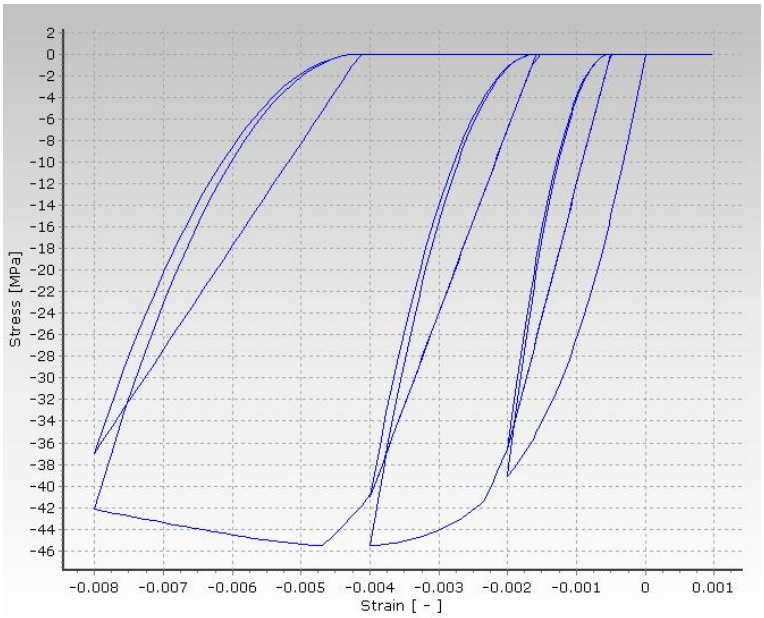

Figure 20 – Constitutive relationship for concrete C30/37 (sample plot – confinement factor = 1,2)

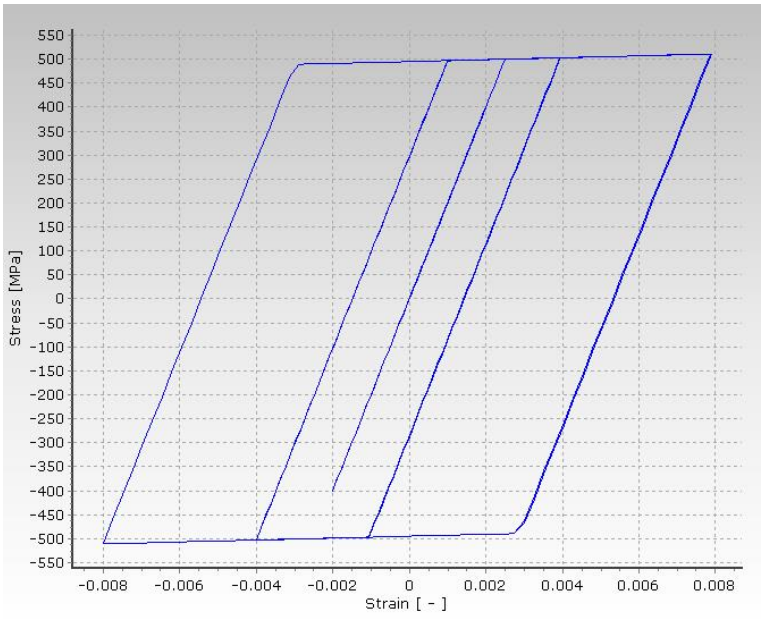

Figure 21 – Constitutive relationship for reinforcing steel A500

Table 10 - Mechanical properties of the Concrete C30/37

f_{cm} **(kPa)**	38000
f_{ctm} **(kPa)**	0
E_c **(kPa)**	32836568
ε_{co} **(‰)**	2,162
Υ **(kN/m^3)**	24,0

Table 11 - Mechanical properties of the Reinforcement A500

E_s **(kPa)**	200000000
f_y **(kPa)**	500000
μ **(-)**	0,010
ε_{su} **(‰)**	75,000
Υ **(kN/m^3)**	78,5

The ultimate reinforcement strain (ε_{su}) adopted was in accordance with the value of the characteristic reinforcement strain at maximum force suggested by Eurocode 2 Part 1-1, 3.2.2(2) for reinforcement bars of Class C. Taking into consideration that the value of the ultimate reinforcement strain was fixed, the value of the strain hardening parameter (μ) chosen directly influenced the maximum reinforcement stress achieved. Please note that the strain hardening parameter is the ratio between the post-yield stiffness and the initial elastic stiffness.

The higher the value of the strain hardening parameter, the greater is the ultimate reinforcement stress obtained. The greater the difference between the ultimate and yield reinforcement stresses, the greater will be the spread of plasticity along the plastic hinges length. Brito (2011) emphasised the importance of the plastic hinges length, considering the fact that it is in those regions that the post-yield deformations concentrate due to the stiffness reduction. Brito (2011) further stated that the smaller the plastic hinges length, the higher the curvatures necessary to guarantee a certain rotation between the extremities of the plastic hinge, in other words, the higher the ductility demand will be, in terms of curvatures for a certain imposed displacement. Considering everything stated above, the value chosen for the strain hardening parameter was of 1%, which ensured that the ultimate reinforcement stress was about 1.3 times the yield reinforcement stress.

It is also important to mention that the specific weight (Υ) directly influences the structural analysis in terms of the elements' self-weight. As a consequence, in the analysis where the effects of the self-weight were not intended to be studied, the specific weight defined in the materials module was considered to be equal to 0kN/m^3.

Lastly, the Poisson coefficient considered in SeismoStruct is either 0.2 for concrete or 0.3 for steel.

3.2.2. Sections

In the sections module, it was possible to define the different cross-sections of the inelastic force-based elements. The definition of these sections serves the purpose to specify the various integration sections necessary to build the beams and the columns of the desired structural model. It is worth mentioning that to represent the changes in reinforcement detailing it was not necessary to discretise the elements even further. This is mainly because a single inelastic force-based element allows the definition of integration sections with different reinforcement details as long as the geometry and the type of materials used in the section remain unaltered.

A rectangular reinforced concrete cross-section was used to define the beams and the columns. In terms of dimensions, both the beams and the columns have 0.50 x 0.30 m^2 cross-sections. The beams will experience bending about the axis of more inertia (major axis) while the columns will bend about the axis of lower inertia (minor axis). This is due to the orientation of the elements and the direction in which the loadings are applied. This point will be discussed in a subsequent chapter. The concrete cover considered was of 0.025m in terms of thickness measured from the exterior of the stirrups.

The reinforcement chosen for the columns was between the minimum and maximum values allowed by Portuguese National Annex of Eurocode 2 Part 1-1. Both these values are solely dependent on the area of cross-section. The minimum value ($A_{s,min} = 0{,}002\ A_c$) for the longitudinal reinforcement is 3cm^2 while the maximum value ($A_{s,max} = 0{,}04\ A_c$) is 60cm^2.

In order to ensure the formation of plastic hinges on the beams, the longitudinal reinforcement of the beams was so that the resisting moment of the columns was 30% higher than the resisting moment of the beams. This avoids the development of a soft-storey type of failure and improves the structure performance under a strong seismic action. The importance of having a weak beam/strong column mechanism has been emphasised by Park and Paulay (1976), cited in Priestley (2000, p.1), Priestley (1996), Brito (2011) and the Eurocode 8 Part 1.

Regarding the confinement factor, the program SeismoStruct allows the users to take into consideration the level of confinement of each section by either automatically calibrating its value based on the transverse reinforcement specified or allowing the user to define the confinement factor to be considered in the structural analysis. The second approach was chosen. The calculation of the confinement factor was done with detail following every step suggested by Mander et al. (1988). In Appendix A, there is a table showing the various parameters that were necessary for the calculation of the confinement factors.

3.2.3. Structure

The structure to be studied represents part of one storey of a reinforced concrete frame structure consisting of two beams 5.00m long, two columns 2.80m tall and stairs starting at the left end node of the bottom beam and finishing at the mid-height level of the right column, as depicted in Figure 22. The left column also serves the purpose of comparing both columns.

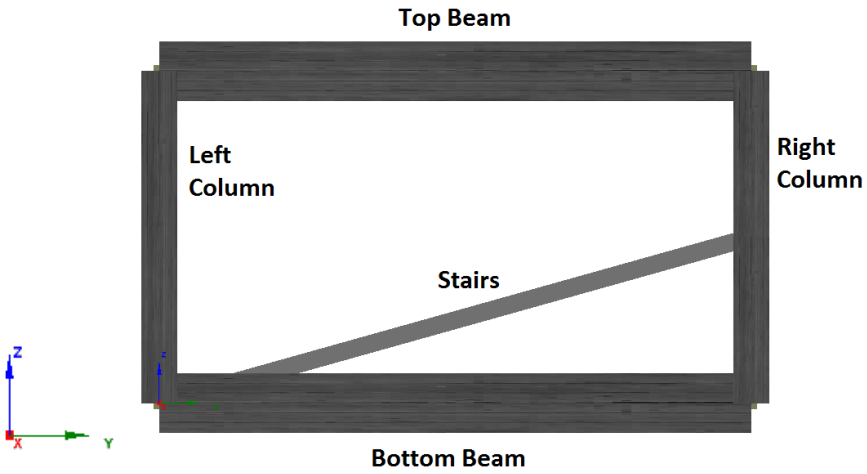

Figure 22 – Elements nomenclature

3.2.4. Restraints

All the analyses performed will be two-dimensional in the Y-Z plane, as such, all the structural nodes considered in a given model will have their out of plane degrees-of-freedom restrained which are the translation along X and the rotations about Y and Z. Additionally, the translation along Z of the bottom beam end nodes will be restrained as well as the translation along Y which will be restrained only in the left end node of the bottom beam.

3.2.5. Loading Phases

In this module, the type of loading strategy employed in the pushover analysis was defined. The type of loading chosen consisted on controlling the response of a particular degree-of-freedom of the structure. By this mean, a target displacement and the respective number of steps, which subdivided the displacement, were defined. During the course of the analysis, the displacement was incrementally increased, according to the number of steps previously defined, until the target was reached. Each step was associated with a load factor automatically estimated by the software in a procedure regarded as Response Control Phase.

This load factor enabled the calculation of the load value associated with the displacement being imposed, in the same degree-of-freedom. The load value could be a force or a displacement. It should be noted that the incremental load had to be numerically specified in the Applied Loads module before the beginning of the analysis. Consequently, as the imposed displacement was being incrementally increased, the load value associated with it was only a percentage of the incremental load previously specified. In other words, the load factor is a percentage of the load specified in the Applied Loads module. Overall, the applied loads included permanent forces in the vertical direction and an incremental displacement in the transversal direction.

3.2.6. Performance Criteria

This SeismoStruct tab allowed the monitoring of the concrete core crushing, as well as the reinforcement steel yielding and respective fracture. The types of criteria used for this monitoring were material strains.

For instance, for the concrete core crushing, the ultimate compressive strains were introduced in the program. These strains are dependent on the quantity of confining reinforcement. For this reason, these strains are only presented in Appendix A. The other strains considered were the value 0,0025 for the steel yielding (ε_{sy}) and 0,075 for the ultimate reinforcement strain (ε_{su}).

It is important to mention that, once the criteria were reached, there was a possibility to stop or continue the analyses considering or not strength degradations. Given the alternatives, the entire pushover analyses were performed without the consideration of strength degradations, which according to SeismoStruct User Manual (2016) possibly avoided the surge of numerical instabilities.

3.3. Model Selection

3.3.1. Type of Discretisation

Essentially, three different types of discretisation were considered for the selection of the structural model to carry out the nonlinear analyses of the next chapter. The first type (Discretisation A) studied is a minimal discretisation characterised by having the beams and the left column represented by a single inelastic element. The right column is represented by two inelastic elements in order to ensure the existence of a mid-height node to connect the stairs to the right column, as illustrated below in Figure 23.

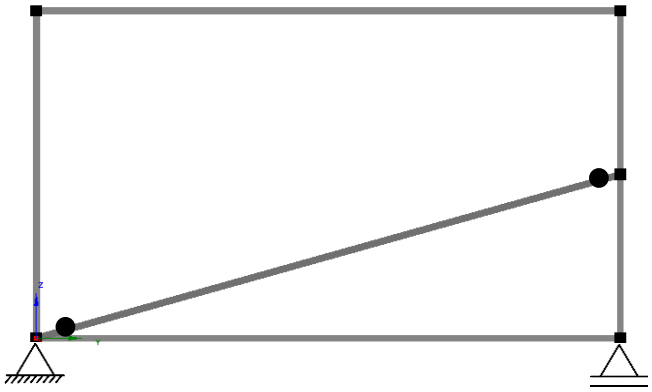

Figure 23 – Localisation of the nodes in Discretisation A

The second type of mesh refinement (Discretisation B), which is showed in Figure 24, is characterised by having all the beams and columns divided into two elements. The discretisation of the right column is identical to the one in Discretisation A.

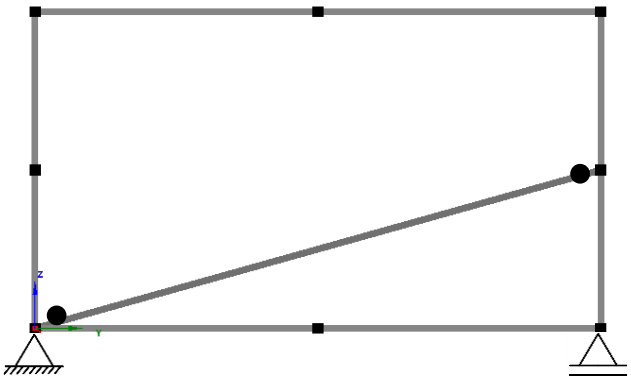

Figure 24 – Localisation of the nodes in Discretisation B

Finally, the third (Discretisation C) consists in dividing the inelastic elements into smaller members in the extremities and in the zone where the stairs meet the right column. The influence of the stairs can be considered to be a localisation issue which justifies the need to further discretise the region where the stairs connect with the right column.

Therefore, the beams and the left column are divided across their length in terms of percentages in the following manner: 15%; 35%; 35% and 15%. On the other hand, the right column is divided into: 7.5%; 17.5%; 17.5%; 7.5%; 7.5%; 17.5%; 17.5%; 7.5%. Consequently, the mesh is more refined in the areas where great variations of curvature are expected to occur. Figure 25 shows the third type of discretisation.

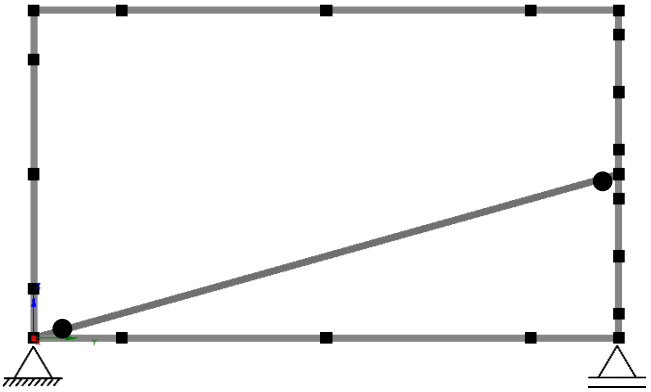

Figure 25 – Localisation of the nodes in Discretisation C

3.3.2. Type of Loadings

For each type of discretisation, two distinct types of loadings were applied. The first did not consider the self-weight of the beams, the columns and the stairs. The only loads considered were a 900kN compressive permanent force applied directly above both columns and an incremental displacement on top of the right column which compressed the stairs (Figure 26).

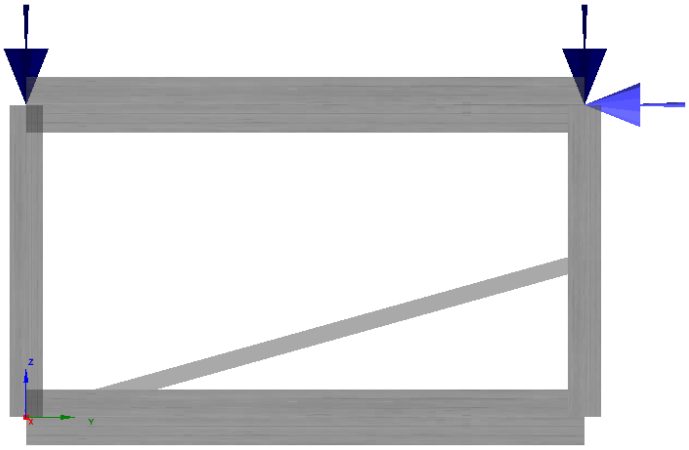

Figure 26 – First type of loading considered

Even though the effects of the stairs will be studied herein in a single floor, caution should be taken considering current buildings usually have more than two floors. For this reason, the 900kN axial force exists to take into account the permanent loadings derived from the weight of the fictitious floors above the floor being studied. The influence of this axial force will be discussed in more detail, once the model is chosen at the end of the calibration phase, considering different values for this force.

The second type of loading, not only considered the same loadings from the first one but it also considered the self-weight of all the elements (beams, columns and stairs) as well as a 25kN/m distributed load applied on the beams (Figure 27). This distributed load is attributable to the weight of a fictitious reinforced concrete slab with 0.15x5.00 m^2 and other permanent loads (which was considered to be approximately 6kN/m). Generally, in framed buildings, the slabs transfer their loadings to the beams, as it is considered herein.

The self-weight of the beams and the columns were specified separately in the materials module as 24kN/m^3 for the concrete class C30/37 and as 78.5kN/m^3 for the reinforcing steel A500. The stairs' specific weight was defined in the elements class module as 0.46 ton/m.

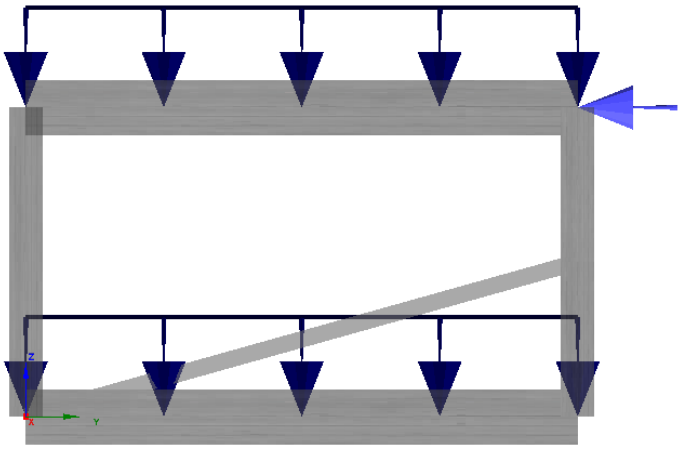

Figure 27 – Second type of loading considered

Please note that the direction in which the permanent loads were applied coincided with the direction of the minor axis of the beams, hence the bending about major axis. On the other hand, the displacement was applied in the direction of the longitudinal axis of the beams. Subsequently, both the displacement and the permanent loads caused bending about minor axis in the columns.

3.3.3. Element Classes

In all the following models, the representation of columns and beams was made through the use of inelastic force-based frame elements. The specificities of these elements were changed throughout the development of the different models, which is why they will only be discussed in the subsequent subchapter.

The representation of the stairs was made through the use of a single elastic frame element with the bending moments released near the end supports. It is worth mentioning that, if the stairs were to be inelastic then, according to SeismoStruct User Manual (2016), these bending moment releases could potentially cause convergence issues thus disabling an appropriate spread of plasticity in the other structural elements. Another reason for defining the stairs as an elastic element was due to the fact that the effects of having the stairs plastified were not intended to be studied. Also, stair elements are often designed separately to only withstand vertical loadings and are not included in the global modelling of buildings.

In terms of modelling, the only function of the element that represents the stairs is to transmit its axial force to the surrounding structural elements. The parameters necessary to define an elastic frame element are the axial, flexural and torsional stiffness. Table 12 exposes those elastic properties of the reinforced concrete stairs which were roughly estimated (not considering the reinforcing bars) for a cross-section with these dimensions: 1.20x0.15 m^2.

Table 12 – Defining parameters of the stairs

EA **(kN)**	5,90 x 10^6
EI_1 **(kN.m^2)**	11000
EI_2 **(kN.m^2)**	710000
GJ **(kN.m^2)**	17000
PP **(ton/m)**	0,00 or 0,46

It is worth mentioning that both the flexural and torsional stiffness are somewhat irrelevant to this analysis. Firstly, as mentioned above, the end nodes of the stairs will have their bending moments about minor and major axis released. Subsequently, the results will not be influenced by the value of flexural stiffness. And, secondly, the static pushover analysis to be performed will be two-dimensional, thus turning the definition of the torsional stiffness inconsequential. Therefore, the most important property in the modelling of the stairs is the axial stiffness which is expected to greatly influence the results.

The properties of the stairs will remain unchanged through the entire calibration phase. On the other hand, as mentioned above, the inelastic elements will suffer some changes regarding the number of integration sections and fibres.

3.3.4. Modelling

At this stage, it is possible to start discussing all the procedures performed to maximise both the imposed displacement and the level of curvatures achieved. Overall, six different type of structural analyses were carried out.

The first analysis is mainly characterised by having all the inelastic elements with ten integration sections. Therefore, the Discretisation A models have 50 controlling points, the Discretisation B has 80 and the Discretisation C has in total 200 integration points.

Each integration section has 150 fibres, following the suggestion of the SeismoStruct User Manual (2016) which states that cross-sections of inelastic elements constituted by more than one type of material should have more than 100 fibres. Hence the employment of 150 fibres in the first model to help decide whether or not it was sufficient to capture the high levels of inelasticity of the frame structure being studied.

In what concerns the reinforcement, the 5.00m beams have 4ϕ20+2ϕ16 for the longitudinal reinforcement distributed along 1.00m measured from both end supports. The rest of the beam span has 4ϕ20. The transverse reinforcement is constant and equal to ϕ6//0.125. Figure 28 and Figure 29 shows the position of the reinforcing steel on the beams.

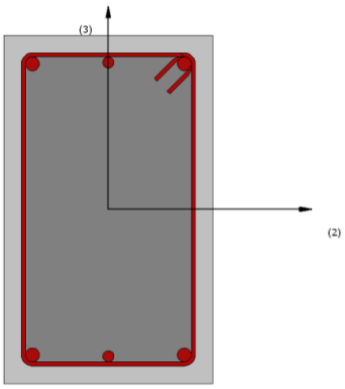

Figure 28 – End support Beam Reinforcement

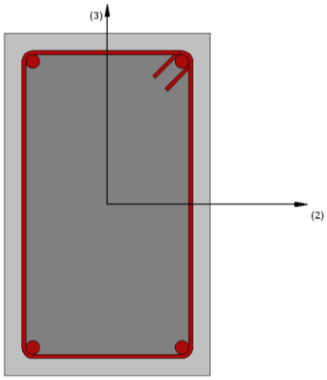

Figure 29 – Mid-span Beam Reinforcement

The columns longitudinal reinforcement is 10ϕ25 along their height, ϕ8//0.10 for the transverse reinforcement over 0.45m away from the extremities and ϕ8//0.20 for the rest of the column. The 0.45m distance is the potential plastic hinge region of the columns. Figure 30 shows the reinforcement of the columns.

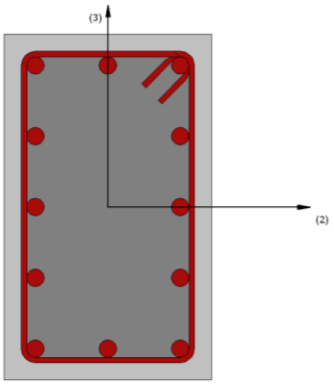

Figure 30 – Reinforcement detailing of the columns

The second model has the curtailment zone of the longitudinal beams' reinforcement at 1.50m away from the end supports as opposed to the 1.00m initially established to avoid plasticity near the supports of the beams. It should be noted that the following models will not suffer any changes with regards to the reinforcement positioning.

The third model is very similar to the second one, with the only difference being the number of sectional fibres considered at each integration section – 250 fibres rather than the initial 150 fibres.

The fourth has all the inelastic force-based elements with five integration sections with 150 fibres. Consequently, Discretisation A has 15 controlling points, Discretisation B has 40 and Discretisation C has in total 100 integration sections.

The fifth consists in having all the inelastic elements with three integration sections with 150 fibres each. In terms of the controlling points, Discretisation A has 15, Discretisation B has 24 and Discretisation C has 60 integration points.

The sixth final model is only for the Discretisation A and includes seven integration sections with 150 fibres for all the inelastic elements. In total, there are 35 integration points. It was not deemed relevant to study the effects of having seven integration sections in the Discretisation B and Discretisation C, since the results of the previous models showed no improvements on having inelastic elements fairly discretised with many integration sections.

3.3.5. Discussion of Results

The main results that will be discussed in this subchapter are the levels of ductility achieved in terms of displacements and curvatures in the different structural models. In addition, the variation of curvatures along the beams and columns of some models will be analysed while making comments regarding the variation of the bending moments' diagrams.

Firstly, before the main results, it is important to present the reasons that led to the end of the analyses as seen in Table 13. The analyses ended either because of the emergence of convergence problems or the occurrence of concrete failure.

Table 13 – Reasons that led to the end of the analyses

Type of model	1st model	2nd model	3rd model	4th model	5th model	6th model
A1[3]	convergence problems	concrete failure	convergence problems	concrete failure		
B1	concrete failure		convergence problems	concrete failure		
C1	convergence problems			concrete failure		
A2	concrete failure	convergence problems	concrete failure			
B2	convergence problems		concrete failure			
C2	concrete failure	convergence problems		concrete failure		

The convergence problems experienced are concentrated in the first three models. These models are precisely the ones that consider ten integration sections on each of the discretised elements. Clearly, there is a relation between the number of integration sections considered and the possibility of convergence problems emerging; the higher the number of integration sections, the stronger is the possibility of convergence problems occurring. Furthermore, in general, the Discretisation C type suffered the most with the convergence problems which indicates that a large number of integration sections together with a tight mesh refinement also contributes negatively to this problem.

Attempts were made to try solving the convergence difficulties encountered such as increasing the number of steps in which the displacement was incremented or changing the convergence criteria tolerance. Nevertheless, the convergence problems still continued and the maximum applied displacement almost did not change.

Concerning the last three models, all of the analyses ended because of the concrete failure at the mid-height section of the right column, immediately below the stairs. The ultimate concrete strain that the mid-height section could endure was reached. It can be said that the mid-height section of the right column is what conditions the collapse of these last three models.

The data in Table 14 indicates the applied displacement on top of the right column at which the mid-height section of the right column starts to yield. It is noteworthy to mention that the displacement values represented, consider the mid-height section of the right column as a reference point. In other words, these displacements concern the displacement endured by the top half of the right column. It should also be noted that mid-height section of the right column is not the first to yield in the structure. The first sections to yield are the ones near the extremities of the beams since the structure was designed to have a weak beam/strong column type of mechanism.

[3] The first character denominates the type of discretisation used, which in this case is Discretisation A. The second character, which is a number, designates the type of loading considered. The number one considers models without the self-weight loading while the number two considers models with the self-weight loading.

Table 14 – Yield displacement values for all the analyses

$\Delta\delta_y$ (mm)						
Model	1st	2nd	3rd	4th	5th	6th
A1	23,53	23,24	24,15	23,24	23,55	23,04
B1	23,54	23,24	24,05	23,04	22,94	
C1	23,54	23,34	24,15	23,44	23,64	
A2	24,11	23,70	24,60	23,82	24,17	23,60
B2	24,39	23,96	25,00	23,81	23,54	
C2	24,46	24,05	25,09	24,28	24,48	

Table 15 shows the maximum applied displacements on top of the right column at which convergence problems emerge or the mid-height section of the right column suffers concrete failure. Similarly to the previous table, the displacement values represented consider the mid-height section of the right column as a reference point.

Table 15 – Maximum displacement values for all the analyses

$\Delta\delta_u$ (mm)						
Model	1st	2nd	3rd	4th	5th	6th
A1	36,64	35,76	36,57	43,31	79,42	38,03
B1	36,76	35,47	36,57	43,20	79,39	
C1	35,26	35,15	35,29	35,66	38,93	
A2	35,31	35,20	35,80	41,89	74,37	36,61
B2	35,51	35,18	35,87	41,97	74,12	
C2	34,89	34,39	35,65	35,52	37,78	

Table 16 shows the displacement ductility values for all the analyses. The displacement ductility was obtained as the ratio between the values represented in Table 15 and Table 14.

Table 16 – Displacement ductility values for all the analyses

$\mu_{\Delta\delta}$						
Model	1st	2nd	3rd	4th	5th	6th
A1	1,56	1,54	1,51	1,86	3,37	1,65
B1	1,56	1,53	1,52	1,88	3,46	
C1	1,50	1,51	1,46	1,52	1,65	
A2	1,46	1,49	1,46	1,76	3,08	1,55
B2	1,46	1,47	1,43	1,76	3,15	
C2	1,43	1,43	1,42	1,46	1,54	

It is possible to observe in the table above that the smaller the number of integration sections considered, the higher is the displacement ductility availability. As previously mentioned, the first three models consider ten integration sections, the fourth model considers five, the fifth considers three and the sixth model considers seven integration sections.

The values of yielding displacements achieved are all numerically close except the ones from the third model, which are slightly higher. The main differences lie with the maximum displacements achieved. The maximum displacements achieved follow the same trend as the displacement ductility, where the smaller the number of integration sections considered, the higher is the maximum displacement achieved.

It can also be stated that the consideration of the self-weight loadings in the models, decreases the displacement ductility. The consideration of the self-weight loadings increases the internal axial forces of the columns. The negative effects of the axial forces in the ductility availability will be discussed with detail in the next chapter.

The conclusions regarding the type of discretisation considered and the displacement ductility achieved is not linear. Nevertheless, in the majority of the models, the displacement ductility decreases with the increase of the discretisation. Only in the fourth and fifth models, from the Discretisation A to Discretisation B, the ductility faintly increases.

Table 17 summarises the curvature ductility values of the regions where plastic hinges form. Since the left column and the right node of the bottom beam usually do not plastify for the imposed displacement levels, their curvature values are neither analysed nor shown in the table below. Hence, the only curvatures presented are from the mid-height node of the right column, which is connected to the end support of the stairs, the left end node of the bottom beam as well as the left and right end nodes of the top beam.

It should be noted that the curvature ductility values of the right column concern the value immediately below the mid-height node, as this is the most relevant section to assess the safety of the structure. In all the structural models, the value immediately above the mid-height node of the right column is smaller. There is a discontinuity in the curvature diagrams. The reason for this situation is intrinsically related to the variation of the axial forces in the column imposed by the presence of the stairs.

In this particular case, with the stairs under compression, the bottom half of that column is less compressed when in comparison with the top half of the column. As a result, the section of the right column immediately above the mid-height node is subjected to a higher level of axial force when comparing with the section immediately below the mid-height node.

Considering that both sections are subjected to the same levels of bending moments, for any given displacement, it is possible to state that the neutral axis depth is higher in the most compressed section, which is the one immediately above. As the analysis progresses, the difference in terms of axials forces between the halves of column increases, in other words, the differences in terms of neutral axis depths between the sections at the mid-height level of the column increases.

The section with the highest level of axial force exhibits higher concrete stresses and concrete strains. Therefore, it could be expected for the concrete failure to occur at this section. However, that is not the case, since the section with the smallest neutral axis depth (the one immediately below) is the first to yield, leading to a higher penetration into the descending branch of the concrete constitutive relationship, leading to a higher neutral axis depth. In this case, this effect is stronger than the effect of

the axial force. The stress-strain relationships of the mid-height sections of the right column will be studied with detail in the next chapter.

Table 17 –Curvature ductility values on different structural elements for all the analyses

Section	Model	1st	2nd	3rd	4th	5th	6th
Mid-height node of the right column	A1	7,86	8,52	6,80	8,00	7,78	8,37
	B1	8,58	7,94	7,26	8,11	7,97	
	C1	6,00	6,34	3,96	8,20	8,05	
	A2	6,01	6,67	9,08	7,10	6,89	7,93
	B2	6,94	6,53	5,97	7,14	7,07	
	C2	9,83	4,60	4,15	7,26	6,80	
Left node of the bottom beam	A1	5,35	5,69	6,25	5,88	5,49	7,64
	B1	3,03	6,03	6,70	8,97	10,12	
	C1	4,87	5,82	6,28	5,76	7,40	
	A2	5,30	5,73	6,19	5,69	5,18	7,14
	B2	10,23	10,22	10,74	14,02	10,67	
	C2	12,09	11,84	12,64	11,90	13,81	
Left node of the top beam	A1	8,85	8,80	9,11	5,38	4,90	7,66
	B1	7,93	7,77	8,43	9,89	8,88	
	C1	7,65	7,77	8,01	7,78	7,77	
	A2	6,75	6,89	7,33	4,00	4,14	5,00
	B2	12,90	12,05	12,44	12,98	9,29	
	C2	15,89	14,50	15,04	14,88	13,30	
Right node of the top beam	A1	16,00	15,85	15,98	13,72	9,13	19,83
	B1	15,85	16,23	16,51	21,20	16,86	
	C1	15,89	15,34	15,97	16,28	18,27	
	A2	16,16	16,28	16,34	13,95	8,79	19,75
	B2	8,58	10,96	11,09	13,67	13,96	
	C2	5,07	7,18	7,48	7,25	7,01	

One of the issues of the first model was related to the early plastification of the sections where the longitudinal reinforcement details changed (curtailment zone) at the bottom and top beams. Figure 31 illustrates two curvature diagrams of the bottom beam for the Discretisation C, where in one of the diagrams this particular situation occurs.

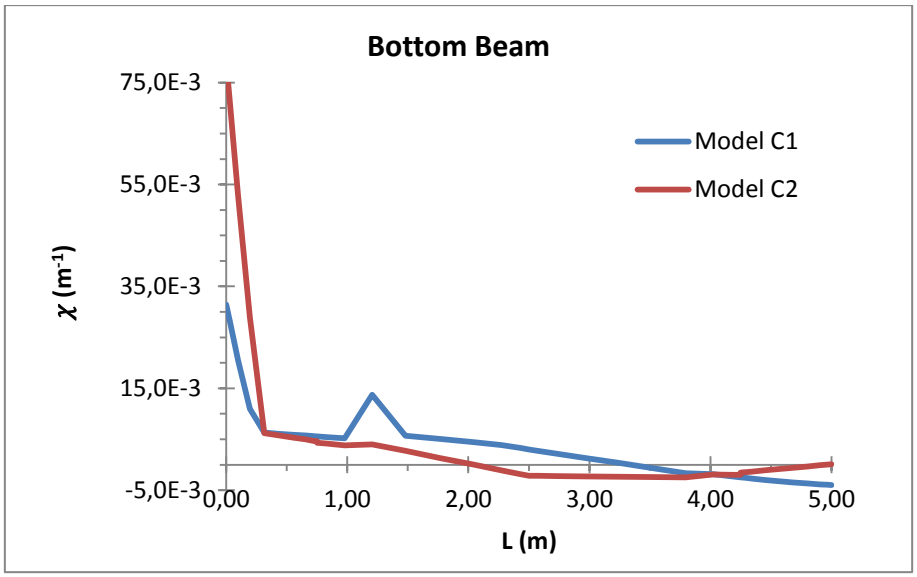

Figure 31 – Curvature diagram of the 1st Model - Discretisation C

If this early plastification, exactly at 1.21m, had not occurred in the Model C1 than the extremities of the beam would, most certainly, plastify more like Model C2. The early plastification is an indication that the curtailment zone of the longitudinal reinforcement is too close to the end support. Furthermore, there are some numerical issues with the bending moment diagrams. For no apparent reason, near the mid-height node of the right column the bending moment diagram near the end of the analysis has a discontinuity that ranges from 1kN.m to 15kN.m in all types of discretisation. Figure 32 shows the bending-moment diagram of the right column which exhibits a discontinuity near the mid-height node.

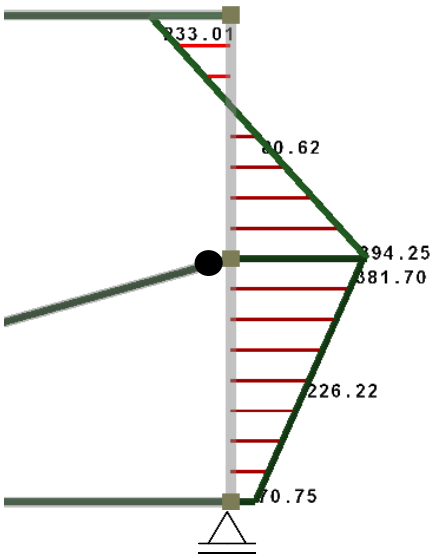

Figure 32 – Bending-moment diagram of the right column by the end of the analysis of 1st Model (A1)

Essentially because of the peaks experienced, the curtailment zone in the second model was changed to avoid plasticity in that region. In the new model, in general, the curvatures are the same as the last model, except for the beam curvatures near the end nodes which are remarkably higher because the reinforcement plastification no longer occurs in the curtailment zone.

With Discretisation C, however, the curvature diagram of the top beam has a small peak (see Figure 33) which coincides with the location of the node that separates two elements, even though the type of section considered before and after is exactly the same. The presence of this small peak at 4.25m may negatively influence the level of curvature achieved at 5.00m. One possible reason for this peak might be the fact that the structure is too discretised or simply has too many integration sections.

In the third model, the number of fibres used was changed to assess the influence in the obtained results. It was observed that the maximum applied displacements were slightly higher but so were the yield displacements. As a result, the displacement ductility values were very similar to the previous models (first and second models), and so were the curvatures ductility values. It was concluded that the increase in the number of fibres, from 150 to 250, did not influence greatly the obtained results. As a consequence, the remaining models used 150 fibres. Moreover, Discretisation C still has a problem with a discontinuity in the curvatures diagrams, only now in the bottom beam instead of the top beam, precisely near the node that separates both elements at 4.25m. The curtailment zone is at 4.00m, which probably means that the change in reinforcement is not influencing that peak.

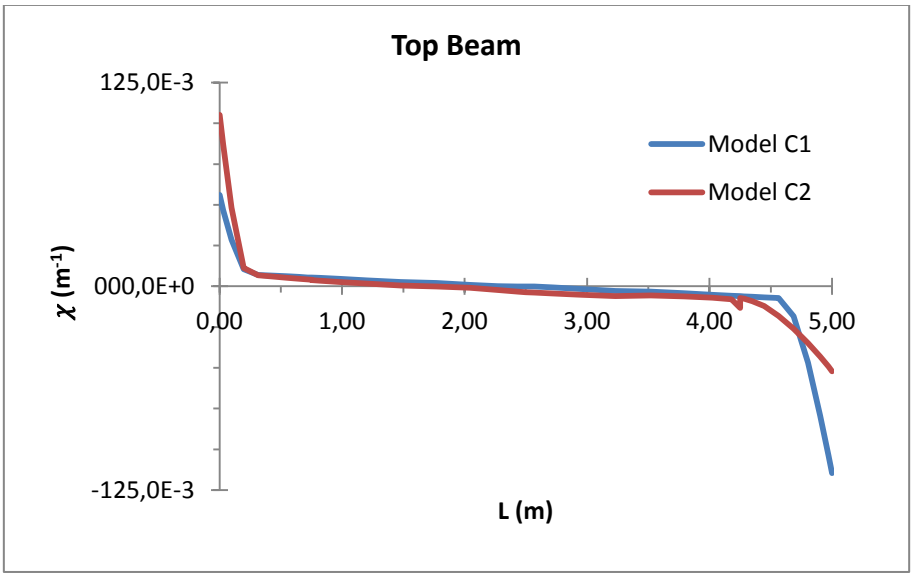

Figure 33 – Curvature diagram of the 2nd Model - Discretisation C

The fourth model still does not solve the previously identified problems (the peak in Discretisation C still exists) but the levels of displacement ductility are higher and the curvatures ductility are generally higher. The bending moment diagrams do not exhibit any discontinuities unlike the previous models.

In order to minimise the convergence problems even further in the inelastic force-base elements adopted, SeismoStruct User Manual (2016) advocates the use of three integration sections, especially in the cases where the elements are very refined and the reinforcement details change. This is how the fifth model was developed. The obtained results are particularly different since the levels of displacement ductility are significantly higher, especially for the Discretisation A and Discretisation B. The curvatures ductility levels, on the other hand, are quite similar to the ones from the fourth model. The top beam in Discretisation C still has that discontinuity that coincides with the discretisation node that separates elements within the beam. The bending moment diagrams do not have any

discontinuities. For Discretisation A and Discretisation B, the employment of three integration sections does not simulate the spread of inelasticity along the elements in an acceptable way because of the total number of controlling points, three or six, is simply insufficient as seen in Figure 34. Consequently, the results are not very reliable.

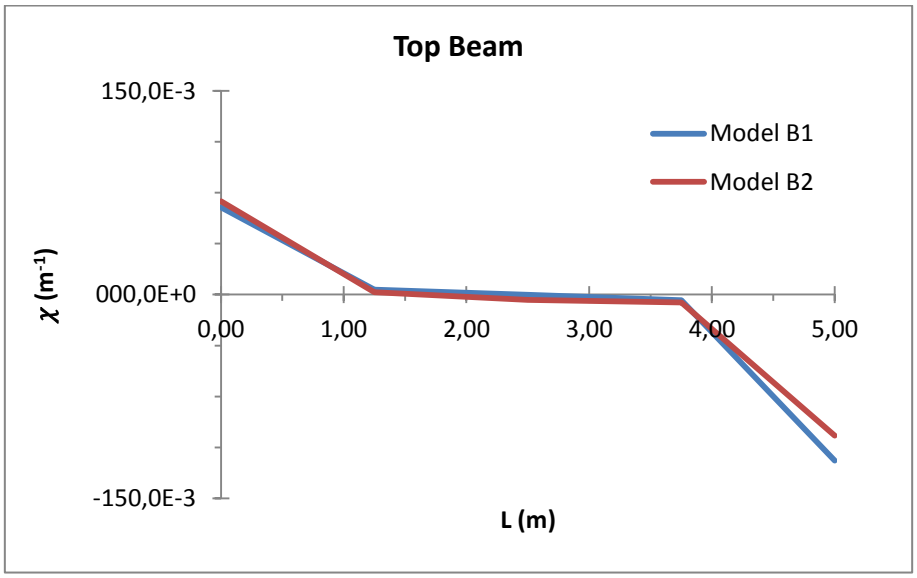

Figure 34 - Curvature diagram of the 5th Model - Discretisation B

The sixth model emerges to test if the increase in the number of integration sections in Discretisation A contributes to the obtainment of better results. The other types of refinement were not tested because the fourth model, with five integration sections, proved to achieve almost the same results as the second one, with ten integration sections, regarding the ductility in terms of curvatures. The displacements ductility values of the sixth model are smaller than the ones of the fourth and fifth models while the curvatures ductility values are higher when comparing within the same type of discretisation. However, the number of integration points to model the spread of plasticity near the end supports of the beams is still insufficient, that zone requires a tighter refinement.

Take everything into consideration, the model that was chosen to progress for the following analyses was the Discretisation C of the fifth one. Firstly, the type of discretisation seems to be more adequate, especially for the right column where the presence of the stairs restrains the horizontal displacements. Secondly, the need to have the elements discretised leads to the need to have a smaller number of integration sections in order to be able to continue the analyses up to higher levels of displacement without experiencing convergence difficulties. The only problem with this model lies in the discontinuity, which probably is a numerical issue, of the curvatures diagram of the beam when considering the self-weight loadings. Figure 35 illustrates the different curvature diagrams for the Discretisation C of the fifth model.

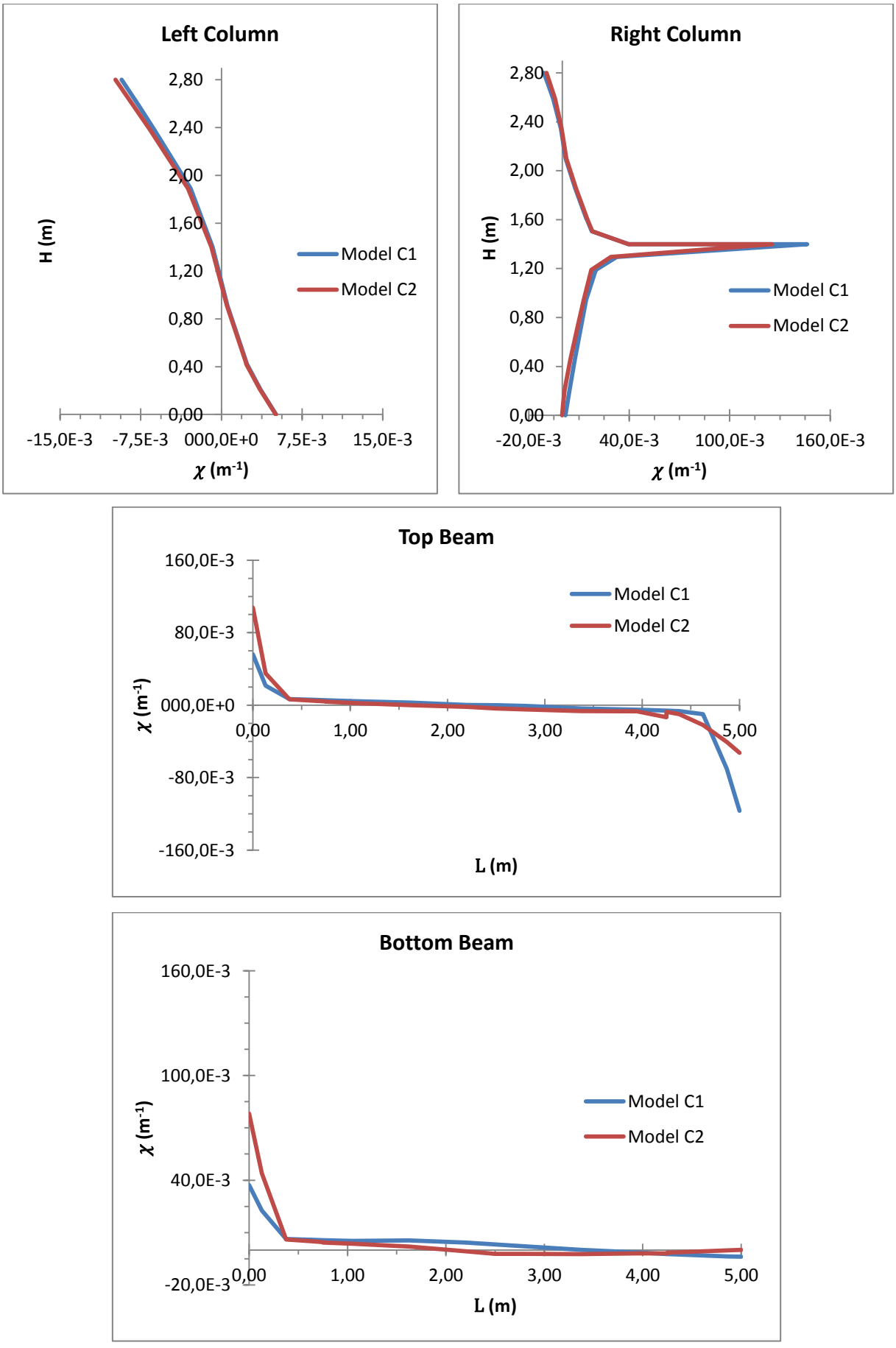

Figure 35 – Curvature diagrams of the 5th Model – Discretisation C

4. Structural Analyses

The objective of this chapter is to study the various effects produced by having a stairs landing at a mid-height level of a column.

Firstly, static analyses with non-variable loadings will be performed to evaluate the internal forces achieved both in a simple framed structure without stairs and in a structure with the stairs.

Afterwards, several static pushover analyses will be executed, while considering changes in terms of the reinforcement details and applied loadings, to study the overall performance of the structure considered in terms of displacements, curvatures and bending moments achieved.

4.1. Static Analyses

4.1.1. Modelling Description

A static analysis of two different elastic framed models with non-variable loadings was performed. The first model, which will be addressed as Model A, was a simple structure with two beams supported by two columns, as depicted in Figure 36. The second model, which will be Model B, was a structure with two beams, two columns and a stairs connecting the end left node of the bottom beam to the mid-height node of the right column, as illustrated in Figure 37. In all models the vertical displacements of the end nodes of the bottom beam and the horizontal displacement of the left node of the bottom beam are restrained.

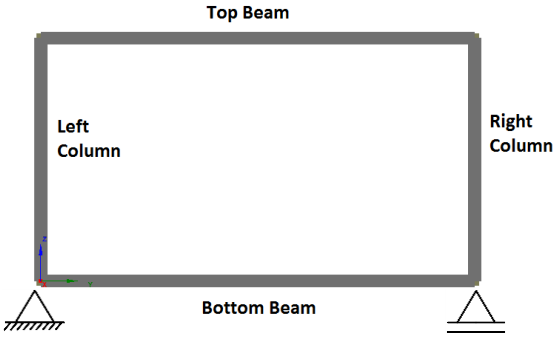

Figure 36 – Structural elements of Model A

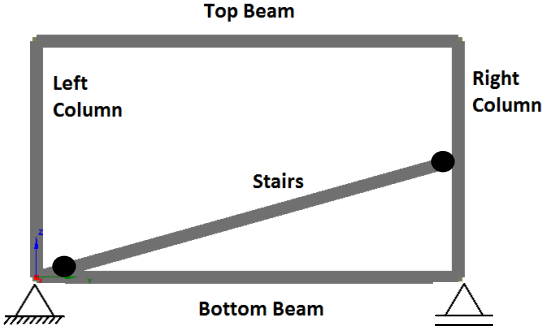

Figure 37 – Structural elements of Model B

Table 18 displays the various properties defined for the beams, columns and stairs. These were the only mechanical properties necessary to build the elastic models. The materials and sections were not needed in this type of analysis. The definition of materials and sections would only be necessary if the elements considered were inelastic.

Table 18 – Properties of the elastic frame elements

Elastic Frame Elements	Beams	Columns	Stairs
EA (kN)	4,93E+06	4,93E+06	5,90E+06
EI_1(kN.m^2)	18471	18471	5500
EI_2 (kN.m^2)	51309	51309	355000
PP (ton/m)	0,38	0,40	0,46

It has been stated by the Eurocode 8 – Part 1, 4.3.1 (7) and 9.4 (3), that in order to take into account the effects of concrete cracking, it is possible to reduce by half the flexural stiffness considered in the non-cracked gross sections. As a result, all the different flexural stiffnesses considered in these elastic models were reduced by half. On the contrary, the axial stiffness considered corresponds to the gross sections.

Moreover, the self-weight of these elements was also considered. Besides these loads, a 900kN compressive force was applied above both columns, a 25kN/m distributed load on the beams and a 0,01m horizontal displacement from right to left on the top node of the right column, which compresses the stairs in Model B. All these loadings are permanently applied. The displacement value considered ensures a response within the elastic range before the steel yielding. According to SeismoStruct User Manual (2016), if the displacement value was such that forced the structure to respond in a nonlinear manner, then the program during the analysis would have to perform additional iterations until convergence was reached.

Similarly to what was done in the Model Calibration phase, the moments were released at the end nodes of the stairs in Model B. Also, the dimensions of the beams, columns and stairs were the same as those considered in the previous chapter.

In what concerns the subdivision of the elements, several structural analyses were performed to assess whether the elements' discretisation influenced the obtained results. It was observed that the type of discretisation used had little impact on the results regarding the internal forces diagrams obtained. In spite of this fact, each column member was divided into 100 elements to enable the drawing of the internal forces diagrams in Excel as displayed in the next subchapter.

4.1.2. Discussion of Results

Figure 38 shows the bending moments, shear and axial forces of the left and right columns for both Model A and Model B.

Regarding the left column, there is no significant difference in terms of moments and forces in Models A and B. This result was expected considering the fact that in both models there is no obstacle preventing the deformation due to the applied displacement. In other words, the displacements are absorbed along the entire height of the column.

In relation to the right column, the differences between Model A and Model B are quite noticeable for the same level of displacement. The internal forces of Model A follow the same trend of the internal forces of the left column in both models.

In Model B, the presence of the stairs at the mid-height level of the right column significantly alters the level of internal forces obtained along the column. The bending moment and shear forces on the right column are significantly higher. The level of axial and shear forces achieved at the top and bottom halves of the column are different, which was expected considering that the stairs transmit an inclined force that has to be absorbed by the right column.

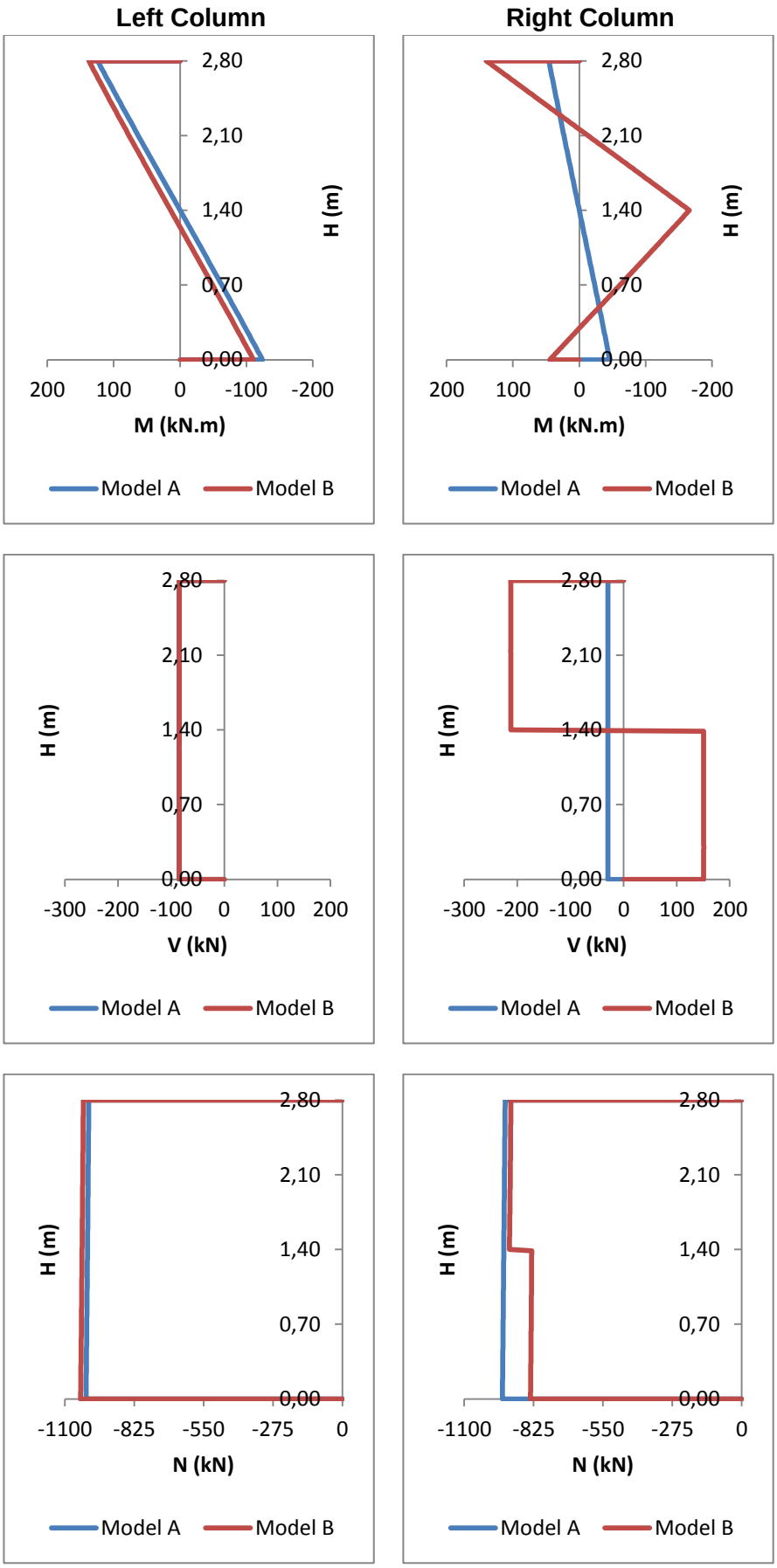

Figure 38 – Internal forces diagrams

The results obtained derive from a well-known occurrence, commonly referred as being the short column effect. As pointed out by Lopes (2008), a landing of stairs, at a mid-height level of a column, restrains the horizontal displacements at that same level. The bottom half of the column is almost unable to deform, which forces that only the top half solely absorb the applied horizontal displacement. In this case, since the top half of the right column is obviously shorter than the left column, the deformations and internal forces imposed on the right side are higher. Special care should be taken with the levels of shear forces obtained because of the looming possibility of shear failure occurring. The shear influence on the structure will be discussed in the next subchapter.

Taking into account the level of internal forces of these elastic analyses, with the imposed horizontal displacement, according to current design procedures, there is a tendency to increase in Model B the amount of flexural reinforcement of the right column to counteract the high bending moments experienced due to the presence of the stairs. Nevertheless, the non-linear effects that the stairs produce in the structure are the ones that should be studied with attention. In the next subchapter, non-linear analyses will be performed on the structure with the stairs while testing whether it is preferable to have an increase in the flexural reinforcement (like the elastic analysis suggests) or if, on the other hand, is it preferable to have an increase in the amount of transversal reinforcement, in the right column, to improve the performance of the structure.

4.2. Static Pushover Analyses

4.2.1. Modelling Description

As discussed in the previous subchapter, it is now important to study the non-linear effects the stairs produce in the structure. Three different models were created. These models will be addressed onwards as Model C, Model D and Model E. The difference between each of these non-linear models lies in the reinforcement used in the right column. When comparing to Model C, Model D has an increase in the amount of longitudinal reinforcement used while Model E has an increase in the amount of transverse reinforcement around the mid-height level of the right column, where a plastic hinge is expected to form.

The reinforcement of the remaining inelastic elements, such as the left column as well as the top and bottom beams, remained unchanged. The chosen model in the calibration phase (5^{th} Model – Discretisation C) served as the starting point for the creation of the non-linear models. In this sense, the elastic properties of the stairs (Table 12) and the reinforcement of the beams (Figure 28 and Figure 29) are the ones that were considered in the 5^{th} Model. Table 19 shows the beams' reinforcement along their length as well as the elements' labels used. The beams were discretised into four elements with three integration sections each. The different length levels correspond to the different integration sections.

Table 19 – Bottom and Top Beams' Reinforcement along the different integration sections

Element Label		L (m)	Integration Section		Reinforcement
BB1	BT1	0,00	BB1(a)	BT1(a)	4ϕ20+2ϕ16; ϕ6//0,125
		0,38	BB1(b)	BT1(b)	
		0,75	BB1(c)	BT1(c)	
BB2	BT2	0,75	BB2(a)	BT2(a)	
		1,63	BB2(b)	BT2(b)	4ϕ20; ϕ6//0,125
		2,50	BB2(c)	BT2(c)	
BB3	BT3	2,50	BB3(a)	BT3(a)	
		3,38	BB3(b)	BT3(b)	
		4,25	BB3(c)	BT3(c)	
BB4	BT4	4,25	BB4(a)	BT4(a)	4ϕ20+2ϕ16; ϕ6//0,125
		4,63	BB4(b)	BT4(b)	
		5,00	BB4(c)	BT4(c)	

It should be noted that the initial longitudinal reinforcement of the columns in Model C was slightly reduced in order to allow an increase in the following Model D. The longitudinal reinforcement considered in the third chapter was very close to the maximum allowed in the Eurocode 2 Part 1-1, which is 60cm^2, taking into account the section dimensions.

Table 20 shows the reinforcement adopted in the left column along the different integration sections for all the non-linear analysis. The left column was discretised into four elements with three integration sections each and the different height levels correspond to the different integration sections of the elements.

Table 21 shows the reinforcement adopted in the right column along the different integration sections and across the different models created. It is worth noticing that the right column was discretised into eight elements with three integration sections each.

Table 20 – Left Column Reinforcement along the different integration sections

Element Label	H (m)	Integration Section	Reinforcement
CL1	0,00	CL1(a)	10ϕ25; ϕ8//0,10
	0,21	CL1(b)	
	0,42	CL1(c)	
CL2	0,42	CL2(a)	
	0,91	CL2(b)	10ϕ25; ϕ8//0,20
	1,40	CL2(c)	
CL3	1,40	CL3(a)	
	1,89	CL3(b)	
	2,38	CL3(c)	10ϕ25; ϕ8//0,10
CL4	2,38	CL4(a)	
	2,59	CL4(b)	
	2,80	CL4(c)	

Table 21 – Right Column Reinforcement across the different models studied

Element Label	H (m)	Integration Section	Model C	Model D	Model E
CR1	0,00	CR1(a)	10ϕ25; ϕ8//0,10	12ϕ25; ϕ8//0,10	10ϕ25; ϕ8//0,10
	0,11	CR1(b)			
	0,21	CR1(c)			
CR2	0,21	CR2(a)			
	0,46	CR2(b)	10ϕ25; ϕ8//0,20	12ϕ25; ϕ8//0,20	10ϕ25; ϕ8//0,20
	0,70	CR2(c)			
CR3	0,70	CR3(a)			
	0,95	CR3(b)			
	1,19	CR3(c)			10ϕ25; ϕ8//0,10
CR4	1,19	CR4(a)			
	1,30	CR4(b)			
	1,40	CR4(c)			
CR5	1,40	CR5(a)			
	1,51	CR5(b)			
	1,61	CR5(c)			
CR6	1,61	CR6(a)			
	1,86	CR6(b)			10ϕ25; ϕ8//0,20
	2,10	CR6(c)			
CR7	2,10	CR7(a)			
	2,35	CR7(b)			
	2,59	CR7(c)	10ϕ25; ϕ8//0,10	12ϕ25; ϕ8//0,10	10ϕ25; ϕ8//0,10
CR8	2,59	CR8(a)			
	2,70	CR8(b)			
	2,80	CR8(c)			

Figure 39 pinpoints the location of the different element labels used on the previous tables to identify the discretised elements of the beams and columns of the structure. Figure 40 magnifies the mid-height zone of the right column while identifying the localisation o the integration sections.

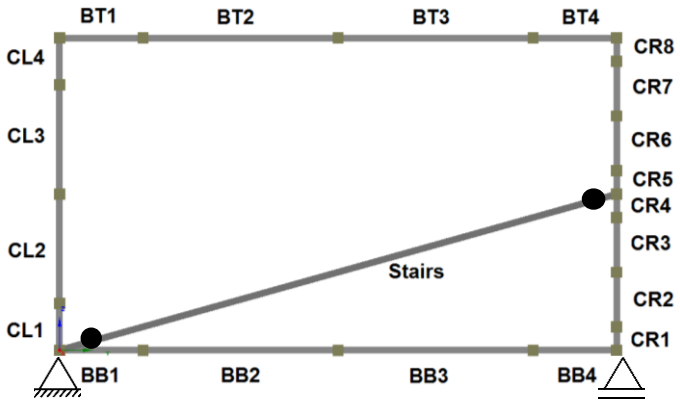

Figure 39 – Identification of the elements labels on the structure

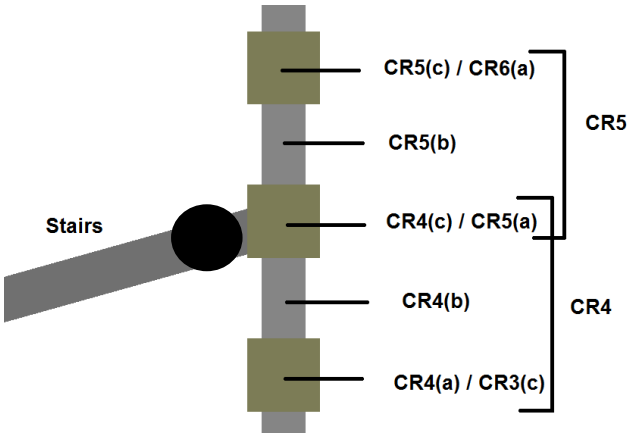

Figure 40 – Magnification of the mid-height zone of the right column

Figure 41 and Figure 42 shows the reinforcement detailing used in the columns of the non-linear models. The flexural reinforcement used was either 10ϕ25 or 12ϕ25. The reinforcement distribution of the former was done near the extremities parallel to the flexural axis. It has been shown by Brito (2011) and Camacho (2012) that this type of distribution maximises the deformation capacity of the cross-section. If, for instance, some of the longitudinal bars were to be distributed closer to the flexural axis, then when comparing to the situation of having the reinforcement near the extremities parallel to the flexural axis and in the advent of having the section subjected to a certain bending moment, the longitudinal bars under compression would contribute less to the absorption of the compressive forces. As a consequence, the concrete would have to contribute more and the neutral axis depth would have to be higher, which would diminish the overall ductility availability.

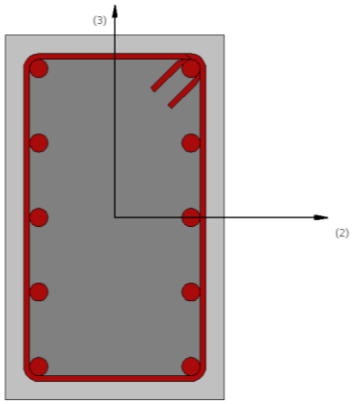

Figure 41 - Reinforcement detailing for 10ϕ25

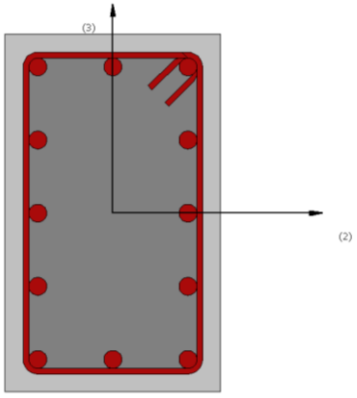

Figure 42 – Reinforcement detailing for 12ϕ25

In general, the same loadings applied in the model calibration phase were applied in these non-linear analyses. The self-weight of all the elements as well as the beams' distributed loadings due to the slabs' weight were considered. The compressive forces applied on top of the columns were also considered, only with the difference that three different compressive loadings were applied: 450kN, 900kN and 1500kN, which correspond to the following normalised axial forces values of 15%, 30% and 50%. These different values enabled the study of the influence that different levels of column compression exert in the curvatures and displacements achieved in the various non-linear analyses. The highest level of compression simulates a ground floor whereas the lowest compression level is

intended to represent a higher floor of a ten storey building. In addition to these loadings, two types of displacement were applied on top of the right column. One from right to left, causing the stairs to be under compression (Type I) and another from left to right, causing the stairs to be under tension (Type II). Overall, with the different reinforcements and applied loadings considered, there are in total 18 different structural models.

4.2.2. Assumptions regarding the Shear Forces

It has been shown in the elastic analyses that the right column, in the presence of the stairs, exhibits a very high level of shear force due to the short-column effect. Since the bottom half of the column deforms significantly less than the top half, it can be said that the deformation of the right column is somewhat restrained. Unlike the right column, the left column can deform freely along its entire height and the levels of shear forces are significantly lower.

It is said by Brito (2011) and Camacho (2012) that concrete elements with a compact cross-section, a quantity of transverse reinforcement not excessively small and a small or moderate level of axial force, are not highly susceptible to experiencing shear failure for shear ratio values higher than three. Below this value, shear effects may reduce the available ductility and energy dissipation capacity.

Furthermore, it is also said that straight elements subjected to linear bending moment diagrams with a sign change are not likely to have a relevant shear effect provided that the ratio between the element free height and the section dimension perpendicular to the flexural axis is higher than six ($L/h > 6$). This ratio is also known as being the shear span ratio. In the left column, the shear span ratio is relatively high, around 9.33. This means that the ductility of this member is not expected to be greatly influenced by shear. In the right column, this quotient diminishes to a value around 4.67 because the free height is smaller. This indicates that shear strength corresponding to the flexural strength might negatively influence the ductility and reduce the plastic hinges lengths as compared.

If shear failure occurs before the plastic hinges can achieve their ultimate curvatures possible, then the section failure occurs to a smaller level of curvature. In other words, the deformation capacity of the plastic hinges might be reduced. This emphasises the importance of having a structure that follows the capacity design principles developed by Park and Paulay (1976), cited in Priestley (2000, p.1), where brittle failure type of mechanisms, such as shear failure or even axial failure, are to be avoided.

It was assumed, throughout the analyses, that the shear strength corresponding to the transverse reinforcement of the right column was high enough to support the shear corresponding to the flexural strength. Even if the assumption made was not true, the analyses would continue without any restrictions since the user would have to specify their end due to shear failure.

To take into account the shear effect, the shear capacity of the sections would have to be manually calculated or automatically calculated by SeismoStruct (2016). In the Performance Criteria tab, the program offers the possibility of choosing the equation A.12 from Eurocode 8 Part 3, A.3.3.1 for the calculation of the shear capacity. Once the shear capacity had been obtained, then it would have to be compared with the shear acting on the member. If the shear acting on the member were to be greater

than its shear capacity, then it would be reasonable to assume that shear failure had occurred. In terms of modelling, depending on what the user would choose, the analysis would either stop or continue with some strength degradations or without them.

Quantitatively, the manual confirmation of this calculation process would be fairly complex, which is why this assumption concerning the shear influence was made. SeismoStruct User Manual (2016) stated that the shear strength depends on many factors, such as, the amount of transverse reinforcement, the concrete contribution, the level of axial force and the displacement ductility. In design, shear failure must be avoided at all costs, for the reasons stated above, by adopting an adequate amount of transverse reinforcement in the plastic hinge regions.

In numerical terms, the results interpretation or the concepts interrelation is not jeopardised because the analyses continue unaffected. Indeed in a real situation, this assumption could not be made in such a lightly manner where the structure would most certainly be affected. This shear failure type of mechanism must be avoided at all costs, for the reasons stated above, by adopting an adequate amount of transverse reinforcement in the plastic hinge regions.

4.2.3. Discussion of Results

First of all, it is important to discuss some global response parameters such as the maximum structural displacements (δ_u) achieved on the 18 different models. Table 22 summarises these maximum applied displacements at the top of the right column.

Table 22 – Maximum displacements at the top of the right column

N (kN)	δ_u (cm)					
	Analyses of Type I			Analyses of Type II		
	Model C	Model D	Model E	Model C	Model D	Model E
450	-6,77	-4,99	-6,77	3,60	3,10	4,07
900	-4,65	-3,86	-6,46	2,78	2,70	3,31
1500	-3,29	-3,37	-3,70	2,46	2,49	2,75

It is possible to observe that the maximum displacements decrease with the increase of the axial forces applied on top of the columns. Within the same levels of axial forces, the Models E analyses present higher displacement values in comparison with Models C and Models D analyses. The only exception is for the analyses of Type I, where an axial force of 450kN is being applied, in which the displacement achieved of -6,77cm in Model C is exactly the same as the displacement achieved in Model E. The explanation to this result will be given later while evaluating the reasons that led to the end of both analyses.

Moreover, the level of displacements achieved on the analyses of Type I are higher than those achieved on the analyses of Type II. As previously mentioned, the only difference between these two types of analyses is the direction in which the displacement is being applied. In the Type I analyses, the displacement compresses the stairs while in the Type II analyses, the displacement places the stairs under tension. The discussion regarding the variation of the levels of displacement achieved on

the different models will be addressed later while analysing the deformed shape of the structure and the neutral axis depth at failure of some critical integration sections. At present, it is relevant to establish a connection between the maximum applied displacements and the reasons that contributed to the end of the analyses.

Considering that the structure followed the capacity design principles where the deformation is assumed to be mainly by flexure, the structure collapse is expected to occur either by the concrete failure under compression or the reinforcement failure under tensile strains. These two possibilities along with the convergence problems that might arise are the reasons that might lead to the end of the analyses. The data in Table 23 and Table 24 summarises those reasons for all the analyses performed while indicating the sections where failure occurred or in the case where convergence problems emerged, indicating the section where failure would most likely occur, had the analysis continued.

Table 23 – Reasons that led to the end of the analyses of Type I

<table>
<tr><th rowspan="2">N (kN)</th><th colspan="3">Analyses of Type I</th></tr>
<tr><th>Model C</th><th>Model D</th><th>Model E</th></tr>
<tr><td>450</td><td>Convergence Problems BT1(a)</td><td>Concrete Failure CR4(c)</td><td rowspan="2">Convergence Problems BT1(a)</td></tr>
<tr><td>900</td><td colspan="2">Concrete Failure CR4(c)</td></tr>
<tr><td>1500</td><td colspan="3">Concrete Failure CR4(c)</td></tr>
</table>

Table 24 – Reasons that led to the end of the analyses of Type II

<table>
<tr><th rowspan="2">N (kN)</th><th colspan="3">Analyses of Type II</th></tr>
<tr><th>Model C</th><th>Model D</th><th>Model E</th></tr>
<tr><td>450</td><td colspan="2" rowspan="3">Concrete Failure CR5(a)</td><td>Reinforcement Failure BT4(c)</td></tr>
<tr><td>900</td><td rowspan="2">Concrete Failure CR5(a)</td></tr>
<tr><td>1500</td></tr>
</table>

The integration sections that condition the end of the analyses are either on the right column or on the top beam. In the right column, the integration section that conditions the end of the analyses is the one at mid-height near the end node of the stairs due to concrete failure. In the top beam, the integration sections that usually condition the end of the analyses are the ones near the extremities due to the excessive deformation of the tensile reinforcement.

It is also interesting to notice that when concrete failure occurs, it occurs at the CR4(c) section for the analyses of Type I and at the CR5(a) section for the analyses of Type II. When reinforcement failure occurs or is on the verge of occurring due to convergence problems, it happens at the BT1(a) section

for the analyses of Type I and at the BT4(c) section for the analyses of Type II. A reason that might explain the occurrence of reinforcement failure is the fact that in those analyses the level of axial forces being applied on the columns is relatively low, 450kN as opposed to 900kN and 1500kN. Therefore, the mid-height sections of the right columns are able to resist longer to the imposed displacement. Furthermore, in the Models E analyses, the confinement level at the mid-height section is greater than the confinement level of Models C and Models D, which positively delays the occurrence of concrete failure at that section.

It was previously stated that for the analyses of Type I where an axial force of 450kN is being applied, the displacement values achieved for Model C and Model E were exactly the same. Table 23 shows that for both models, convergence problems emerged and BT1(a) section was on the verge of experiencing reinforcement failure. This explains why the displacement values achieved were the same, considering that near failure the reinforcing steel strains of the BT1(a) section in both models were also the same and close to their ultimate value. If, for instance, the analyses had terminated due to the concrete failure of the mid-height section of the right column, then the displacement values achieved would most certainly be different, considering that in those sections the confinement level is different because the transverse reinforcement considered is also different.

Other relevant results to be discussed are the variation of the bending-moment diagrams. These diagrams provide information on how the structure deforms by flexure. In this sense, Figure 43 and Figure 44 show generic bending-moment diagrams at failure regarding the analyses of Type I and Type II while Table 25 and Table 26 show the respective values of some notable points in the structure. It should be noted that the representation of the bending-moment diagrams is done in this manner because these diagrams follow the same configuration in the different models within the same type of analyses.

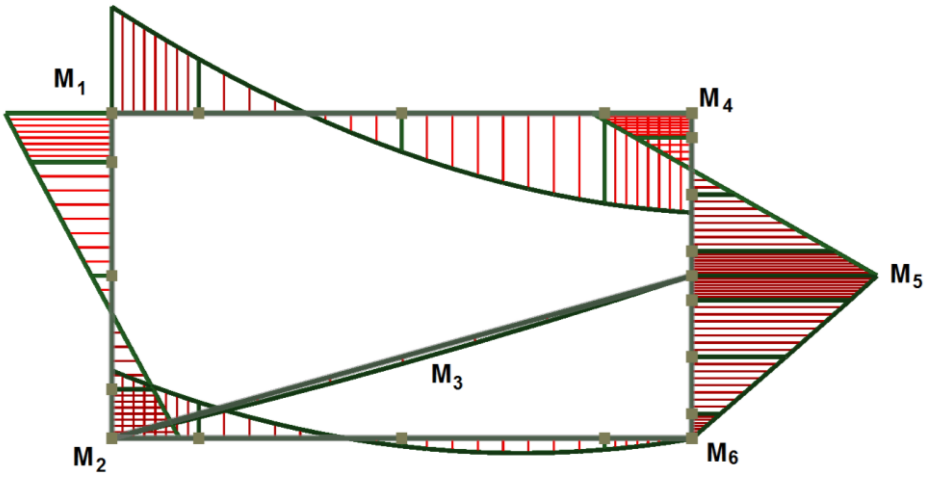

Figure 43 – Bending moment diagram shape at failure for the analyses of Type I

The adopted notation was "M_1" for the bending-moment at the end node of the top of the left column and the left side of the top beam, "M_2" for the end node coinciding with the left column and the bottom beam, "M_3" for the stairs mid-span bending-moment, "M_4" for the end node coinciding with the top

beam and the right column, "M_5" for the bending-moment at mid-height of the right column and "M_6" for the bending-moment at the end node coinciding with the bottom beam and the right column.

Table 25 – Bending moment values for the analyses of Type I

Analyses of Type I		N=450kN	N=900kN	N=1500kN
Model C	M_1(kN.m)	256,84	238,09	226,17
	M_2(kN.m)	170,84	157,35	142,34
	M_3(kN.m)	14,60	14,60	14,60
	M_4(kN.m)	230,87	220,32	212,07
	M_5(kN.m)	340,30	372,10	386,83
	M_6(kN.m)	14,22	5,91	-1,60
Model D	M_1(kN.m)	240,48	230,98	226,70
	M_2(kN.m)	156,69	148,26	140,63
	M_3(kN.m)	14,60	14,60	14,60
	M_4(kN.m)	223,43	216,71	212,60
	M_5(kN.m)	375,45	379,58	398,06
	M_6(kN.m)	2,45	-1,54	-2,57
Model E	M_1(kN.m)	256,83	253,75	229,70
	M_2(kN.m)	170,81	163,96	145,79
	M_3(kN.m)	14,60	14,60	14,60
	M_4(kN.m)	230,87	226,83	214,00
	M_5(kN.m)	340,46	381,42	399,86
	M_6(kN.m)	14,19	-16,68	1,66

The bending-moments "M_1", "M_2" and "M_4" are in accordance with the expected structural deformed shape considering that in the analyses of Type I, the applied displacement is from right to left. The bending-moment "M_6" tends to be on the outside of the structure, in other words, it tends to be positive if the orientation of the bottom beam bar is considered from left to right or if the orientation of the right column is considered to bottom to top. In the table above, some "M_6" values are negative because that bending-moment is on the inside of the structure and contrary to the representation in Figure 43. The "M_5" bending-moment at failure is the one that suffers most variations from model to model. As the axial forces on the columns increase, this bending-moment also increases. As expected, the bending-moment "M_3" is the same in all models, considering the fact that the end-nodes of the element that represents the stairs have their bending-moments released. The mid-span moment value is due to the consideration of the stairs' self-weight.

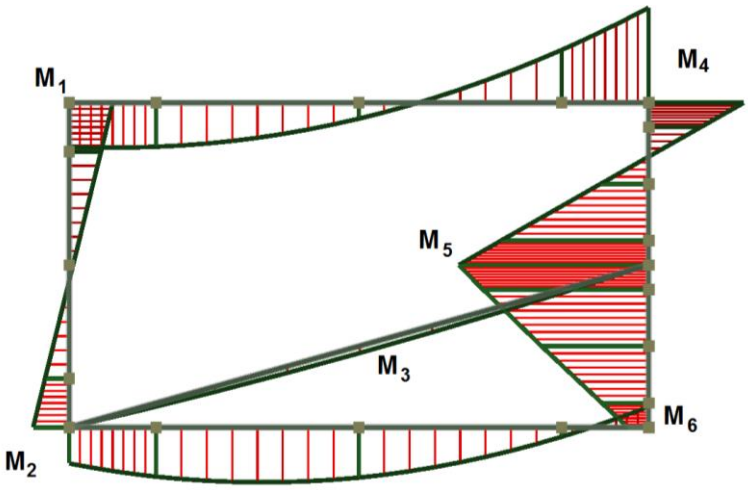

Figure 44 - Bending moment diagram shape at failure for the analyses of Type II

Table 26 - Bending moment values for the analyses of Type II

Analyses of Type II		N=450kN	N=900kN	N=1500kN
Model C	M_1(kN.m)	114,46	93,51	83,76
	M_2(kN.m)	94,72	73,87	65,94
	M_3(kN.m)	14,60	14,60	14,60
	M_4(kN.m)	211,32	204,54	201,80
	M_5(kN.m)	365,01	382,15	395,16
	M_6(kN.m)	44,19	41,23	42,33
Model D	M_1(kN.m)	98,42	90,59	84,81
	M_2(kN.m)	78,89	71,01	67,07
	M_3(kN.m)	14,60	14,60	14,60
	M_4(kN.m)	207,62	203,93	202,25
	M_5(kN.m)	384,97	396,03	402,81
	M_6(kN.m)	32,32	35,01	40,04
Model E	M_1(kN.m)	128,84	111,05	94,03
	M_2(kN.m)	109,29	93,15	77,69
	M_3(kN.m)	14,60	14,60	14,60
	M_4(kN.m)	213,14	210,46	205,08
	M_5(kN.m)	371,77	394,70	409,58
	M_6(kN.m)	47,03	46,48	44,58

In the analyses of Type II, similarly to the analyses of Type I, the bending-moments "M_1", "M_2" and "M_4" are in accordance with the expected structural deformed shape considering that the applied displacement is from left to right. The bending-moment "M_6" is always on the inside of the structure, in other words, it is negative if the orientation of the bottom beam bar is considered from left to right or if the orientation of the right column is considered to bottom to top. The "M_5" bending-moment at failure is the one that suffers most variations from model to model. As the axial forces on the columns

increase, this bending-moment also increases. The bending-moment "M_3" is exactly the same as the one in the analyses of Type I.

At last, the variation of the right column curvatures near structural collapse are represented in Figure 45 and Figure 46 for the analyses of Type I and Type II. Table 27 and Table 28 indicate the ultimate curvatures (χ_u) of the CR4(c) and CR5(a) sections of the analyses of Type I and II, respectively.

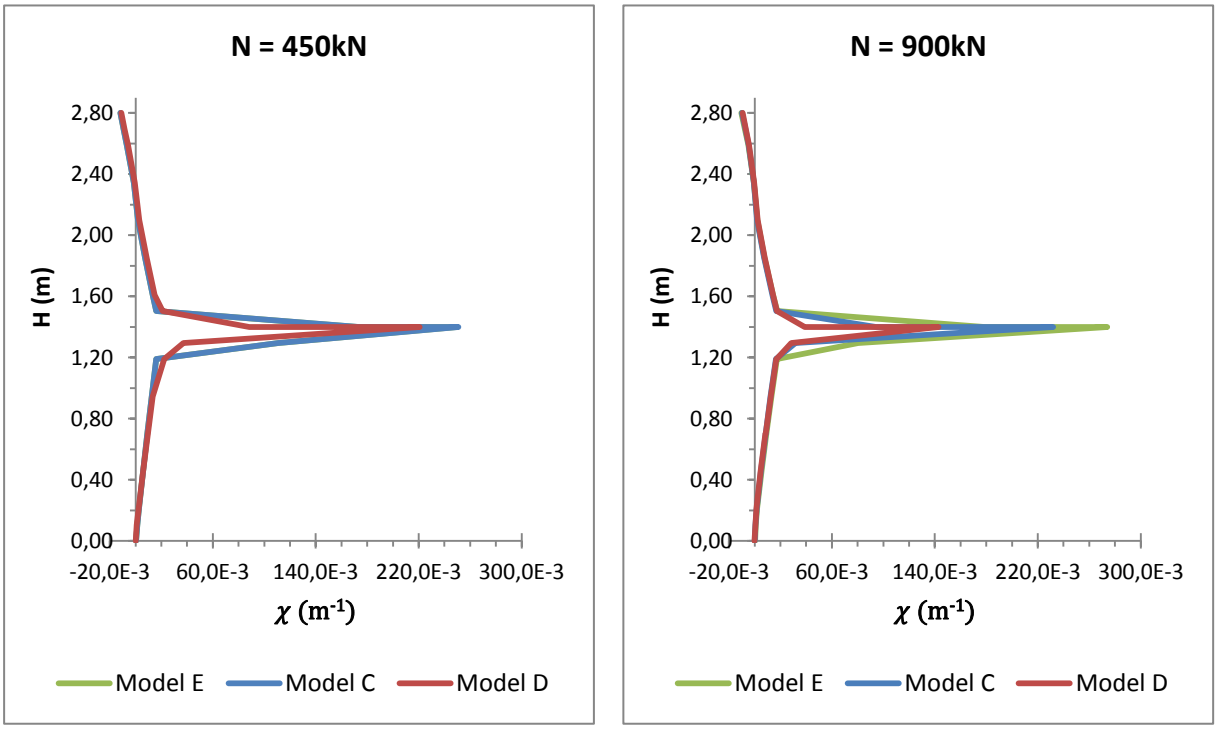

Note: Graphically, Model C coincides with Model E

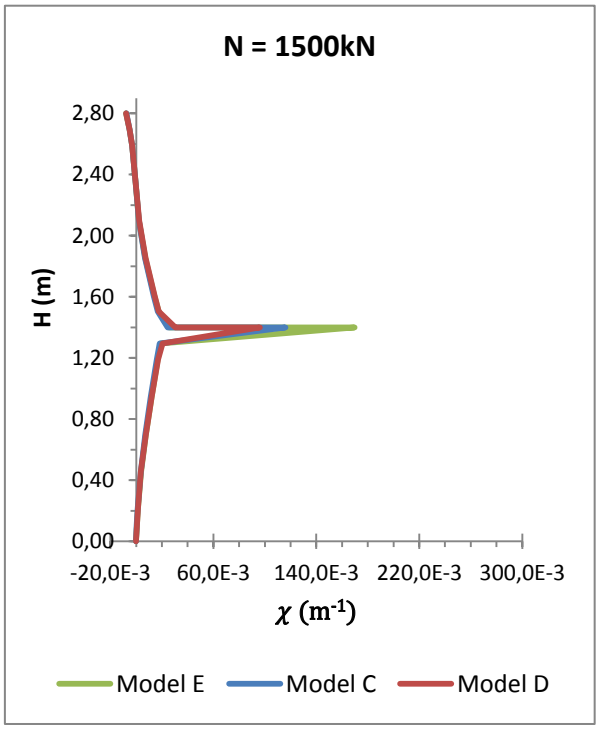

Figure 45 – Right column curvatures diagrams near structural collapse for the analyses of Type I

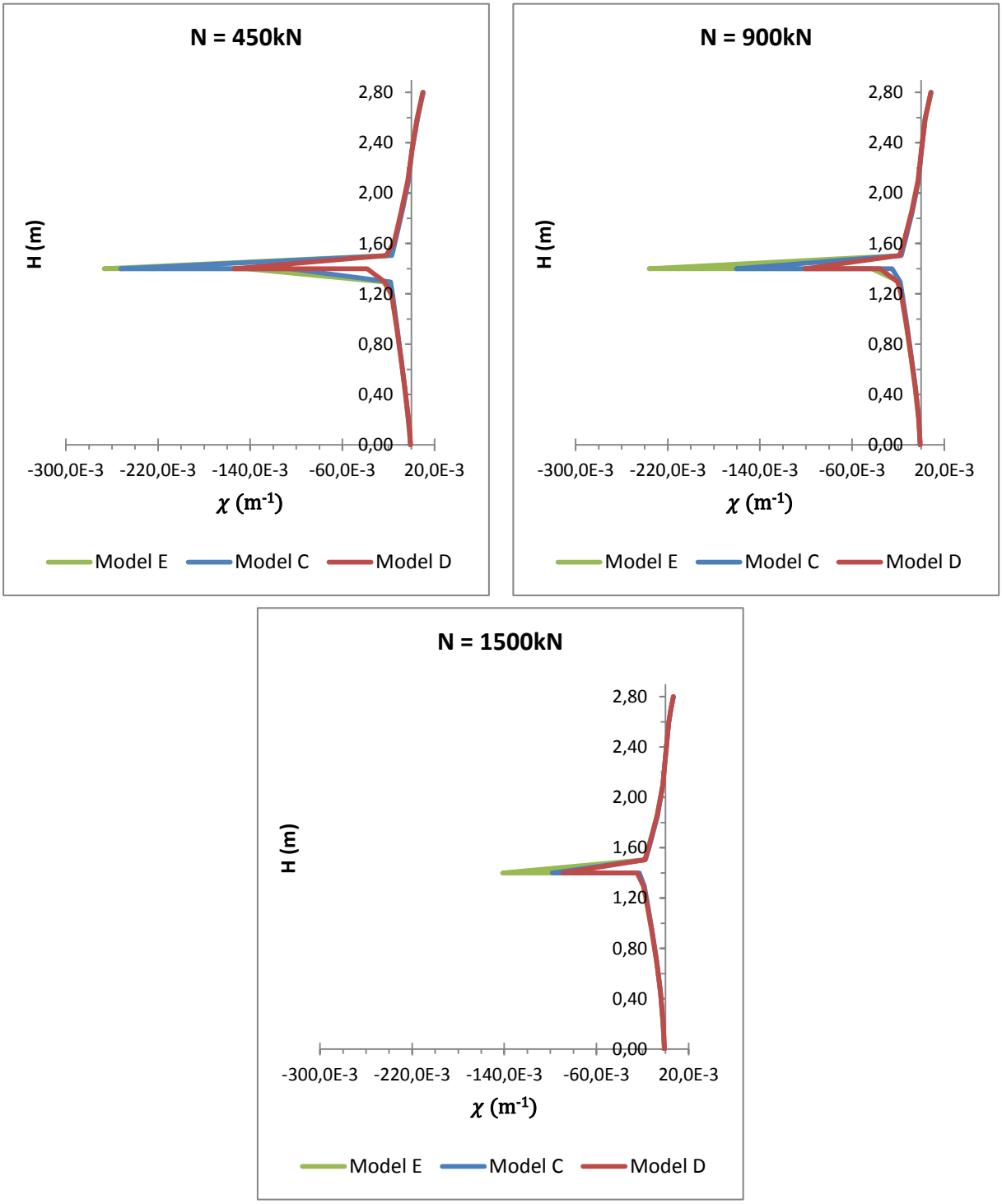

Figure 46 – Right column curvatures diagrams near structural collapse for the analyses of Type II

Table 27 – Ultimate curvatures at CR4(c) section of the right column of the analyses of Type I

N (kN)	χ_u (‰/m)		
	Model C	**Model D**	**Model E**
450	250,71	220,81	249,76
900	231,96	142,97	273,96
1500	116,04	96,02	169,79

Table 28 – Ultimate curvatures at CR5(a) section of the right column for the analyses of Type II

N (kN)	χ_u (‰/m)		
	Model C	**Model D**	**Model E**
450	-252,46	-154,14	-266,85
900	-160,49	-101,05	-236,00
1500	-98,41	-89,14	-141,47

It is possible to notice the negative effects of the compressive force on the columns in all of the analyses. As the compressive force increases, the ultimate curvature decreases, similarly to the displacements trending. It can also be observed that the variations in terms of the flexural and transverse reinforcement have a major influence in the values of the ultimate curvatures. The increase in the flexural reinforcement, from Model C to Model D, considerably decreases the ultimate curvatures achieved. Conversely, the increase in the transverse reinforcement, from Model C to Model E, increases the ultimate curvatures reached because of the higher level of confinement.

As the ultimate curvatures were presented, it is of interest to study the strain values and the neutral axis depths of the integration sections that suffered failure due to the concrete or due to the reinforcement. It is important to have the ultimate strains of the materials in question indicated to interpret the following results. The ultimate reinforcement strain, which is 0.075, was already presented in Table 11. The ultimate concrete strains, for every type of section considered, are presented in the Appendix A. As seen previously, in the majority of the studied cases, the cross-section that most led to end of the analyses was the mid-height section of the right column due to the excessive concrete deformation. This situation was compatible with the results of the elastic models, where the right column was subjected to higher levels of bending moments and shear forces due to the presence of the stairs. Table 29 indicates the reinforcement used in that section as well as the confinement factors and the ultimate concrete strains. These strains are dependent on the confinement factor considered, which, in turn, are dependent on the reinforcement used.

Table 29 – Reinforcement, confinement factors and ultimate concrete strains for the mid-height section

Model	**C**	**D**	**E**
Reinforcement	10ϕ25; ϕ8//0,20	12ϕ25; ϕ8//0,20	10ϕ25; ϕ8//0,10
f'_{cc}/f'_{co}	1,056	1,061	1,165
ε_{cu}(‰)	8,022	8,003	11,291

By observing the table above, it is possible to notice that from Model C to Model D the ultimate concrete compressive strain (ε_{cu}) decreases despite the slight increase of the confinement factor (f'_{cc}/f'_{co}). This situation makes sense, considering the fact that the transverse reinforcement is the same in both models. Therefore, the total transversal volumetric reinforcement ratio (ρ_s) is also the same. Looking at the equation (17) to obtain the ultimate concrete compressive strain in chapter 2, if the total transversal reinforcement volumetric ratio is the same in both models, then the bigger the confinement factor is, the bigger is the compressive strength of the confined concrete (f'_{cc}) and the smaller is the ultimate concrete compressive strain (ε_{cu}). The reason for the increase in the confinement factor from Model C to Model D is mainly because of the reduction of the clear distance between longitudinal bars. This situation positively contributes to the confinement effect yet negatively contributes to the ultimate concrete strains because the stirrups diameter and spacing is exactly the same.

Comparing Model C to Model E, the decrease in terms of spacing of the transverse reinforcement not only increases the confinement factor but it also increases the ultimate concrete compressive strain. Unlike the previous situation, the decrease of the stirrups spacing, from Model C to Model E, significantly increases the total transversal volumetric reinforcement ratio. As a result, in Model E the compressive strength and strain of the confined concrete are higher because of the higher value of the confinement factor.

Table 30 and Table 31 show the concrete and reinforcement strains as well as the neutral axis depths of the beams' sections where reinforcement failure occurred in the analyses of Type I and II, respectively. In addition, these tables also show the strains and neutral axis depths of all the mid-height sections of the right column. In the majority of these mid-height sections, concrete failure was experienced since the ultimate compressive strain was achieved. The analyses in which concrete failure was not reached, convergence problems due to imminent reinforcement failure or reinforcement failure itself were felt.

Table 30 – Ultimate strains and neutral axis depths of the most relevant sections in the Analysis Type I

Model	Integration Section	L or H (m)	N (kN)	ε_{cu} (‰)	ε_{su} (‰)	c_u (m)
C	BT1(a)	0,00	450	-3,142	74,895	0,017
	CR4(c)	1,40	450	-4,691	50,236	0,019
			900	-8,038	42,781	0,035
			1500	-8,762	16,660	0,076
D	CR4(c)	1,40	450	-8,030	40,345	0,036
			900	-9,654	21,668	0,068
			1500	-8,924	12,112	0,093
E	BT1(a)	0,00	450	-3,142	74,895	0,017
	CR4(c)	1,40	450	-4,631	50,088	0,019
	BT1(a)	0,00	900	-3,090	74,998	0,017
	CR4(c)	1,40	900	-8,925	51,094	0,033
			1500	-11,679	25,519	0,069

Table 31 - Ultimate strains and neutral axis depths of the most relevant sections in the Analysis Type II

Model	Integration Section	L or H (m)	N (kN)	ε_{cu} (‰)	ε_{su} (‰)	c_u (m)
C	CR5(a)	1,40	450	-8,023	47,288	0,032
			900	-8,103	27,057	0,050
			1500	-8,833	12,726	0,090
D	CR5(a)	1,40	450	-8,151	25,619	0,053
			900	-8,290	13,848	0,082
			1500	-8,742	10,788	0,098
E	BT4(c)	5,00	450	-2,202	74,979	0,012
	CR5(a)	1,40	450	-7,037	51,301	0,026
			900	-11,435	40,292	0,048
			1500	-11,417	19,577	0,081

What can be firstly said is that, within the same models, the neutral axis depth near failure increases with the increase of the axial force applied on top of the columns (N). Even though, the ultimate curvatures achieved will only be examined in the next subchapter, as a direct consequence, the ultimate curvatures achieved decrease with the increase of the extension of the neutral axis depth (c_u). This influence in the deformation capacity in terms of maximum curvatures has been emphasised by Brito (2011).

From Models C to D, within the same levels of axial force, the increase in the flexural reinforcement significantly increases the neutral axis depth. As seen in Table 29, the ultimate concrete strains (ε_{cu}) of Models C and D at the mid-height section are numerically very close. As a result, the ultimate curvatures in this plastic hinge region of Model D are considerably lower.

On the contrary, from Models C to E, the increase in the transverse reinforcement slightly reduces the neutral axis depth yet significantly increases the ultimate curvatures achieved because the concrete can support higher levels of strains.

It is possible to observe that, in the cases where the reinforcement failure of the beams occurred, the neutral axis depth was very small, which means that the concrete contribution to balance the tensile stresses of the reinforcement was small. This situation makes sense considering that there was a small quantity of flexural reinforcement on the beams precisely to encourage the formation of plastic hinges near the end nodes of the beams. It has been stated by Brito (2011) that this type of failure commonly occurs in sections where the flexural reinforcement is concentrated in the extremities of the cross-section end.

As the beams reached their maximum deformation capability, the expected mid-height region of the right column did not fail. For instance, the CR4(c) section in Model C of the Analysis Type I subjected to a compressive force of 450kN, was only sustaining a compressive strain about 40% lower than its maximum capability. The level of axial force was not that high, and consequently, the neutral axis depth was small in the CR4(c) section, as seen in Table 30. On the other hand, in the analyses regarding Model E where the reinforcement failure of the beams occurred, the sudden increase of the

ultimate compressive concrete strain in the right column, made it difficult for the maximum values to be achieved under the circumstances of having a small level of axial force. In this sense, the deformation capacity of the mid-height section of the right column was not entirely explored because, as previously mentioned, the deformation capacity of this section significantly improved due to the increase of the confinement level.

When comparing the neutral axis depths near failure between the analyses of Type I and Type II, within the same levels of axial force on top of the columns, the neutral axis depths of the CR5(a) sections of the Type II analyses are higher than the neutral axis depths of the CR4(c) sections of the Type I analyses. This difference can be explained while evaluating the deformed shape of structure. Following the line of thought that the bending-moment diagrams give an indication of the expected deformed shape of the structure, it is possible to confirm in the next figures that the deformed shape of the structure somewhat follows the trend of the bending-moment diagrams.

Figure 47 and Figure 48 depict this deformed shape near failure for the particular case of Model E subjected to a 900kN axial force for the analysis Type I and II, respectively. The colour blue highlights the members whose integration sections yielded. The deformed shapes of the remaining analyses were not depicted since they are analogous to the ones presented herein.

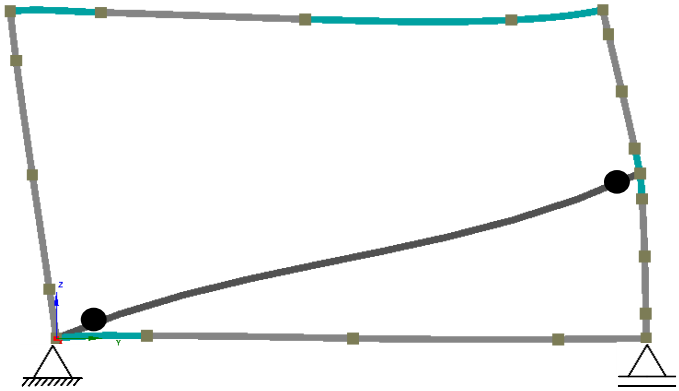

Figure 47 – Deformed Shape of the Structure in Type I Analysis

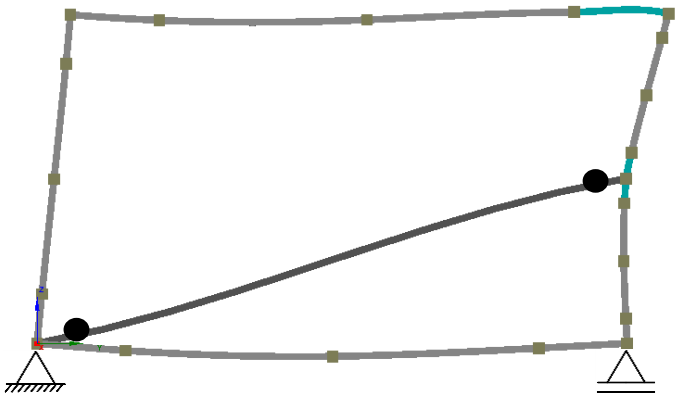

Figure 48 – Deformed Shape of the Structure in Type II Analysis

In the analysis Type I, with the displacement being applied from right to left, the structure has to sustain an anti-clockwise rotation. In the analysis Type II, is the exact opposite, the displacement is

being applied from left to right and the structure has to withstand a clockwise rotation. As a result, the right column in the analysis Type II is subjected to a higher axial force when comparing to the left side. So, if a comparison is established between the analyses of Type I and Type II, the right column of the analysis Type II, for a certain given displacement, is under a higher level of axial force, and thus, presents higher levels of neutral axis depths. Therefore, the structures in the analyses of Type II will suffer collapse more rapidly than the analyses of Type I. Also, that explains the fact that only one plastic hinge region emerges on the beams. In the analyses of Type I, up to three plastic hinges emerge on the beams. The exception is the region near the right end node of the bottom beam, which almost does not move and deform, due to the axial stiffness of the stairs.

Another relevant point to be assessed and was previously noted is the fact that in the Type I analyses, concrete failure occurs at the CR4(c) section, immediately below the end node of the stairs while in the Type II analyses, concrete failure happens in the CR5(a) section, immediately above the end node of the stairs. A brief explanation will be presented while comparing the levels of strains along different values of imposed displacement on the mid-height sections of the right column of Model E subjected to a 900kN axial force.

Table 32 indicates the concrete strains and the strains of the reinforcement under tension, most far apart from the neutral axis, for the mid-height sections of the right column in the Type I analyses. Four different sets of values, corresponding to different levels of displacements, are presented. The first set of strains is before the sections yield. The second is after the yielding of the CR4(c) section but before the yielding of the CR5(a) section. The third and fourth are after the yielding of the CR5(a) section. In addition to this table, the strains diagrams drawings are represented in Figure 49 to facilitate the visualisation of these strains.

Table 32 – Values of strains for specified applied displacements in the analyses of Type I

Identification Letter	δ (cm)	ε_c^- (‰)		ε_s^+ (‰)	
		CR4(c)	CR5(a)	CR4(c)	CR5(a)
A	1,00	-0,718	-0,730	0,885	0,825
B	2,50	-1,534	-1,471	3,322	2,410
C	3,00	-2,816	-1,686	14,905	3,418
D	5,00	-6,591	-3,633	42,132	21,140

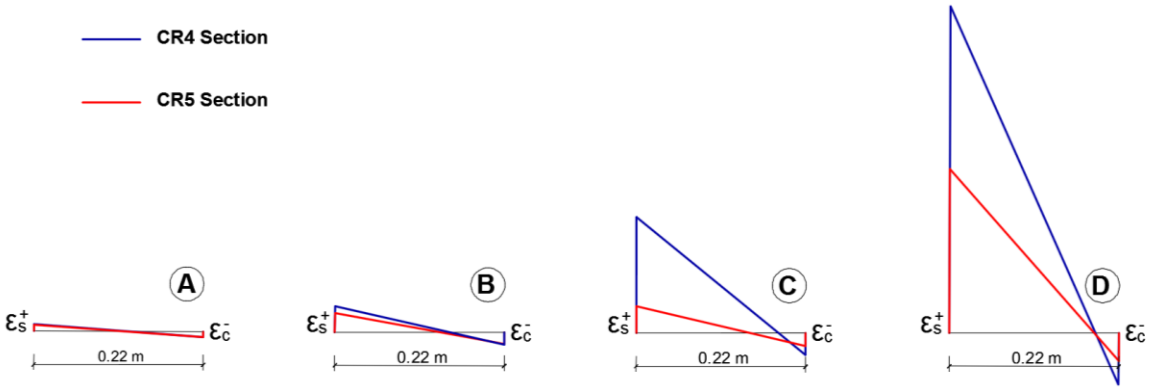

Figure 49 – Comparison of the strains evolution of the mid-height sections of the right column for the analyses of Type I

During the first phase of the analysis (situation A), the differences between the strain values are not significant. However, the concrete strains of the CR5(a) section are slightly higher than the ones in the CR4(c) section. This is due to the axial force being mobilised by the stairs under compression, which forces the top half of the right column to be more compressed than the bottom half.

Since both sections are under the same levels of bending moments at any given step, as a consequence, the neutral axis depth of the CR5(a) section is the most extensive one. This small variation prompts the tensile reinforcement of the CR4(c) section to yield first, as the Figure 49 illustrates in situation B.

As the tensile reinforcement yields, with the progress of the analysis, the effects of the compressive reinforcement, not yet yielded, start to be more felt and the concrete does not contribute as much as it did previously. This accentuates the differences between the neutral axis depths of the mid-height sections until the yielding of the CR5(a) section (situation C).

Similarly to the CR4(c) section, the concrete under compression of the CR5(a) section starts to contribute less and the neutral axis depth starts decreasing at a faster pace. Then, the concrete of the CR4(c) section enters in the descending portion of its constitutive relationship, where the strains increase while the stress levels decrease. At this point, the compressive reinforcement has also yielded and the concrete is forced to contribute more in terms of area. As a result, the neutral axis depth of the CR4(c) section slightly increases and near the end of the analysis (situation D), the differences between the neutral axes depths for both CR4(c) and CR5(a) sections are not substantial.

By the time the concrete of the CR5(c) section enters in the descending portion of the stress-strain relationship, the analysis is already reaching its end, so the neutral axes depths are close. In this particular case, the end of the analysis coincides with the emergence of convergence problems due to the imminent beam section failure related to the excessive reinforcement deformation. Figure 50 depicts the stress-strain relationships of the concrete and reinforcement of the mid-height sections of the right column for the analysis Type I.

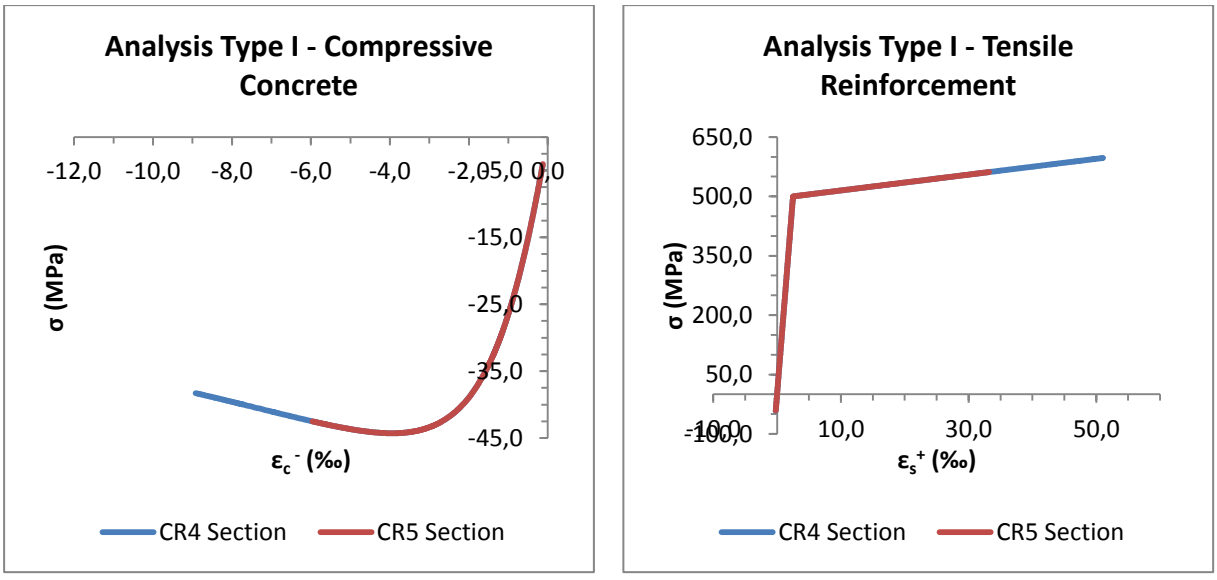

Figure 50 – Stress-Strain relationships of the mid-height sections of the analysis Type I

Analogously to what was done in the Type I analysis, Table 33 shows the strain values of the Type II analysis, Figure 51 represents the evolution of those strains and Figure 52 illustrates the stress-strain relationships of the mid-height sections.

Table 33 - Values of strains for specified applied displacements in the analyses of Type II

Identification Letter	δ (cm)	ε_c^- (‰)		ε_s^+ (‰)	
		CR4(c)	CR5(a)	CR4(c)	CR5(a)
A	1,00	-1,001	-0,979	1,162	1,261
B	2,00	-1,728	-1,841	2,409	3,553
C	2,50	-2,050	-3,636	3,616	17,267
D	3,00	-2,366	-7,183	5,253	32,448

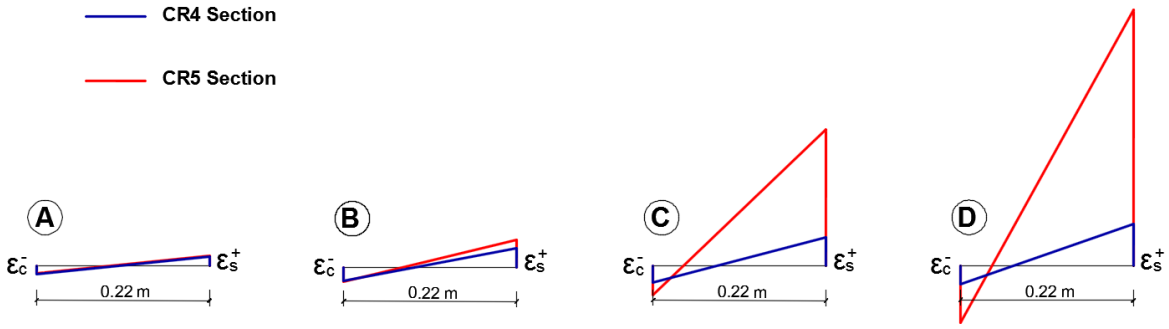

Figure 51 - Comparison of the strains evolution of the mid-height sections of the right column for the analyses of Type II

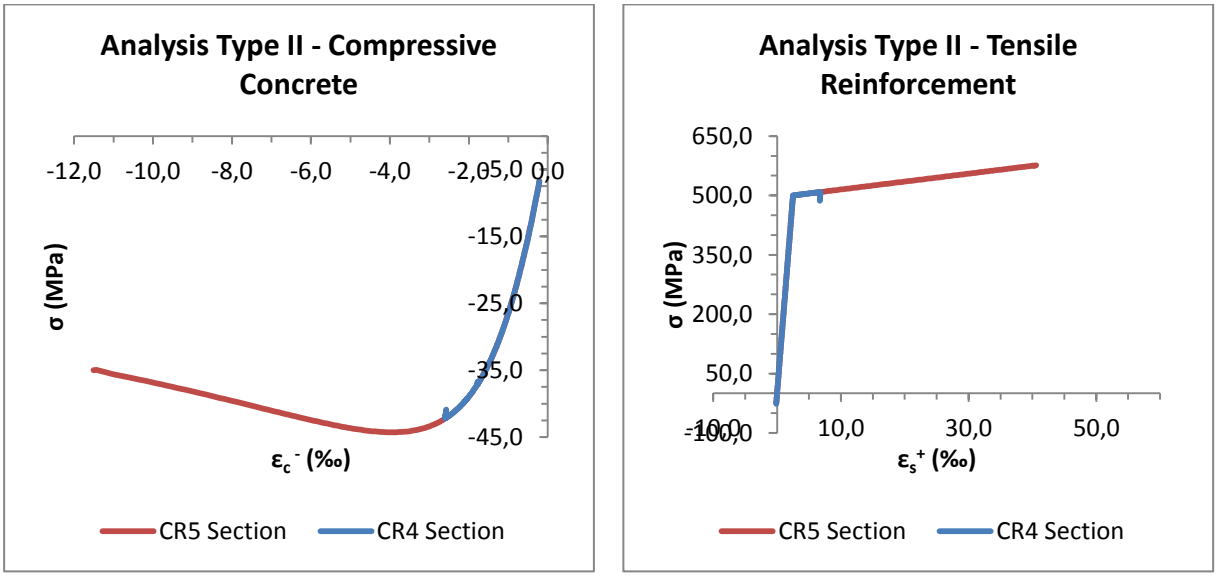

Figure 52 – Stress-Strain relationships of the mid-height sections of the analysis Type II

The interpretation for the Type II analysis, where the applied displacement causes the stairs to be under tension, is now reverse. The bottom half of the right column is more compressed than the top half and, as a result, the CR5(a) section is the first to yield because the neutral axis depth is smaller.

The differences between the neutral axes depths of the mid-height sections increase until the yielding of the CR4(c) section. Then, the concrete of the CR5(a) section enters in the descending portion of its constitutive relationship, causing the neutral axis depth to increase, until the analysis ends due to concrete failure. The CR4(c) section does not enter in the descending portion of the concrete stress-strain relationship, so the differences between the neutral axes depths of the mid-height sections CR4(c) and CR5(a) are more noticeable than the differences in the Type I analyses. Another reason for this difference being more noticeable is also the fact that the axial forces in the right column of the Type II analyses are greater than the Type I because of the direction in which the displacement is being applied. Figure 53 illustrates the variation of the axial forces in the right column for both types of analyses, under the same displacement of 3,00cm, in Models E.

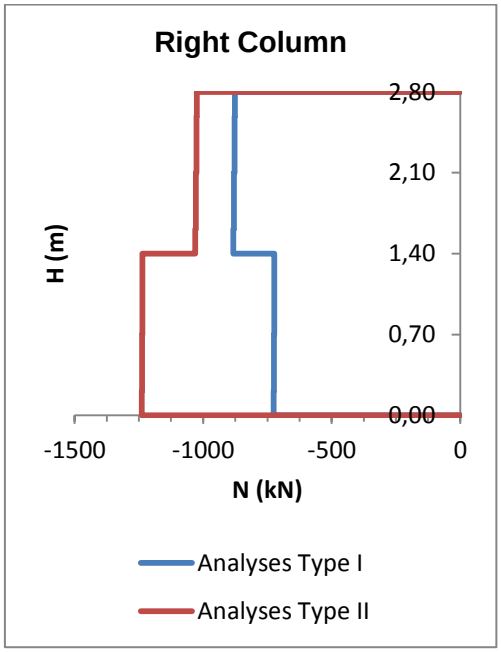

Figure 53 – Variation of the axial forces along the right column for the two types of analyses

4.2.4. Displacement-Curvature Diagrams

The data in Table 34 indicates the displacement values on top of the right column at which the CR4(c) section for the analyses of Type I and the CR5(a) section for the analyses of Type II yield.

Table 34 – Displacements at which the mid-height section of the right column yields

N (kN)	δ_y (cm)					
	Analyses of Type I			Analyses of Type II		
	Model C	Model D	Model E	Model C	Model D	Model E
450	-2,24	-2,35	-2,25	1,79	1,85	1,79
900	-2,44	-2,51	-2,45	1,93	1,97	1,93
1500	-2,69	-2,74	-2,69	2,10	2,13	2,11

Analysing the tables above, it is possible to observe that, as the compressive forces applied in the columns increase, the yielding displacements also increase. It was previously seen that the maximum displacements decreased with the increase of the compressive force. This means that the overall ductility in terms of displacements is negatively influenced by the presence of axial forces in the columns. In the Type II analyses the axial force influence is even more exacerbated because of the direction in which the displacement is being applied that, as previously mentioned, compresses even further the right side of the structure.

The yielding displacements of Models C and E, within the same compressive forces, are practically the same, which was expected considering that both models have the same flexural reinforcement. In Model D, since the flexural reinforcement considered is higher, the tensile forces at the yielding phase are also higher. Therefore, the concrete contribution to equilibrate those forces has to be greater, causing an extension of the compressed zone and reducing the zone under tension, which delays the section yielding.

Table 35 indicates the yielding curvatures (χ_y) of the sections CR4(c) and CR5(a) of the analyses of Type I and II, respectively. Figure 54 depicts the displacement-curvature diagrams of the mid-height sections of the right column for the analyses of Type I and II, respectively.

Table 35 – Yielding curvatures at the mid-height sections of the right column

N (kN)	χ_y (‰/m)					
	Analyses of Type I – CR4(c)			Analyses of Type II – CR5(a)		
	Model C	Model D	Model E	Model C	Model D	Model E
450	16,28	17,06	16,81	-17,33	-17,92	-17,66
900	18,19	18,37	18,29	-19,19	-19,57	-19,34
1500	20,22	20,28	20,15	-21,19	-21,30	-21,23

As the compressive force increases, the yield curvature also increases. It was previously seen that the ultimate curvatures decreased. As a result, the deformation capacity diminishes with the increase of the compressive force. Brito (2011) studied with detail the negative influence of the axial forces on the ductility of reinforced concrete structures. The higher the compressive force, the higher is the extension of the compressed zone at the cross-section level, and consequently, the concrete failure of the cross-section occurs under a smaller curvature value.

It can also be observed that the variations in terms of the flexural and transverse reinforcement have little influence in the values of the yield curvature. The same cannot be said about the ultimate curvatures. The increase in the flexural reinforcement, from Model C to Model D, considerably decreases the ultimate curvatures achieved because, as seen in the previous subchapter, the neutral axes depths are higher near failure.

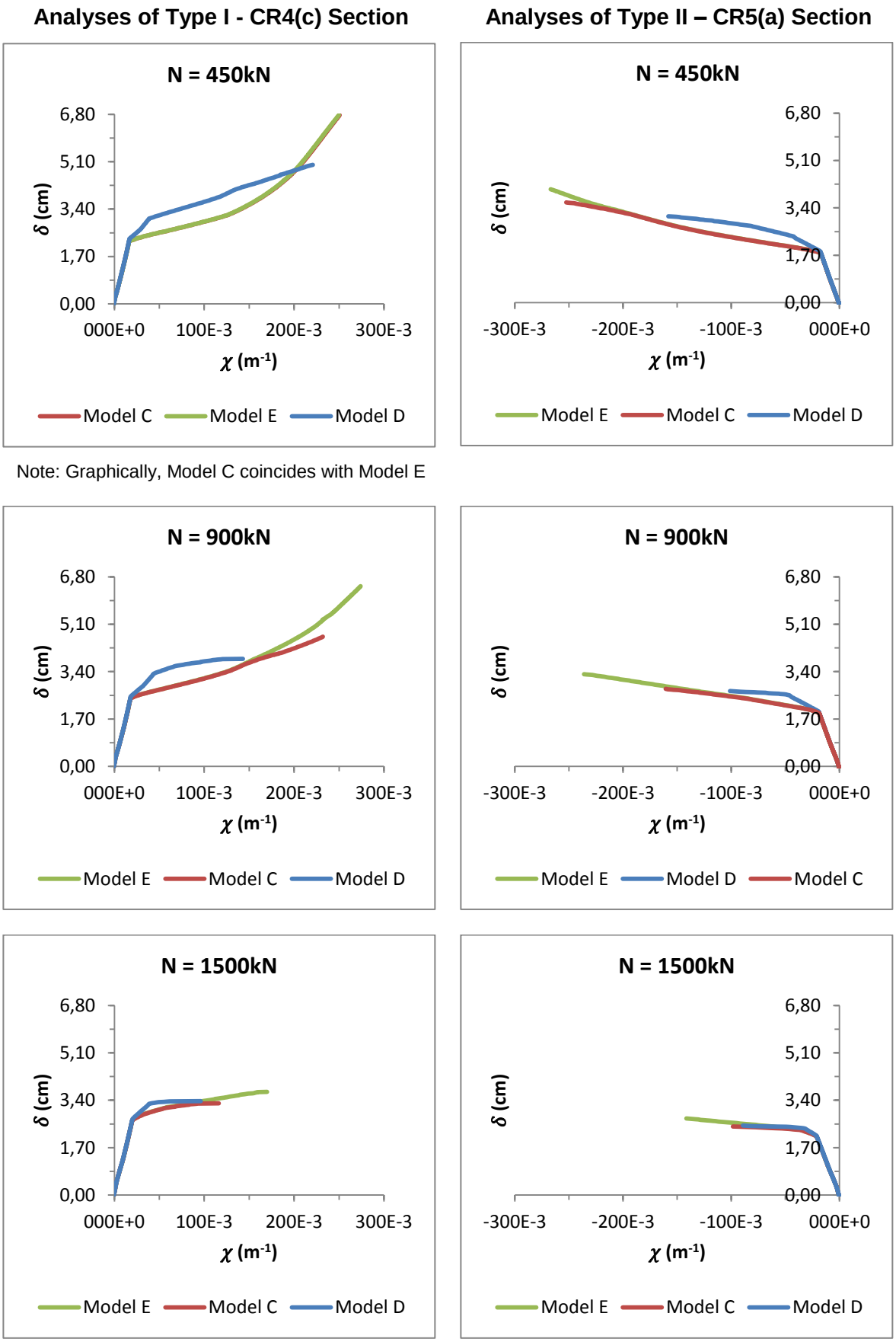

Note: Graphically, Model C coincides with Model E

Figure 54 – Displacement-Curvature diagrams at the mid-height sections of the right columns

One factor that has not yet been discussed and contributes to the higher depth level of neutral axes in Model D is the ratio between the flexural reinforcement under compression and the flexural reinforcement under tension. The influence of this ratio in the concrete structures ductility has been discussed by Brito (2011) and Camacho (2012). In Models C and E, the longitudinal reinforcement was all concentrated in the extremities parallel to the flexural axis of the cross-section. Therefore, as the analyses progress, the quantity of flexural reinforcement under tension was equal to the quantity of flexural reinforcement under compression.

Nevertheless, in Model D, the quantity of flexural reinforcement under tension is slightly higher than the quantity of flexural reinforcement under compression. As a consequence, the concrete has to compensate the smaller compression force that the reinforcement mobilises and the neutral axis depth has to be higher leading to smaller ultimate curvatures.

Conversely, the increase in the transverse reinforcement, from Model C to Model E, increases the ultimate curvatures reached because of the higher level of confinement. Taking into account the fact that yield curvatures of all models are approximately the same, it can be said that the curvatures ductility in the Models E are, in general, far greater than the ones in Models C and D. The increase in the transverse reinforcement increases the confinement factor and, as a consequence, also increases the ultimate compressive concrete strain that the cross-section can support.

4.2.5. Moment-Curvature Diagrams

Table 36 and Table 37 show the yielding (M_y) and ultimate bending moments (M_u) achieved at the CR4(c) section for the Type I analyses and the CR5(a) section for the Type II analyses, respectively.

Table 36 – Yielding and maximum bending moments at the CR4(c) section of the analyses of Type I

N (kN)	M_y (kN.m)			M_u (kN.m)		
	Model C	Model D	Model E	Model C	Model D	Model E
450	296,41	310,90	296,81	340,30	375,50	340,46
900	337,61	347,60	337,60	372,10	379,60	381,42
1500	385,92	391,30	385,80	386,83	398,10	399,90

Table 37 – Yielding and maximum bending moments at the CR5(a) section of the analyses of Type II

N (kN)	M_y (kN.m)			M_u (kN.m)		
	Model C	Model D	Model E	Model C	Model D	Model E
450	323,06	335,18	323,32	365,01	383,60	371,77
900	362,70	371,25	362,72	382,15	396,03	394,70
1500	407,65	411,33	407,97	395,16	402,81	409,58

It is possible to notice in the tables above that the axial force on top of the columns increases both the yielding and ultimate bending moments achieved at the cross-sections. In addition, as expected, the yielding bending moment in Model D is the highest one because this model considers the highest level of flexural reinforcement. The values of bending moments achieved seem to have a directly proportional variation with the increase of flexural reinforcement considered, which strongly influences

the resistant capacity of the cross-section. Previously, it was noticed that the values of yield curvatures in the D models were practically identical to the yield curvatures of the other models, within the same range of axial forces. Taking into account these factors, it is possible to state that, near yielding, the flexural stiffness of the cross-section is highly dependent on the quantity of flexural reinforcement considered. It has been referred in the literature review chapter, of this dissertation, that one of the common misconceptions in which the current design codes rely is assuming that the flexural stiffness of the cross-sections is not influenced by the quantity of flexural reinforcement and, therefore, it is assumed that an increase in the flexural reinforcement will proportionally increase the yield curvature and potentially deter the formation of plastic hinges. The assumption that serves as the basis for the linear elastic analyses is not adequate for levels of internal forces close to or larger than the ones at yielding.

In what concerns Models C and E, those models consider the same amount of flexural reinforcement, thus the yielding bending moments are almost identical. Only the ultimate bending moments are different because the confinement level due to the transverse reinforcement considered was different in those models. The mid-height section of the right column is more confined in Model E than Model C.

In some of the analyses, the ultimate bending moment does not coincide with the maximum bending moment felt at the cross-sectional level because the maximum bending moment occurs before the end of the analyses. As soon as this maximum value is reached, the spread of plasticity comes to a standstill, because the value of the bending moment can no longer increase and the concrete deformability capacity is not completely exploited. For this reason, it is presented on Table 38 the ratios between the maximum and yielding bending moments for all the analyses executed. It is also of interest to analyse as well the bending-moment-curvature diagrams represented in Figure 55 for the analyses of Type I and II, respectively.

Table 38 – Quotients between maximum and yielding bending moments

N (kN)	$M_{máx}/M_y$ (-)					
	Analyses of Type I – CR4(c) Section			**Analyses of Type II - CR5(a) Section**		
	Model C	**Model D**	**Model E**	**Model C**	**Model D**	**Model E**
450	1,15	1,21	1,15	1,13	1,16	1,15
900	1,10	1,15	1,13	1,06	1,13	1,09
1500	1,05	1,09	1,05	1,05	1,06	1,05

From the table above, it is possible to observe that the differences between the maximum and yielding bending moments diminish with the increase of the compressive force being applied on top of the columns. In practical terms, this means that the spread of plasticity decreases with the increase of the normalised axial force. Brito (2011) stated that the smaller the plastic hinge length, the greater will be the demand of curvatures on the plastic hinge region. Moreover, the ductility availability of the plastic hinge regions decreases with the increase of the axial forces being applied on the columns, because of the greater depth of the neutral axis. Consequently, the end of the analyses occurs under smaller values of displacements and curvatures.

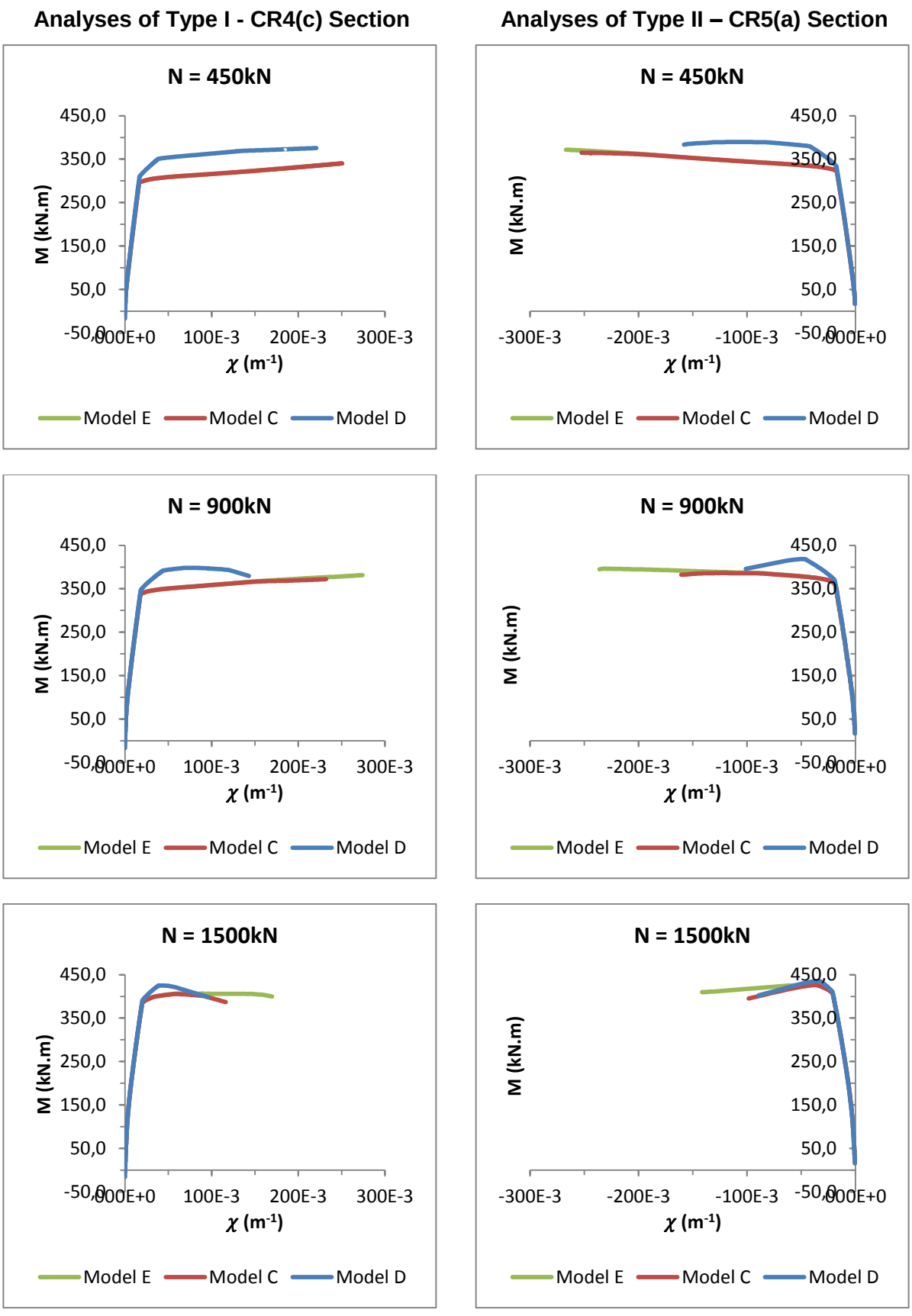

Figure 55 – Moment-Curvature diagrams at the mid-height sections of the right columns

For the smallest levels of the compressive force, the maximum bending moments occur at the end of the analyses. Exceptions to this statement are the diagrams corresponding to the Model D analyses. Those Model D diagrams along with the analyses submitted to a 1500kN axial force have their bending moments reaching a maximum value before the end of the analyses. After attaining their maximum bending moments, the moment-curvature diagrams of these analyses exhibit a descending portion leading to the obtainment of ultimate bending moments, in some cases, smaller than the values of yielding bending moments. This highlights the fact that the concrete stress-strain behaviour becomes more relevant than the reinforcing steel constitutive relationship and the curvatures ductility are smaller in those analyses. In the other analyses that do not exhibit a descending portion in the moment-curvatures diagram, it can be said that the reinforcing steel hardening considered was possibly enough to prevent that decrease in the values of bending moments.

In conclusion, it can be said that the greater the ratio between maximum and yielding bending moments, the greater will be the spread of plasticity. The models under a smaller level of compressive force will have larger plastic hinges and, therefore, the curvatures ductility demand in those models will be smaller. When comparing within the same levels of compressive force, the Models D have the highest ratios. However, when observing the particular case of having a 900kN axial force applied on the columns, despite Model D having the highest ratio between the maximum and yielding bending moment, Model D has a maximum peak in moment-curvatures diagrams which restricts the potential length of the plastic hinge and, consequently, restricts the spread of plasticity that the concrete could endure. On the contrary, Models C and E, despite having quotients slightly smaller, take full advantage of the concrete deformation capacity because the maximum bending moments achieved coincide with the sections failure. When comparing Model C and Model E, the highest confinement level in Model E positively contributes to the obtainment of greater plastic hinges length – the quotient between maximum and yielding bending moments is higher in Models E. Furthermore, it can be said that the confinement level in Model E seems to reduce the importance of the descending portion of concrete stress-strain relationship since it delays the obtainment of the maximum concrete stress.

5. Conclusions

5.1. General Considerations

The present dissertation focused on the study of the nonlinear effects produced by imposed displacements on a column supporting a slab of stairs at middle height between floors. It has been shown that performing an elastic analysis on a reinforced concrete framed structure subjected to a horizontal displacement, wherein one of the columns supports a slab of stairs at middle height between floors, leads to the obtainment of high levels of bending moments and shear forces at that same column (see point 4.1.2.). The stairs have a considerable axial stiffness that restrains the deformation capacity in the horizontal direction of the column in question, causing a short-column effect. This effect forces the column to absorb the imposed displacement along a smaller height than in the situation of not having the presence of stairs.

The increase of the internal forces felt in the column in the elastic analysis, particularly the bending moments, would indicate that the quantity of flexural reinforcement without considering the effect of the stairs was insufficient. As a result, there would be a need to increase the strength, in order to withstand those high levels of internal forces experienced due to the stairs. Nevertheless, increasing the flexural reinforcement would start a cycle that, as it was shown, not only would it increase the bending moments but, as a consequence, it would also increase the levels of shear force experienced (see point 4.2.3., Tables 25 and 26). It is noteworthy to mention that an increase in the levels of shear forces would have the inconvenience of potentially escalating the occurrence of shear induced type of failures.

Following the elastic analysis, a nonlinear analysis of the structure being studied was performed. Emphasis was laid on the examination of the available ductility, in terms of displacements and curvatures, while considering different types of longitudinal and transverse reinforcement.

It was noticed that increasing the column flexural reinforcement to resist an imposed displacement did not improve the structure's performance (see point 4.2.3., Table 22 and Tables 25 to 28). Despite the greater flexural stiffness for deformations at or higher than yielding (see point 4.2.5., Figure 55), the available curvatures ductility was considerably smaller (see point 4.2.3., Tables 27 and 28). Furthermore, it was observed that variations in the flexural reinforcement did not produce significant variations in the values of yield curvatures achieved (see point 4.2.4., Table 35). This proves that these values are independent of strength, which completely opposes to what is assumed in the current seismic design codes. By this mean, increasing the quantity of flexural reinforcement to withstand imposed displacement does not avoid or delay the structural yielding.

Conversely, increasing the transverse reinforcement in the plastic hinges regions of the column ensured a better performance and increased the deformation capacity, as the displacements and curvatures ductility obtained were higher (see point 4.2.3., Tables 22, 27 and 28). The level of confinement and, subsequently, the ultimate compressive concrete strains were greater, which

enabled a higher ductility availability to withstand the applied horizontal displacement (see point 4.2.3., Table 29).

In addition, it has been demonstrated that the larger the intensity of the axial forces being applied on the column, the smaller were the overall displacements and curvatures ductility (see point 4.2.3., Tables 22, 27 and 28 and point 4.2.4., Table 35) because there was a significant increase in the depths of the neutral axis on the cross-sections (see point 4.2.3., Tables 30 and 31). On the other hand, the bending moments, at yield and at the end of the analyses, expectedly increased with the increase of the axial forces (see point 4.2.5., Tables 36 and 37).

In what concerns the moment-curvature diagrams, it was noticed that, for the strongest intensities of axial force and for the smallest confinement levels, the descending portion of the concrete stress-strain relationship, after the attainment of the maximum stress, strongly influenced the moment-curvature diagrams by inducing a descending branch, which restricted the maximum concrete deformability potentially achieved on the structural elements (see point 4.2.5., Figure 55), as it increases the neutral axis depth at rupture. Moreover, it was also noticed that the ratios between the maximum and yielding bending moments and the plastic hinges length decreased with the increase of the levels of axial forces being applied on the columns (see point 4.2.5, Table 38).

5.2. Recommendations

This thesis placed emphasis on the nonlinear analyses of seismic effects produced by stairs supported at middle height of columns. Nevertheless, it is important to bear in mind that in the current design practice nonlinear analyses are not commonly executed, mainly, due to their inherent complexity. Instead, elastic analyses are made where seismic actions are defined through the use of elastic response spectrums and the structural nonlinear behaviour is taken into account with the use of behaviour coefficients. Taking into consideration these facts, some recommendations will be made in the following paragraphs.

It has been shown that when imposing horizontal displacements to columns supporting stairs at a mid-height level, the column's structural behaviour is strongly influenced by the presence of stairs. As previously stated, in the design practice, stairs are usually not included in the global modelling of buildings. As a consequence, this procedure severely underestimates the effects on the columns that support stairs. Therefore, those columns may not be adequately reinforced to withstand a seismic movement and the structural collapse may be potentially induced. To prevent the underestimation of seismic effects on those columns and the entailed consequences, it is vital to include the consideration of stairs on the analytical models of building structures under seismic actions.

The most important effect to consider is the ductility demand on the region where the stairs connect to the columns, which in this case was the mid-height level of the column. It was demonstrated that in the mid-height region, a plastic hinge was formed and for this situation, Eurocode 8 – Part 1 already states in section 5.2.3.4 (2) a) that a sufficient curvature ductility shall be provided in all critical regions of primary seismic elements, including column ends. In this sense, the mid-height region of any given column supporting stairs should be considered a critical region considering the potential formation of a

plastic hinge on that same region. Eurocode 8 – Part 1 further states in section 5.4.3.2.2 (4) the definition of the critical regions, offering the possibility to calculate the critical length, measured from both end sections of a primary seismic column. If the clear length of a certain column supporting stairs at an intermediate level is considered to be half the column, then the mid-height region is considered to be a critical region as well as the bottom and top regions of the column and all these critical regions should, according to Eurocode 8, be reinforced accordingly. However, as it was said previously, stairs are usually not included on the analytical models. As a result, if Eurocode 8 guidelines are followed and the analytical model does not include stairs, then the mid-height region of columns supporting stairs is not considered to be critical and, thus, it does not need to be reinforced accordingly. So, in order to avoid misinterpretations, Eurocode 8 should explicitly include guidelines to design columns that support stairs at an intermediate level, such as the necessity to have an adequate amount of confinement especially at the regions where plastic hinges are expected to be formed, namely the mid-height level and the top and bottom ends of the column. It should also be included the fact that the longitudinal reinforcement does not need to be increased due to the short column effect. As it was demonstrated, increasing the longitudinal reinforcement, does not improve the overall behaviour of the structure. On the other hand, increasing the amount of transverse reinforcement counteracts the aggravated effect of the higher levels of shear forces and increases the concrete confinement to overcome the increase of the ductility demand.

5.3. Suggestions for Future Research

To conclude, some suggestions for future research will be drawn in the following paragraphs. It would be of interest to pursue the detailed studying of problems that are conceptually equivalent to the effects produced by stairs on columns of buildings.

For instance, it would be interesting to analyse the effects produced by masonry infilled frames on columns subjected to imposed displacements. Unlike the stairs that are considered to be secondary structural elements, masonry infills are considered to be non-structural elements. Nevertheless, similarly to stairs that are supported on columns, partially infilled frames also restrain the deformation of columns under imposed displacements and, in this sense, can also cause the emergence of the short column effect since the columns free height to withstand the imposed displacement is reduced. This short column effect can strongly influence negatively the local behaviour prompting, for example, the occurrence of shear failure.

Additionally, some other suggestions that are more related to the work presented in this dissertation may include a thorough quantitative evaluation of the effects of the shear forces on columns under imposed displacements that support slabs of stairs. Another possibility is to study a whole building in a two-dimensional plane, with its respective loadings and multiple stairs connecting storeys, to compare the results obtained with the entire structure and the substructure studied in this thesis. Also, it could be interesting to study a building in a three-dimensional model to take into account the torsional effects due to seismic actions that the stairs may induce in the building. As a final suggestion, the

landing of the stairs could also be structurally modelled to study their influence on the structural behaviour.

References

Brito, A. 2011. *Dimensionamento de estruturas subterrâneas de betão armado sujeitas a acções sísmicas*. PhD Thesis in Civil Engineering, Instituto Superior Técnico, Universidade Técnica de Lisboa.

Calabrese, A., Almeida, J. P. and Pinho, R. 2010. Numerical issues in distributed inelasticity modelling of RC frame elements for seismic analysis. *Journal of Earthquake Engineering and Engineering Vibration* 14(S1). pp. 38-68.

Calvi, G. M., Sullivan, T. 2009. Development of a model code for direct displacement based seismic design. *The state of Earthquake Engineering Research in Italy: the ReLUIS-DPC 2005-2008 Project* .pp. 141-171.

Camacho, V. 2012. *Optimização do Projecto de Pontes para a Acção Sísmica*. MSc Dissertation in Civil Engineering, Instituto Superior Técnico, Universidade Técnica de Lisboa.

Correia, A. A., Virtuoso, F. B. E. 2006. Nonlinear Analysis of Space Frames. *Proceedings of the Third European Conference on Computational Mechanics: Solids, Structures and Coupled Problems in Engineering*. Mota Soares et al. (Eds.), Lisbon, Portugal.

EN 1992-1-1. "Eurocode 2: Design of concrete structures – Part: 1-1: General rules and rules for buildings". 2010.

EN 1998-1. "Eurocode 8: Design of structures for earthquake resistance – Part 1: General rules. seismic actions and rules for buildings". 2010.

EN 1998-2. "Eurocode 8: Design of structures for earthquake resistance – Part 2: Bridges". 2011.

EN 1998-3. "Eurocode 8: Design of structures for earthquake resistance – Part 3: Assessment and retrofitting of buildings". 2005.

Lopes, M. 2008. Breve referência à história da engenharia sísmica. *Sismos e Edifícios (Cap.1)*. Amadora: Edições Orion, pp. 1-14.

Lopes, M. 2008. Concepção de estruturas. *Sismos e Edifícios (Cap.5)*. Amadora: Edições Orion, pp. 189-265.

Mander, J. B., Priestley, M. J. N. and Park, R. 1988. Theoretical stress-strain model for confined concrete. *Journal of Structural Engineering* 114(8). pp. 1804-1826.

Priestley, M. J. N. 1996. Displacement-Based Seismic Assessment of Reinforced Concrete Buildings. *Journal of Structural Engineering* 1 (1). pp. 157-192.

Priestley, M. J. N. 2000. Performance Based Seismic Design. *Proceedings 12th World Conference on Earthquake Engineering*. Auckland. Paper nº 2831.

Seismosoft. 2016. "*SeismoStruct 2016 – A computer program for static and dynamic nonlinear analysis of framed structures".* Available at: http://www.seismosoft.com/ [Accessed: 1 August 2016].

Smith, R. S. H., Tso, W. K. 2002. Inconsistency of Force-Based Design Procedure. *Journal of Seismology and Earthquake Engineering* 4 (1). pp.47-54.

Appendix A – Confinement Factor Calculation Table

The data in the Table below indicates the several parameters values necessary to obtain the confinement factors of the different types of sections used in the various structural non-linear analyses, according to the methodology proposed by Mander et al. (1988). In addition, the values of the ultimate reinforcement strains and ultimate concrete strains are also presented below.

Reinforcement type	**1**	**2**	**3**	**4**	**5**	**6**
Longitudinal reinforcement	4ϕ20+2ϕ16	4ϕ20	12ϕ25		10ϕ25	
Transverse reinforcement	ϕ6//0,125	ϕ6//0,125	ϕ8//0,10	ϕ8//0,20	ϕ8//0,10	ϕ8//0,20
h **(m)**	0,500					
b **(m)**	0,300					
A_S **(cm²)**	16,59	12,57	58,90	58,90	49,09	49,09
s **(m)**	0,125	0,125	0,100	0,200	0,100	0,200
s' **(m)**	0,119	0,119	0,092	0,192	0,092	0,192
c **(m)**	0,025					
f'_{co} **(kPa)**	38000					
f_{yh} **(kPa)**	500000					
d_c **(m)**	0,244		0,242			
b_c **(m)**	0,444		0,442			
A_c **(m²)**	0,1083	0,1083	0,1070	0,1070	0,1070	0,1070
A_e **(m²)**	0,0328	0,0278	0,0688	0,0448	0,0637	0,0414
$\sum w_i^2$ **(m²)**	0,350	0,395	0,073	0,073	0,115	0,115
A_i **(m²)**	0,0583	0,0659	0,0122	0,0122	0,0192	0,0192
ρ_{cc}	0,0153	0,0116	0,0551	0,0551	0,0459	0,0459
A_{cc} **(m²)**	0,1067	0,1071	0,1011	0,1011	0,1021	0,1021
k_e	0,307	0,260	0,681	0,443	0,624	0,406
f'_{lx} **(kPa)**	285	241	1414	460	1296	422
f'_{ly} **(kPa)**	156	132	774	252	709	231
f'_l **(kPa)**	211	178	1046	340	959	312
f'_{cc}/f'_{co}	1,038	1,032	1,179	1,061	1,165	1,056
f'_{cc} **(kPa)**	39446	39225	44805	40313	44269	40123
ε_{co} **(‰)**	2,160					
ε_{cc} **(‰)**	2,571	2,508	3,942	2,764	4,094	2,817
ρ_s	0,0027	0,0027	0,0061	0,0031	0,0061	0,0031
ε_{su} **(‰)**	75,000					
ε_{cu} **(‰)**	7,659	7,679	11,203	8,003	11,291	8,022